CERN-PH-TH/2014-048,
DESY 14-040, IFUM 1024-FT,
LPN14-061, MCnet-14-07,
WUB/14-01

arXiv:1404.0327v2 [hep-ph] 27 Jun 2014

Towards precise predictions for Higgs-boson production in the MSSM

E. Bagnaschi [a,b], R.V. Harlander [c], S. Liebler [d], H. Mantler [e], P. Slavich [a,b] and A. Vicini [f]

[a] *LPTHE, UPMC Univ. Paris 06, Sorbonne Universités, 4 Place Jussieu, F-75252 Paris, France*

[b] *LPTHE, CNRS, 4 Place Jussieu, F-75252 Paris, France*

[c] *Fachbereich C, Bergische Universität Wuppertal, Gaußstraße 20, D-42119 Wuppertal, Germany*

[d] *Universität Hamburg, Luruper Chaussee 149, D-22761 Hamburg, Germany*

[e] *CERN, Theory Division, CH-1211 Geneva 23, Switzerland*

[f] *Dipartimento di Fisica, Università di Milano and INFN, Sezione di Milano, Via Celoria 16, I–20133 Milano, Italy*

Abstract

We study the production of scalar and pseudoscalar Higgs bosons via gluon fusion and bottom-quark annihilation in the MSSM. Relying on the NNLO-QCD calculation implemented in the public code `SusHi`, we provide precise predictions for the Higgs-production cross section in six benchmark scenarios compatible with the LHC searches. We also provide a detailed discussion of the sources of theoretical uncertainty in our calculation. We examine the dependence of the cross section on the renormalization and factorization scales, on the precise definition of the Higgs-bottom coupling and on the choice of PDFs, as well as the uncertainties associated to our incomplete knowledge of the SUSY contributions through NNLO. In particular, a potentially large uncertainty originates from uncomputed higher-order QCD corrections to the bottom-quark contributions to gluon fusion.

e-mail addresses:
bagnaschi@lpthe.jussieu.fr, robert.harlander@uni-wuppertal.de, stefan.liebler@desy.de,
hendrik.mantler@cern.ch, slavich@lpthe.jussieu.fr, alessandro.vicini@mi.infn.it

1 Introduction

The recent discovery of a Higgs boson with mass around 125.5 GeV by the ATLAS and CMS experiments at the Large Hadron Collider (LHC) [1, 2] puts new emphasis on the need for precise theoretical predictions for Higgs production and decay rates, both in the Standard Model (SM) and in plausible extensions of the latter such as the Minimal Supersymmetric Standard Model (MSSM). The current status of these calculations is summarized in the reports of the LHC Higgs Cross Section Working Group (LHC-HXSWG) [3, 4, 5].

In the SM, the main mechanism for Higgs production at hadron colliders is gluon fusion [6], where the coupling of the gluons to the Higgs is mediated by loops of heavy quarks, primarily top and bottom. The knowledge of this process includes: the next-to-leading order (NLO) QCD contributions [7] computed for arbitrary values of the Higgs and quark masses [8, 9, 10, 11]; the next-to-next-to-leading order (NNLO) QCD contributions due to top-quark loops, in the heavy-top limit [12, 13] and including finite top-mass effects [14]; soft-gluon resummation effects [15] and estimates of the next-to-next-to-next-to-leading order (NNNLO) QCD contributions [16]; the first-order electroweak (EW) contributions [17, 18, 19, 20, 21] and estimates of the mixed QCD-EW contributions [22].

The Higgs sector of the MSSM consists of two $SU(2)$ doublets, H_1 and H_2, whose relative contribution to electroweak symmetry breaking is determined by the ratio of vacuum expectation values of their neutral components, $\tan\beta \equiv v_2/v_1$. The spectrum of physical Higgs bosons is richer than in the SM, consisting of two neutral scalars, h and H, one neutral pseudoscalar, A, and two charged scalars, $H^{\pm}$. The couplings of the MSSM Higgs bosons to matter fermions differ from those of the SM Higgs, and they can be considerably enhanced or suppressed depending on $\tan\beta$. As in the SM, one of the most important production mechanisms for the neutral Higgs bosons is gluon fusion, mediated by loops involving the top and bottom quarks and their superpartners, the stop and sbottom squarks. However, for intermediate to large values of $\tan\beta$ bottom-quark annihilation can become the dominant production mechanism for the neutral Higgs bosons that have enhanced couplings to down-type fermions.

If the third-generation squarks have masses around one TeV or even larger, their contributions to the gluon-fusion process are suppressed, and a sufficiently accurate determination of the cross section can be achieved by rescaling the SM results for the top- and bottom-quark contributions by appropriate Higgs-quark effective couplings. If, on the other hand, some of the squarks have masses of the order of a few hundred GeV – a scenario not yet excluded by the direct searches at the LHC – a precise calculation of the contributions to the gluon-fusion cross section from diagrams involving squarks becomes mandatory. The NLO-QCD contributions to scalar production arising from diagrams with colored scalars and gluons were first computed in the vanishing-Higgs-mass limit (VHML) in ref. [23], and the full Higgs-mass dependence was included in later calculations [10, 11, 24]. For what concerns pseudoscalar production, the NLO-QCD contributions arising from diagrams with quarks and gluons are known [8, 9, 10, 11] while diagrams involving only squarks and gluons do not contribute to the gluon-fusion process due to the structure of the pseudoscalar couplings to squarks. In contrast, a

full calculation of the contributions to either scalar or pseudoscalar production arising from two-loop diagrams with quarks, squarks and gluinos – which can involve up to five different particle masses – is still missing. Calculations based on a combination of analytic and numerical methods were presented in refs. [25, 26], but neither explicit analytic formulae nor public computer codes implementing the results of those calculations have been made available so far.

Approximate results for the quark-squark-gluino contributions can however be obtained assuming the presence of some hierarchy between the Higgs mass and the masses of the particles running in the loops. If the Higgs boson is lighter than all the particles in the loops, it is possible to expand the result in powers of the Higgs mass, with the first term in the expansion corresponding to the VHML. This limit was adopted in refs. [27, 28, 29] for the calculation of the top-stop-gluino contributions to scalar production and in refs. [30, 31] for the analogous calculation of pseudoscalar production. Refs. [29, 31] also discussed the reliability of the VHML by considering the next term in the expansion in the Higgs mass.

While an expansion in the Higgs mass is a viable approximation in the computation of the top-stop-gluino contributions to the production of the lightest scalar h, it might not be applicable to the production of the heaviest scalar H and of the pseudoscalar A, if their mass is comparable to the mass of the top quark. Moreover, an expansion in the Higgs mass is certainly useless in the calculation of the bottom-sbottom-gluino contributions, due to the presence of a light bottom quark. All of these limitations can, however, be overcome with an expansion in inverse powers of the superparticle masses. Since it does not assume any hierarchy between the Higgs mass and the mass of the quark in the loop, such an expansion is applicable to both top-stop-gluino and bottom-sbottom-gluino contributions, as long as the squarks and the gluino are heavier than the considered Higgs boson and the top quark. Results for scalar production based on an expansion in the superparticle masses were presented in refs. [32, 33, 34], and analogous results for pseudoscalar production were presented in ref. [31].

In order to improve the accuracy of the MSSM prediction for the gluon-fusion cross section, and to allow for a meaningful comparison with the SM prediction, several contributions beyond the NLO in QCD should be included. The NNLO-QCD contributions to scalar production arising from diagrams with top quarks and the subset of EW contributions arising from diagrams with light quarks can be obtained from the corresponding SM results with an appropriate rescaling of the Higgs couplings to quarks and to gauge bosons. The NNLO-QCD top-quark contributions to pseudoscalar production have also been computed [35]. Approximate results beyond the NLO in QCD also exist for the contributions of diagrams involving superparticles. A first estimate of the NNLO-QCD contributions of diagrams involving stop squarks was presented in ref. [36], and an approximate calculation of those contributions, assuming the VHML and specific hierarchies among the superparticle masses, was recently presented in refs. [37, 38]. Furthermore, a subset of potentially large $\tan\beta$-enhanced contributions from diagrams involving sbottom-gluino or stop-chargino loops can be resummed in the LO cross section by means of an effective Higgs-bottom coupling [39, 40, 41].

In a significant part of the MSSM parameter space, the couplings of the heavier neutral Higgs

bosons H and A to bottom quarks are enhanced by $\tan\beta$ with respect to the corresponding coupling of the SM Higgs, while their couplings to top quarks are suppressed by $\tan\beta$. When that is the case, the bottom-quark contributions to the gluon-fusion process – which for a SM-like Higgs with mass around 125.5 GeV amount to roughly 7% of the cross section – can dominate over the top-quark contributions. The bottom-quark contributions are subject to large QCD corrections enhanced by powers of $\ln(m_\phi^2/m_b^2)$, where ϕ denotes a generic Higgs boson, and so far they have been computed only at the NLO [8, 9, 10, 11]. As a result, the uncomputed higher-order QCD corrections to the bottom-quark contributions can become the dominant source of uncertainty in the cross section for the production of heavy MSSM Higgs bosons in gluon fusion.

On the other hand, as mentioned earlier, when the couplings to bottom quarks are sufficiently enhanced the production of MSSM Higgs bosons through bottom-quark annihilation dominates over gluon fusion. In the four-flavor scheme (4FS), where one does not consider the bottom quarks as partons in the proton, the process is initiated by two gluons or by a light quark-antiquark pair, and the cross section is known at the NLO in QCD [42]. In the five-flavor scheme (5FS), where the bottom quarks are in the initial partonic state, the cross section is known up to the NNLO in QCD [43, 44]. The use of bottom-quark parton density functions (PDFs) in the 5FS allows to resum terms enhanced by $\ln(m_\phi^2/m_b^2)$ that would arise in the 4FS when one or both bottom quarks are collinear to the incoming partons. As in the case of gluon fusion, the $\tan\beta$-enhanced contributions from diagrams involving superpartners can be resummed in the LO result by means of an effective Higgs-bottom coupling. The remaining one-loop contributions from superpartners have been found to be small [45].

A considerable effort has been devoted over the years to making the existing calculations of Higgs production available to the physics community in the form of public computer codes. In the case of the SM, NNLO-QCD predictions of the total cross section for gluon fusion, including various refinements such as EW corrections and finite top-mass effects, are provided, e.g., by `HIGLU` [46], `ggh@nnlo` [47], `HNNLO` [48] and `iHixs` [49]. The code `bbh@nnlo` [50] provides instead a NNLO-QCD prediction of the total cross section for Higgs production in bottom-quark annihilation in the 5FS. For what concerns the production of MSSM Higgs bosons via gluon fusion, `HIGLU` implements the results of ref. [24] for the NLO-QCD contributions arising from diagrams with squarks and gluons, as well as the results of refs. [40, 41] for the resummation of the $\tan\beta$-enhanced squark contributions in an effective Higgs-bottom coupling.

More recently, two codes that compute the cross section for Higgs production including approximate results for the contributions of diagrams with quarks, squarks and gluinos have become available. As described in ref. [51], the NLO-QCD [11, 29, 31, 32, 34] and EW [18, 21] contributions to Higgs-boson production via gluon fusion in the SM and in the MSSM have been implemented in a module for the so-called `POWHEG BOX` [52], a framework for consistently matching NLO-QCD computations of matrix elements with parton-shower Monte Carlo generators, avoiding double counting and preserving the NLO accuracy of the calculation. The code `SusHi` [53], on the other hand, computes the cross section for Higgs-boson production in both gluon fusion and bottom-quark annihilation, in the SM

and in the MSSM. In the case of gluon fusion, `SusHi` includes the exact results of ref. [9] for the NLO-QCD contributions of two-loop diagrams with top and bottom quarks, and the approximate results of refs. [28, 31, 34] and refs. [31, 32] for the NLO-QCD contributions of two-loop diagrams with stop and sbottom squarks, respectively. The NLO-QCD contributions of one-loop diagrams with emission of an additional parton are taken from ref. [33]. The NNLO-QCD contributions from diagrams with top quarks are included via a call to `ggh@nnlo`, and the corresponding contributions from diagrams with stop squarks are estimated following ref. [36]. Finally, the known SM results for the EW contributions [18, 20, 21] are adapted to the MSSM by rescaling the Higgs couplings to top quarks and to gauge bosons. In the case of bottom-quark annihilation, `SusHi` obtains from `bbh@nnlo` the NNLO-QCD result valid in the SM, then rescales it by an effective Higgs-bottom coupling that accounts for the $\tan\beta$-enhanced squark contributions [39, 40].

In this paper we use `SusHi` for a precise study of scalar and pseudoscalar Higgs production in the MSSM. In section 2 we present predictions for the total inclusive cross section for Higgs production in six benchmark scenarios compatible with the LHC results, focusing in particular on a scenario with relatively light stops where the effect of the SUSY contributions can be significant. In section 3 we provide a detailed discussion of the sources of theoretical uncertainty in the calculation of the total cross section for Higgs-boson production in the MSSM. We examine the dependence of the cross sections for gluon fusion and bottom-quark annihilation on the renormalization and factorization scales, on the precise definition of the Higgs-bottom coupling and on the choice of PDFs, as well as the uncertainty associated to our incomplete knowledge of the SUSY contributions through NNLO. In particular, we point out a potentially large uncertainty arising from uncomputed higher-order QCD corrections to the bottom-quark contributions to gluon fusion, which can affect the interpretation of the searches for the MSSM Higgs bosons in scenarios where their couplings to bottom quarks are enhanced with respect to the SM. In section 4 we present our conclusions. Finally, in the appendix we list the cross sections and uncertainties for the production of the three neutral Higgs bosons in selected points of the parameter space for the six benchmark scenarios.

2 Higgs-boson production in viable MSSM scenarios

The discovery of a neutral scalar with mass around 125.5 GeV puts the studies of the Higgs sector of the MSSM in an entirely new perspective. In order to remain viable, a point in the MSSM parameter space must now not only pass all the experimental bounds on superparticle masses, but also lead to the prediction of a scalar with mass, production cross section and decay rates compatible with those measured at the LHC. In particular, the relatively large mass of the SM-like scalar discovered at the LHC implies either stop masses of the order of 3 TeV – which would result in a negligible stop contribution to the production cross section – or a large value of the left-right mixing term in the stop mass matrix (see, e.g., refs. [54, 55]). In the latter case, at least one of the stops could have a mass as low as a few hundred GeV, and induce a significant contribution to the gluon-fusion cross section.

In view of these considerations, we will focus on the set of MSSM scenarios compatible with the LHC findings that has recently been proposed in ref. [56]. We will study the effect of the different contributions to the total cross section for the production of the MSSM Higgs bosons, relying on the approximate NNLO-QCD calculations implemented in `SusHi`.

2.1 The benchmark scenarios

The SM parameters entering our calculations include the Z-boson mass $m_Z = 91.1876$ GeV, the W-boson mass $m_W = 80.398$ GeV, the Fermi constant $G_F = 1.16637 \times 10^{-5}$ and the strong coupling constant $\alpha_s(m_Z) = 0.119$.[1] For the masses of the top and bottom quarks we take the pole mass $m_t = 173.2$ GeV [58] and the SM running mass (in the $\overline{\rm MS}$ scheme) $m_b(m_b) = 4.16$ GeV [59].

At the tree level, the MSSM neutral scalar masses m_h and m_H and the scalar mixing angle α can be computed in terms of m_Z, $\tan\beta$ and the pseudoscalar mass m_A only. However, the radiative corrections to the tree-level predictions can be substantial, and they bring along a dependence on all of the other MSSM parameters. To compute the masses and the couplings of Higgs bosons and superparticles in a given point of the MSSM parameter space we use the public code `FeynHiggs` [60], which includes the full one-loop [61] and dominant two-loop [62, 63, 64, 65, 66] corrections to the neutral Higgs masses. Since the theoretical uncertainty of the Higgs-mass calculation in `FeynHiggs` has been estimated to be of the order of 3 GeV [67],[2] we consider as phenomenologically acceptable the points in the MSSM parameter space where `FeynHiggs` predicts the existence of a scalar with mass between 122.5 GeV and 128.5 GeV and with approximately SM-like couplings to gauge bosons.

In addition to $\tan\beta$ and m_A, the MSSM parameters most relevant to the prediction of the masses and production cross sections of the Higgs bosons are: the soft SUSY-breaking masses for the stop and sbottom squarks, which for simplicity we set all equal to a common mass parameter M_S; the soft SUSY-breaking gluino mass $m_{\tilde{g}}$; the soft SUSY-breaking Higgs-squark-squark couplings A_t and A_b; the superpotential Higgs-mass parameter μ. In our convention for the sign of the latter, the left-right mixing terms in the stop and sbottom mass matrices are $X_t \equiv A_t - \mu\cot\beta$ and $X_b \equiv A_b - \mu\tan\beta$, respectively. It should be noted that in our analysis the soft SUSY-breaking squark masses and trilinear couplings are expressed in an "on-shell" (OS) renormalization scheme, as described in refs. [62, 63] for the stop sector and in refs. [64, 65, 32] for the sbottom sector. Since the two-loop calculation of the Higgs masses implemented in `FeynHiggs` and the NLO-QCD calculation of the production cross section implemented in `SusHi` employ the same OS scheme, the input values of the soft SUSY-breaking parameters can be passed seamlessly from the Higgs-mass calculation to the cross-section calculation. Concerning the parameters $\tan\beta$, μ and m_A, their definition is relevant to the Higgs-mass calculation only. In particular, $\tan\beta$ and μ are expressed in the $\overline{\rm DR}$ scheme, at a renormalization scale that

[1] The SM inputs agreed upon by the LHC-HXSWG are listed on the group's website [57].

[2] To reduce this uncertainty, it would be necessary to include in the mass calculation the remaining two-loop effects [68] and at least the dominant three-loop effects [69, 70]. Note also that there is an additional uncertainty of approximately 1 GeV stemming from the uncertainty of the SM input parameters, especially m_t.

Scenario	M_S [GeV]	X_t [GeV]	μ [GeV]	M_2 [GeV]
$m_h^{\rm max}$	1000	2000	200	200
$m_h^{\rm mod+}$	1000	1500	200	200
$m_h^{\rm mod-}$	1000	-1900	200	200
light stop	500	1000	400	400
light stau	1000	1600	500	200
tau-phobic	1500	3675	2000	200

Table 1: Choices of MSSM parameters for the benchmark scenarios proposed in ref. [56].

`FeynHiggs` takes by default equal to m_t, while m_A is identified with the pole mass of the pseudoscalar. Finally, the choice of renormalization scheme for $m_{\tilde{g}}$ amounts to a higher-order effect, because the gluino mass enters only the two-loop part of the corrections.

A detailed description of the six benchmark scenarios adopted in our analysis can be found in the paper where they were originally proposed, ref. [56]. All of the scenarios are characterized by relatively large values of the ratio X_t/M_S, ensuring that the mass of the SM-like Higgs falls within the required range without the need for extremely heavy stops. In addition, the masses of the gluino and of the first-two-generation squarks are set to 1.5 TeV, large enough to evade the current ATLAS [71, 72] and CMS [73, 74, 75] bounds. The prescriptions of ref. [56] for the parameters M_S, X_t, μ and for the soft SUSY-breaking wino mass M_2 are listed in table 1. We vary the parameters $\tan\beta$ and m_A within the ranges

$$2 \,\leq\, \tan\beta \,\leq\, 50 \;, \qquad\qquad 90 \text{ GeV} \,\leq\, m_A \,\leq\, 1 \text{ TeV} \;. \tag{1}$$

In all scenarios the Higgs-sbottom-sbottom coupling A_b is set equal to A_t, the left-right mixing of the first-two-generation squarks is neglected and the bino mass M_1 is obtained from the GUT relation $M_1/M_2 = (5/3)(m_Z^2/m_W^2 - 1)$, with the exception of the fourth scenario where we set $M_1 = 340$ GeV.[3] Finally, the choices of ref. [56] for the soft SUSY-breaking parameters in the slepton sector have a very small impact on the predictions for the Higgs masses and production cross sections, therefore we do not report them here.

The fourth scenario in table 1, denoted as *light stop*, deserves a special discussion. In this scenario the two stop masses are 324 GeV and 672 GeV; the sbottom masses depend on $\tan\beta$, but the lightest sbottom is always heavier than 450 GeV, while the heaviest one is always lighter than 550 GeV. With such relatively low masses, loops involving squarks can give a sizable contribution to the cross section for Higgs production, but we have to worry about the exclusion bounds from the LHC. Indeed, the ATLAS and CMS collaborations have presented preliminary results for the searches of direct stop- and sbottom-pair production, based on the full 8-TeV data sample, considering the decay chains

$$\tilde{t}_1 \,\to\, t\,\chi_1^0 \,\to\, b\,W\,\chi_1^0 \quad [76, 77] \;, \qquad \tilde{t}_1 \,\to\, b\,\chi_1^\pm \,\to\, b\,W\,\chi_1^0 \quad [76, 77] \;, \qquad \tilde{t}_1 \,\to\, c\,\chi_1^0 \quad [78, 79] \;,$$

[3] The choice $M_1 = 350$ originally proposed in ref. [56] would result in a stop LSP for $\tan\beta \gtrsim 20$.

$$\tilde{b}_1 \;\to\; b\,\chi_1^0 \quad [73,\,80]\,, \qquad\qquad \tilde{b}_1 \;\to\; t\,\chi_1^\pm \;\to\; t\,W\,\chi_1^0 \quad [71,\,74]\,.$$

The allowed values of the stop and sbottom masses depend on the chargino and neutralino masses, as well as on the branching ratios for the different squark decays. With the choice of parameters in table 1, $M_2 = \mu = 400$ GeV, together with $M_1 = 340$ GeV, the masses for the lightest chargino and neutralino have a mild dependence on $\tan\beta$, but they stay within the ranges $m_{\chi_1^\pm} \approx 341$ – 346 GeV and $m_{\chi_1^0} \approx 316$ – 320 GeV for $\tan\beta > 10$. In this case the lightest stop decays almost entirely through the loop-induced, flavor-violating channel $\tilde{t}_1 \to c\,\chi_1^0$. This channel has been investigated by ATLAS [78] and CMS [79], but the resulting bounds only reach to values of $m_{\tilde{t}_1}$ around 250 GeV. For the lightest sbottom, the two-body decays $\tilde{b}_1 \to \tilde{t}_1\,W$ and $\tilde{b}_1 \to b\,\chi_j^0$ (with j up to 3 or 4) are kinematically open. The direct decay of $\tilde{b}_1$ to the lightest neutralino would be constrained by the searches in refs. [73, 80], but *i*) that channel is never dominant in the considered range of parameters and *ii*) the experimental bounds only reach to values of $m_{\chi_1^0}$ below 280 GeV. Finally, the heaviest stop and sbottom can decay through a multitude of channels, and their direct decays to χ_1^0 or $\chi_1^\pm$ are significantly suppressed.

2.2 Cross section for Higgs production

We are now ready to present our precise predictions for the production of MSSM Higgs bosons at the LHC. As mentioned earlier, we rely on the code `SusHi`,[4] which includes all of the available NLO-QCD contributions to the gluon-fusion process, supplemented with the known SM results for the NNLO-QCD contributions in the heavy-top limit and for the EW contributions (both adapted to the MSSM by appropriately rescaling the Higgs couplings). While the results implemented in `SusHi` for the NNLO-QCD top contributions are strictly valid only for a Higgs mass below the top threshold, $m_\phi < 2\,m_t$, a comparison with the NLO results suggests that they provide a decent approximation also for larger values of the Higgs mass [81, 82]. The NNLO-QCD contributions from stop loops are estimated following ref. [36], i.e., neglecting the contributions of three-loop diagrams but retaining the NNLO contributions that arise from the product of lower-order terms. We have also checked that, when all of the NNLO-QCD contributions are omitted, the results of `SusHi` for the gluon-fusion cross section agree with those of the calculation implemented in the `POWHEG BOX` [51], which includes the same NLO-QCD and EW contributions. For what concerns the bottom-quark annihilation process, `SusHi` includes the NNLO-QCD results valid in the SM within the 5FS, also rescaled by the effective Higgs-bottom couplings of the MSSM.

In our study, we fix the center-of-mass energy of the proton-proton collisions to 8 TeV. While the numerical value of the total cross section for Higgs production does obviously depend on the collision energy, we have checked that the relative importance of the various contributions to the production processes and their qualitative behavior over the MSSM parameter space do not change

[4] For a detailed description of the cross-section calculation implemented in `SusHi` we refer to the code's manual [53].

substantially if we set the energy to 13 TeV. By default, we use the MSTW2008 set of PDFs [83], and we fix the renormalization and factorization scales entering the gluon-fusion cross section to $\mu_R = \mu_F = m_\phi/2$ [13, 84], where $\phi = \{h, H, A\}$ denotes the considered Higgs boson. For bottom-quark annihilation, the central values of the scales are chosen as $\mu_R = m_\phi$ and $\mu_F = m_\phi/4$ [43, 44, 85]. In the calculation of the gluon-fusion cross section we relate the bottom Yukawa coupling to the pole mass M_b, computed at the three-loop level [86] from the input value for the running mass, $m_b(m_b)$. In the case of bottom-quark annihilation, on the other hand, we relate the bottom Yukawa coupling to $m_b(m_\phi)$, in turn obtained from $m_b(m_b)$ via four-loop renormalization-group evolution [87]. In both cases, the $\tan\beta$-enhanced SUSY corrections to the relation between mass and Yukawa coupling of the bottom quark are included following refs. [39, 40]. The theoretical uncertainties associated to the choice of PDFs, to the variation of the renormalization and factorization scales and to the definition of the bottom Yukawa coupling will be discussed in detail in section 3.

In figures 1 and 2 we show the total cross section – i.e., the sum of gluon fusion and bottom-quark annihilation – for the production of the scalars (h, H) and of the pseudoscalar (A), respectively, as contour plots in the m_A–$\tan\beta$ plane. For the other MSSM parameters, we adopt the *light-stop* scenario described in section 2.1. Tables for the numerical values of the cross section (and the corresponding uncertainties) in all of the six benchmark scenarios are given in the appendix. In the two plots of figure 1, referring to h (left) and H (right) production, the red lines are contours of equal mass for the corresponding scalar. In this scenario, the prediction for the mass of the lightest scalar reaches a maximum of 123.8 GeV at large $\tan\beta$. The heaviest-scalar mass grows with m_A, and we show only the contour corresponding to 126 GeV to avoid clutter (for large m_A, the contours are roughly at $m_H \approx m_A$ and independent of $\tan\beta$). The x-axis of the plot for h production ends at $m_A = 300$ GeV because, for larger values, the cross section becomes essentially independent of m_A. The x-axis of the plots for H and A ends at $m_A = 500$ GeV because the expansion in the SUSY masses used to approximate the two-loop squark contributions in `SusHi` becomes unreliable when the Higgs mass approaches the lowest squark-mass threshold, which in the *light-stop* scenario corresponds to $2\,m_{\tilde{t}_1} \approx 650$ GeV. The theoretical uncertainty associated with this approximation will be discussed in section 3.4.

The qualitative behavior of the cross sections in figures 1 and 2 can be easily interpreted considering the relations between the scalar and pseudoscalar masses in the MSSM Higgs sector, and how each of the Higgs bosons couples to the top and bottom quarks (the squark contributions are generally sub-dominant, as will be discussed below). In the so-called decoupling limit, $m_A \gg m_Z$, the lightest scalar h has SM-like couplings to quarks, while its mass is essentially independent of m_A and, for $\tan\beta \gtrsim 10$, depends only weakly on $\tan\beta$. The cross section for h production (left plot in figure 1) varies very little in this region, and differs from the SM result for a Higgs boson of equal mass only because of the squark contributions to the gluon-fusion process. For $m_A \lesssim 130$ GeV, on the other hand, the couplings of h to top (bottom) quarks are non-standard, being suppressed (enhanced) by $\tan\beta$. In this narrow region the total cross section for h production is dominated by the contributions of the diagrams that involve the Higgs-bottom coupling, and it grows significantly with $\tan\beta$.

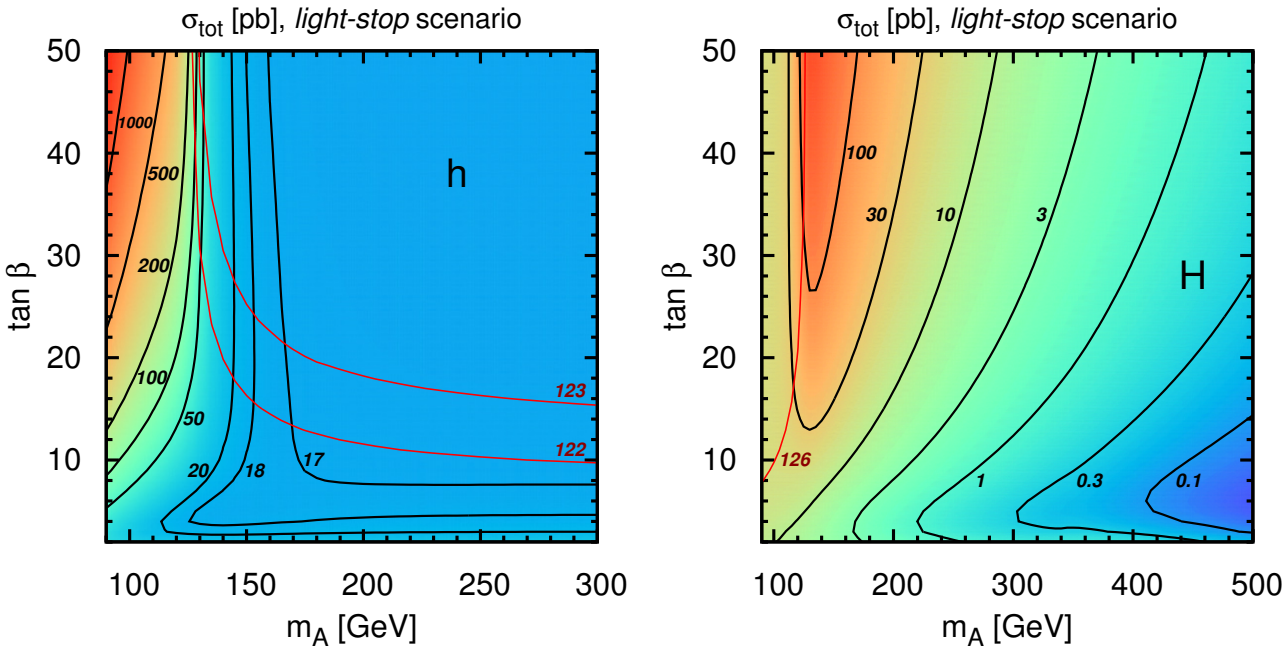

Figure 1: Total cross section in picobarn (pb) for the production of h (left) and H (right), as a function of m_A and $\tan\beta$ in the *light-stop* scenario. The solid red lines are contours of equal mass for each scalar.

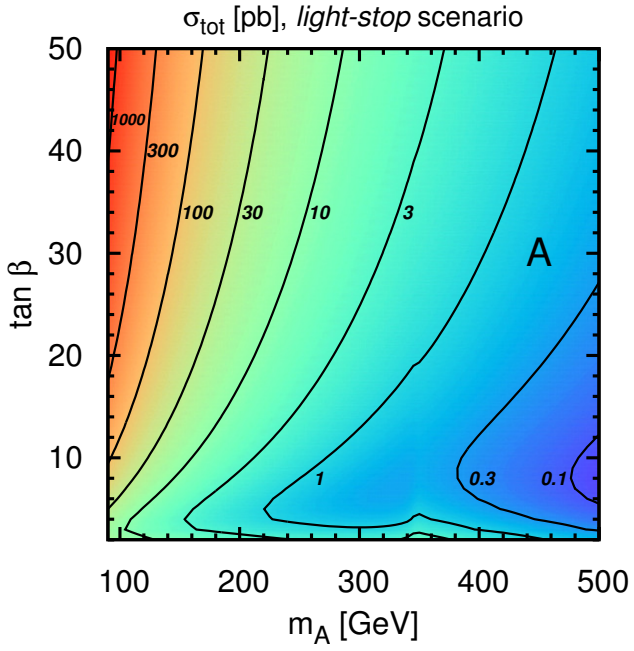

Figure 2: Same as figure 1 for the production of the pseudoscalar A.

The behavior of the cross section for H production in the m_A–$\tan\beta$ plane (right plot in figure 1) is different from – and somewhat complementary to – the one for h production. In the strip where $m_A \lesssim 130$ GeV, the heaviest scalar has a mass around 125 GeV and significant couplings to both top and bottom quarks, and the cross section for its production grows with $\tan\beta$. For larger m_A, on the other hand, m_H grows together with m_A, and the couplings of H to top (bottom) quarks are suppressed (enhanced) by $\tan\beta$. The total cross section for H production is therefore dominated, already for moderate $\tan\beta$, by the contributions of the diagrams that involve the Higgs-bottom coupling. The latter grow significantly with $\tan\beta$, but decrease with m_A, being suppressed by powers of the ratio m_b^2/m_H^2. Finally, the pseudoscalar couplings to top (bottom) quarks are suppressed (enhanced) by $\tan\beta$ for all values of m_A. Therefore, the behavior of the cross section for A production in the m_A–$\tan\beta$ plane, see figure 2, resembles the behavior of h production when $m_A \lesssim 130$ GeV, and the one of H production for larger m_A: in both cases, the cross section grows with $\tan\beta$, but decreases with m_A.

To disentangle the effects of the two main production channels for the MSSM Higgs bosons, we show in figures 3 and 4 the ratio between the gluon-fusion cross section and the sum of gluon-fusion and bottom-quark-annihilation cross sections in the *light-stop* scenario, again as contour plots in the m_A–$\tan\beta$ plane. Predictably, the plots reflect the behavior of the coupling of the considered Higgs boson to bottom quarks. The left plot in figure 3 shows that, when m_A is large enough that the couplings of the lightest scalar are SM-like, gluon fusion is by far the dominant process for h production, and the contribution of bottom-quark annihilation amounts only to a few percent. Only in the strip with $m_A \lesssim 130$ GeV and $\tan\beta \gtrsim 8$, where the coupling of h to bottom quarks is sufficiently enhanced by $\tan\beta$, does bottom-quark annihilation become the dominant process. Conversely, bottom-quark annihilation gives the largest contribution to the cross section for H production (right plot in figure 3) when $m_A \gtrsim 130$ GeV and $\tan\beta \gtrsim 6$, while in the case of A production (figure 4) the cross section is dominated by bottom-quark annihilation already for $m_A \gtrsim 100$ GeV, as long as $\tan\beta \gtrsim 5-8$.

To assess the relevance of the squark contributions to the gluon-fusion cross section in the *light-stop* scenario, we show in figures 5 and 6 the ratio of the total gluon-fusion cross section over the cross section computed including only the contributions of quarks (with appropriate rescaling of the Higgs-quark couplings). The left plot of figure 5 shows that – in this scenario characterized by relatively light squarks – the interference between the top and stop contributions can reduce the cross section for h production by as much as 20% in the decoupling region with large m_A and $\tan\beta$. Remarkably, in this region the partial NNLO-QCD contributions from stop loops that we include following ref. [36] account by themselves for a 6% suppression of the cross section. The theoretical uncertainty associated to these contributions will be discussed in section 3.4. For what concerns H production (right plot of figure 5), the squark contributions reduce the cross section by up to 30% for low values of m_A, and the suppression becomes even stronger with increasing pseudoscalar mass. In particular, near the lower-right corner of the plot, where $m_A \gtrsim 420$ GeV and $\tan\beta$ ranges between 6 and 20, the interference between the quark and squark contributions induce a suppression of the cross section by $70-80\%$. In this region the top contribution is suppressed by $\tan\beta$, while the bottom contribution is

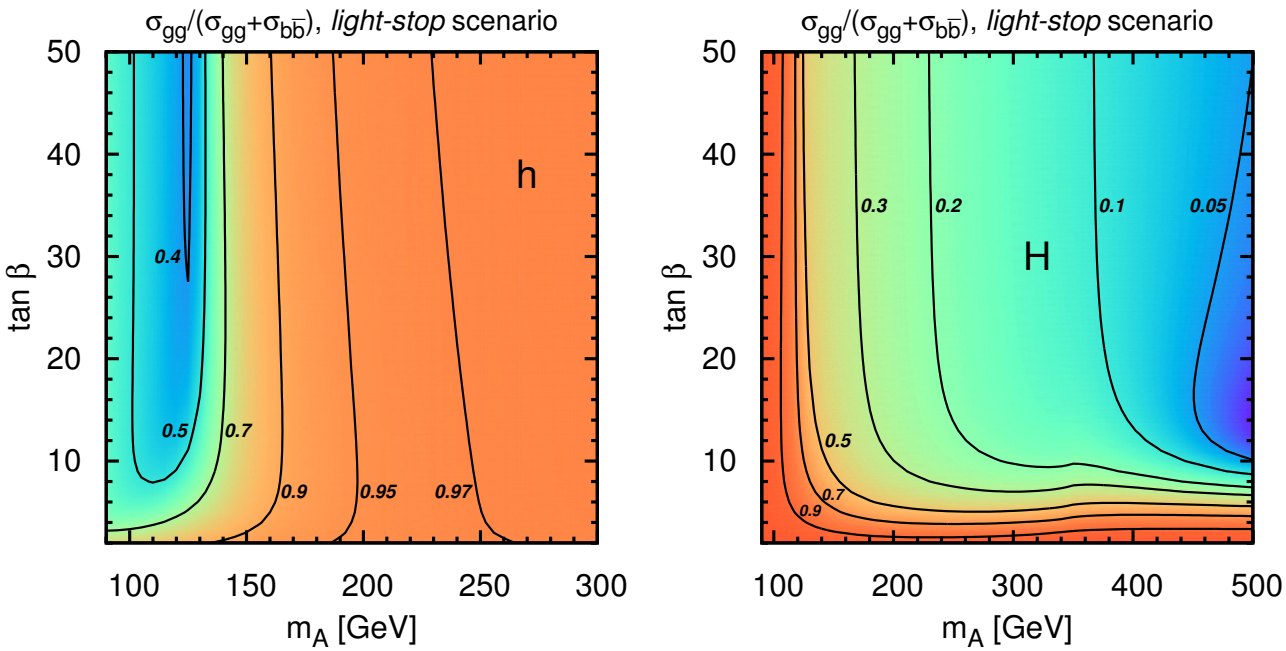

Figure 3: Ratio of gluon-fusion cross section over total cross section for the production of h (left) and H (right), as a function of m_A and $\tan\beta$ in the *light-stop* scenario.

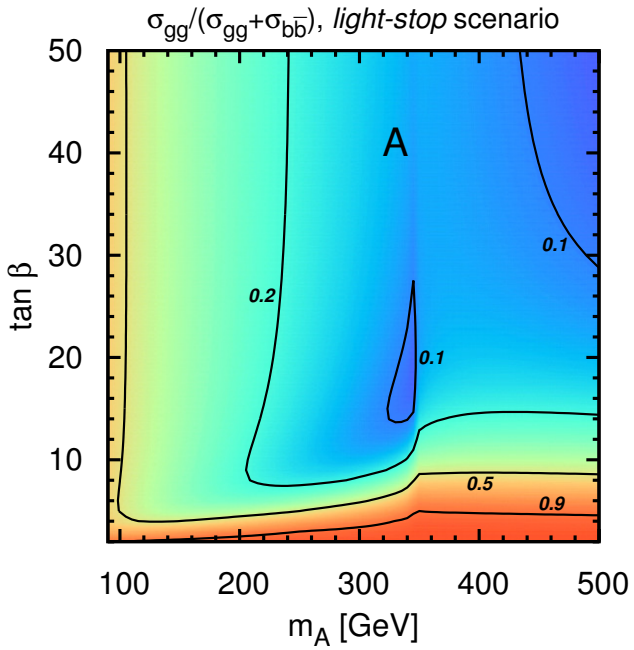

Figure 4: Same as figure 3 for the production of the pseudoscalar A.

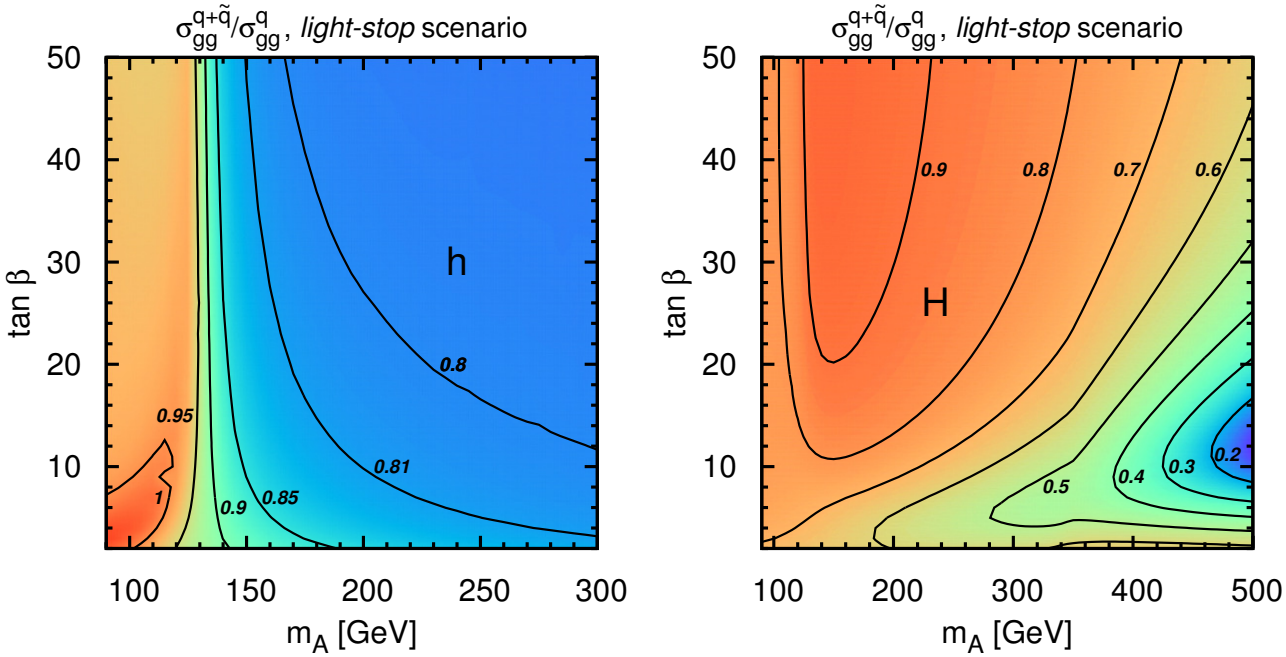

Figure 5: Ratio of gluon-fusion cross section for the production of h (left) and H (right) over the corresponding cross section neglecting squark contributions, as a function of m_A and $\tan\beta$ in the *light-stop* scenario.

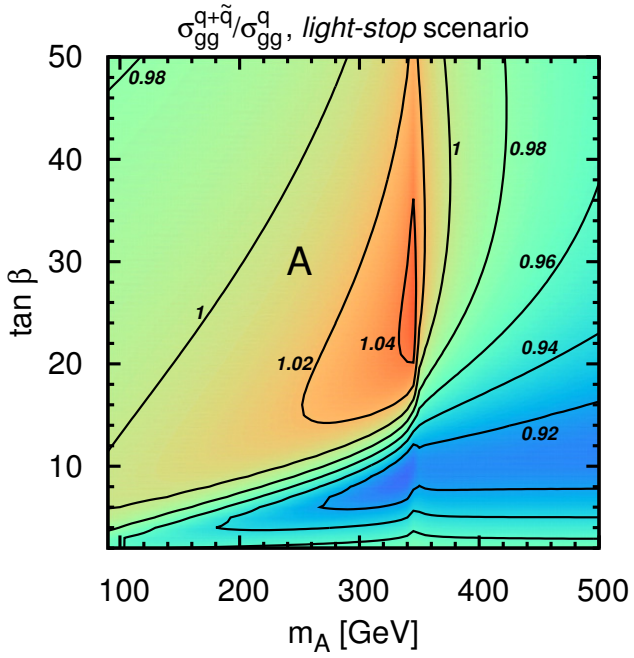

Figure 6: Same as figure 5 for the production of the pseudoscalar A.

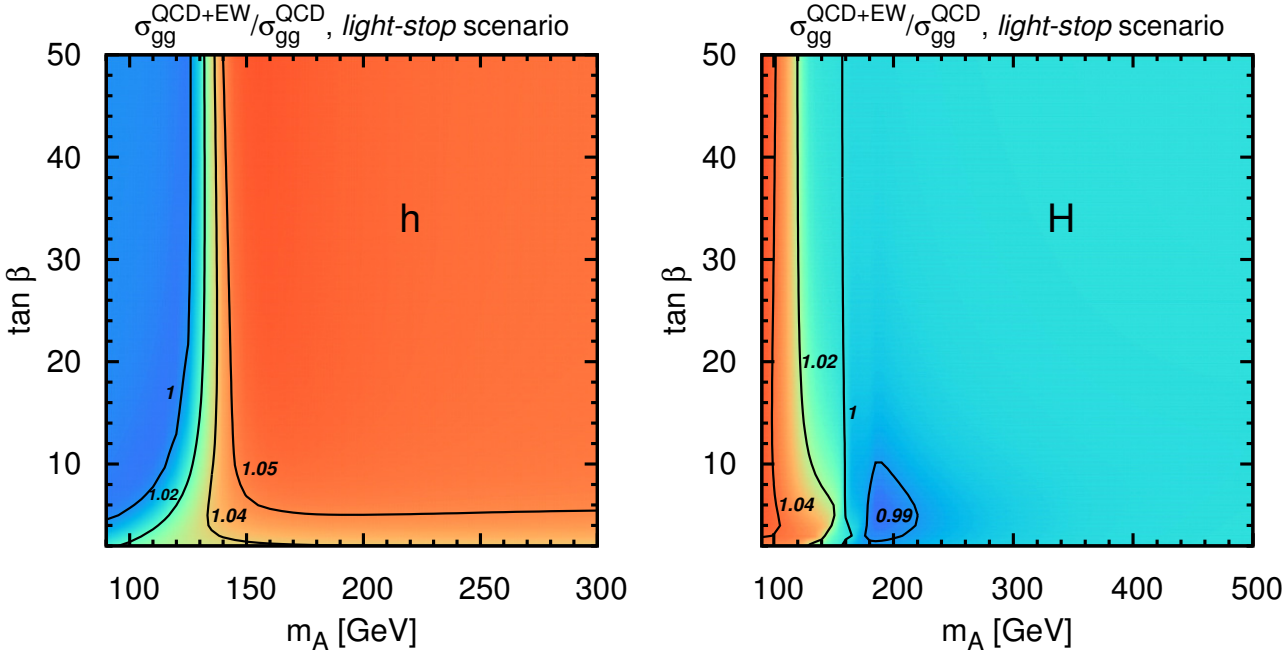

Figure 7: Ratio of gluon-fusion cross section for the production of h (left) and H (right) over the corresponding cross section neglecting EW contributions, as a function of m_A and $\tan\beta$ in the *light-stop* scenario.

suppressed by m_b^2/m_H^2 and only moderately enhanced by $\tan\beta$, so they both become comparable in size with the stop contribution. The resulting gluon-fusion cross section is rather small, of the order of a few femtobarns. Finally, figure 6 shows that, in the case of A production, the effect of the squark contributions on the cross section for gluon fusion in the *light-stop* scenario is always less than 10%. This is due to the fact that the pseudoscalar couples only to two different squark-mass eigenstates, while gluons couple only to pairs of the same squarks. Therefore, there is no squark contribution to the gluon-fusion process at the LO, and the whole effect in figure 6 arises from two-loop diagrams.

For a SM Higgs boson sufficiently lighter than the top threshold, the EW corrections to gluon fusion are well approximated [20, 21] by the contributions of two-loop diagrams in which the Higgs couples to EW gauge bosons, which in turn couple to the gluons via a loop of light quarks (including the bottom). In `SusHi`, these contributions are incorporated in the MSSM calculation of the gluon-fusion cross section by rescaling the two-loop EW amplitude given in ref. [21] with the appropriate Higgs-gauge boson couplings.[5] In figure 7 we investigate the impact of the light-quark EW contributions on the production of the scalars h and H, plotting the ratio of the gluon-fusion cross sections computed with and without those contributions, in the m_A–$\tan\beta$ plane for the *light-stop* scenario. The figure

[5] In fact, `SusHi` implements two alternative procedures for including the EW contributions in the total cross section for gluon fusion. We follow the one described in eq. (37) of the code's manual [53].

shows that the EW corrections tend to increase the cross section, and their impact depends mainly on the strength of the coupling of the considered scalar to gauge bosons. In the case of h production (left plot) the EW corrections become fairly constant, around 6%, in the region of sufficiently large m_A where the lightest scalar has SM-like couplings. Conversely, in the case of H production (right plot) the EW corrections reach a comparable value only in the strip of very low m_A, and they quickly drop below 1% as soon as $m_A \gtrsim 150$ GeV. On the other hand, since the pseudoscalar does not couple to two gauge bosons at tree level, there are no EW contributions from light-quark loops to its production.

For what concerns the remaining sources of EW corrections to gluon fusion, those arising from two-loop diagrams involving top quarks are known to be small for a SM-like Higgs with mass around 125 GeV [20], while in the case of H and A they are suppressed in most of the parameter space by the small (or vanishing) Higgs couplings to top quarks and to gauge bosons. On the other hand, the EW corrections involving the bottom Yukawa coupling, which have not yet been computed because they are negligible for the SM Higgs, could become relevant for the production of H and A. In addition, a full computation of the EW corrections should include the contributions of diagrams involving superparticles. The non-decoupling SUSY effects that dominate at large $\tan\beta$ are indeed included in an effective Higgs-bottom coupling, as discussed in section 3.2.2, but the remaining contributions, so far uncomputed, could become relevant if some of the superparticles are relatively light.

Results for the Higgs-production cross section in the other benchmark scenarios listed in table 1 can be found in the appendix. In the four scenarios denoted as m_h^{max}, $m_h^{\text{mod+}}$, $m_h^{\text{mod}-}$ and *light stau*, the couplings of the Higgs bosons to top and bottom quarks and to gauge bosons are rather similar to the ones in the *light-stop* scenario. Thus, the discussion given above for the qualitative behavior in the m_A–$\tan\beta$ plane of the total cross section, of the EW corrections and of the relative importance of gluon fusion and bottom-quark annihilation applies to those four scenarios as well. However, all of the third-generation squarks have masses around 1 TeV, therefore the impact of the SUSY contributions on the gluon-fusion cross section is considerably smaller than in the case of the *light-stop* scenario. The suppression of the cross section for h production in the decoupling limit never goes beyond 6%. For what concerns H production, the effect of the interference between quark and squark contributions becomes significant only for very large m_A and moderate $\tan\beta$, where the gluon-fusion cross section is tiny anyway. The largest effect, a suppression by 30 – 40%, is found in the *light-stau* scenario for $m_A \gtrsim 850$ GeV and $10 \lesssim \tan\beta \lesssim 20$, where the cross section is of the order of a tenth of a femtobarn. The SUSY contributions to A production, already small in the *light-stop* scenario because they only arise at two loops, are further suppressed in the m_h^{max}, $m_h^{\text{mod+}}$, $m_h^{\text{mod}-}$ and *light-stau* scenarios.

In the last scenario in table 1, denoted as *tau-phobic*, the MSSM parameters are arranged in such a way that, for certain values of m_A and $\tan\beta$, the radiative corrections to the $(1,2)$ element of the CP-even Higgs mass matrix suppress significantly the mixing angle α, so that the coupling of h to taus – which is proportional to $\sin\alpha$ – is in turn suppressed with respect to its SM value. However, the couplings of the scalars to top and bottom quarks are modified as well, in particular the coupling of h to bottom quarks is suppressed. As a result, in the *tau-phobic* scenario the behavior in the

m_A–$\tan\beta$ plane of the various contributions to the Higgs-production cross section differs from the one found in the other scenarios. The total cross section for h production shows some enhancement with $\tan\beta$ even for large values of m_A, while for small m_A the total cross section for H production has a milder dependence on $\tan\beta$ than in the other scenarios. Also, the suppression of the h coupling to bottom quarks makes the contribution of bottom-quark annihilation to h production smaller than in the other scenarios. Finally, the *tau-phobic* scenario is characterized by third-generation squark masses around 1.5 TeV, and by a value of the superpotential Higgs-mass parameter, $\mu = 2$ TeV, much larger than in the other scenarios. Since μ enters the couplings of the Higgs bosons to squarks, the impact of the SUSY contributions on the cross section for scalar production is – despite the heavier squarks – somewhat larger than in the $m_h^{\rm max}$, $m_h^{\rm mod+}$, $m_h^{\rm mod-}$ and *light-stau* scenarios, and in the case of pseudoscalar production it is even larger than in the *light-stop* scenario.

3 Sources of theoretical uncertainty

Like any other quantity evaluated perturbatively, the cross sections for Higgs production in gluon fusion and bottom-quark annihilation suffer from an intrinsic theoretical uncertainty due to the truncation at finite order in the coupling constants. Typically, the residual dependence on the renormalization and factorization scales is used as an estimate of this uncertainty. In section 3.1 we discuss our study of the scale dependence of the cross sections.

In addition, there are sources of uncertainty that are more specific to the Higgs-production processes considered in this paper. As we discuss in section 3.2, one of the most important sources of uncertainty in the production of Higgs bosons with non-standard couplings to quarks is the dependence of the cross section on the precise definition of the bottom-quark mass and Yukawa coupling. The numerical difference between the pole bottom mass and the running mass computed at a scale of the order of the Higgs mass is more than 40%, and – in a fixed-order calculation of the cross sections – the effect of such a large variation cannot be compensated by the large logarithms that are induced at NLO by counterterm contributions. Furthermore, it is well known that the relation between the bottom mass and the corresponding Yukawa coupling is affected by potentially large, $\tan\beta$-enhanced SUSY corrections that must be properly resummed. The dependence of the cross sections on the details of the resummation procedure constitutes a further source of uncertainty.

In section 3.3 we discuss the uncertainties associated to the choice of PDF sets. We also investigate the issue of consistency between the pre-defined value of the bottom mass in the PDFs and the value of the mass used to extract the bottom Yukawa coupling.

Finally, in section 3.4 we discuss two sources of uncertainty arising from our incomplete knowledge of the SUSY contributions to gluon fusion. In particular, we assess the validity of the expansion in inverse powers of the SUSY masses used to approximate the contributions of two-loop diagrams involving superparticles. We also estimate the uncertainty associated to the fact that `SusHi` does not include the contributions of three-loop diagrams involving superparticles.

3.1 Scale dependence of the cross section

In this section we study the dependence of the cross section for Higgs production on the renormalization scale μ_R at which the relevant couplings in the partonic cross section are expressed, and on the factorization scale μ_F entering both the PDFs and the partonic cross section. We recall that, although the complete result for the hadronic cross section does not depend on μ_R and μ_F, its approximation at a given perturbative order retains a dependence on those scales, which is formally one order higher than the accuracy of the calculation. In a given calculation at fixed order, the two scales are arbitrary, and they are typically fixed at some central values $\bar{\mu}_R$ and $\bar{\mu}_F$ characteristic of the hard scattering process. The variation of the scales around their central values provides an estimate of the size of the uncomputed higher-order contributions.

We discuss separately the cases of gluon fusion (section 3.1.1) and of bottom-quark annihilation (section 3.1.2). In the former, μ_R denotes the scale at which we express the strong gauge coupling entering the partonic cross section already at the LO, while in the latter it denotes the scale at which we express both the bottom Yukawa coupling entering at the LO and the strong gauge coupling entering at the NLO. We postpone to section 3.2 a discussion of the dependence of the gluon-fusion cross section on the scale at which we express the bottom Yukawa coupling.

3.1.1 Gluon fusion

The natural hard scale in the production of a Higgs boson ϕ is obviously of the order of m_ϕ. In our study of gluon fusion we take $\bar{\mu}_R = \bar{\mu}_F = m_\phi/2$ as central values for the renormalization and factorization scales, because, with this choice, the cross section shows a reduced sensitivity to scale variations and an improved convergence of the perturbative expansion [13]. Moreover, it has been observed that this choice allows to mimic the effects of soft-gluon resummation in the total cross section [84].

We study the impact of the scale variation around the central choice $(\bar{\mu}_R, \bar{\mu}_F)$ following the LHC-HXSWG prescription [3]: we consider seven combinations of renormalization and factorization scales, defined as the set C_μ of the pairs (μ_R, μ_F) obtainable from the two sets $\mu_R = \{m_\phi/4,\, m_\phi/2,\, m_\phi\}$ and $\mu_F = \{m_\phi/4,\, m_\phi/2,\, m_\phi\}$, with the additional constraint that $1/2 \leq \mu_R/\mu_F \leq 2$ (i.e., we treat the variations of the ratio μ_R/μ_F on the same footing as the variations of the individual scales, discarding the two pairs where the ratio varies by a factor of four around its central value). We then determine the maximal and minimal values of the cross section on the set C_μ,

$$\sigma^- \equiv \min_{(\mu_R,\,\mu_F)\,\in\, C_\mu} \{\sigma(\mu_R,\mu_F)\}\ , \qquad \sigma^+ \equiv \max_{(\mu_R,\,\mu_F)\,\in\, C_\mu} \{\sigma(\mu_R,\mu_F)\}\ , \tag{2}$$

and define the relative scale uncertainty of the cross section as $\Delta_\mu \equiv \Delta_\mu^+ - \Delta_\mu^-$, where

$$\Delta_\mu^+ \equiv \frac{\sigma^+ - \sigma(\bar{\mu}_R,\bar{\mu}_F)}{\sigma(\bar{\mu}_R,\bar{\mu}_F)}\ , \qquad \Delta_\mu^- \equiv \frac{\sigma^- - \sigma(\bar{\mu}_R,\bar{\mu}_F)}{\sigma(\bar{\mu}_R,\bar{\mu}_F)}\ . \tag{3}$$

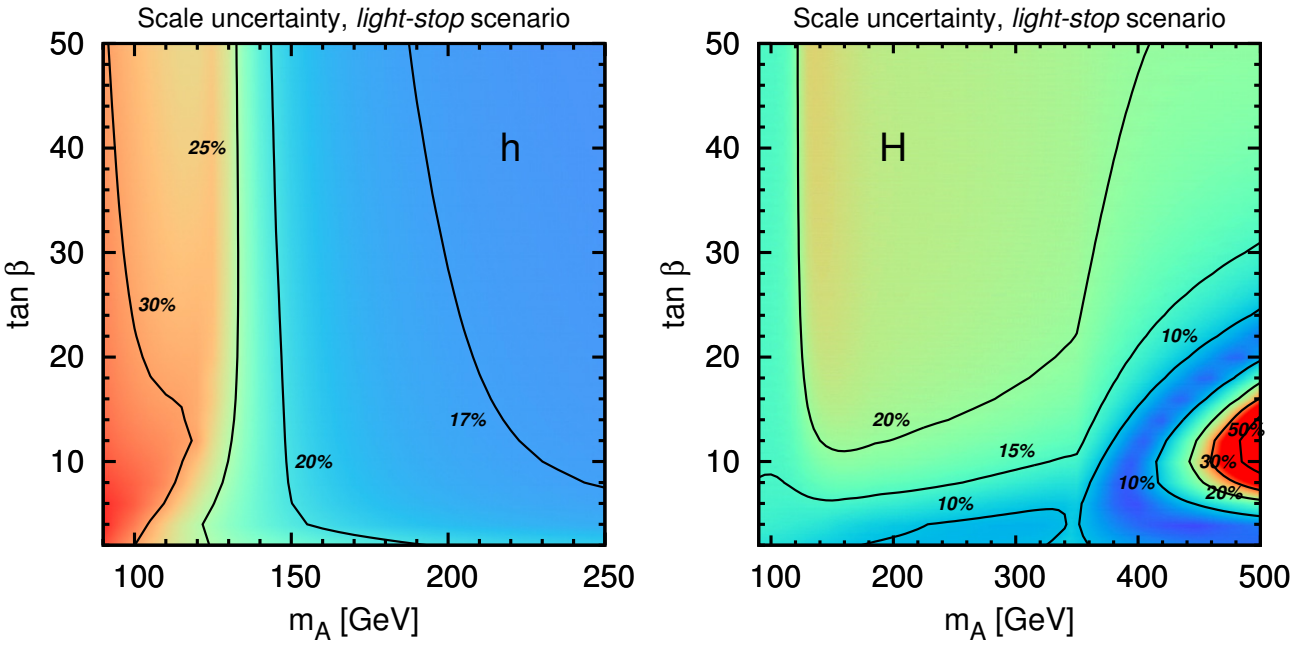

Figure 8: Relative scale uncertainty Δ_μ (in percent) for h production (left) and H production (right) in gluon fusion in the *light-stop* scenario.

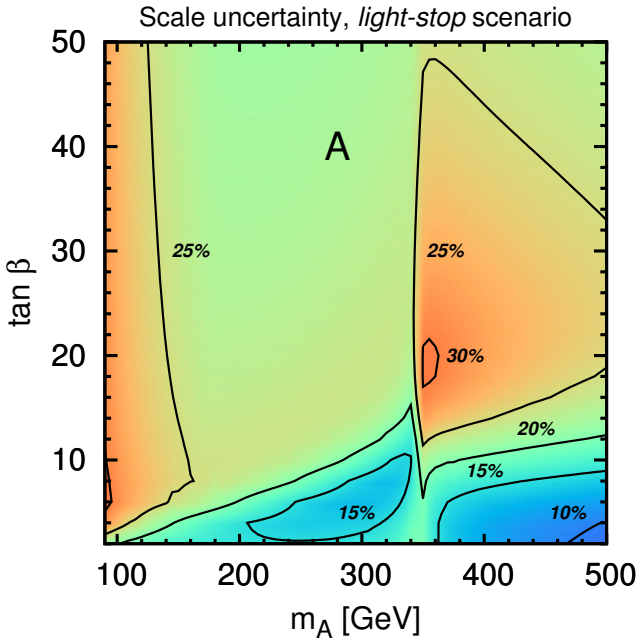

Figure 9: Same as figure 8 for the production of the pseudoscalar A.

In figures 8 and 9 we show the contours of equal Δ_μ for scalar and pseudoscalar production in the m_A–$\tan\beta$ plane, fixing the MSSM parameters as in the *light-stop* scenario. The qualitative features of the plots can be understood by considering that the top, bottom, SUSY and EW contributions to the gluon-fusion cross section are known at different orders in the perturbative expansion. In particular, the top contribution is included in `SusHi` with full mass dependence through $\mathcal{O}(\alpha_s^3)$ (i.e., NLO) and in the VHML at $\mathcal{O}(\alpha_s^4)$ (i.e, NNLO). Its residual scale dependence amounts to an $\mathcal{O}(\alpha_s^5)$ effect, with the exception of some mass-dependent effects at $\mathcal{O}(\alpha_s^4)$, which are known to be numerically small [14]. The bottom and sbottom contributions are included at the NLO and they account for an $\mathcal{O}(\alpha_s^4)$ effect. The stop contributions are included through the NNLO, see section 3.4, but their effect on scale dependence is also of $\mathcal{O}(\alpha_s^4)$ because we neglect the genuine three-loop terms. Finally, while the EW corrections are computed at $\mathcal{O}(\alpha\alpha_s^2)$, their inclusion as a fully factorized term at the NLO causes their effect on scale variation to be of $\mathcal{O}(\alpha\alpha_s^4)$, numerically very small. As a consequence of the varying accuracy of the different contributions, the scale uncertainty for the production of a given Higgs boson depends on which contribution plays the dominant role in the considered region of the m_A–$\tan\beta$ plane. The uncertainty is lowest, around $10-20\%$, where the top contribution dominates: this is the case for h production (left plot in figure 8) in the decoupling region, where the uncertainty stabilizes to roughly 16% at large m_A (i.e., slightly smaller than the 18% we obtain for the same Higgs mass in the SM); for H production (right plot in figure 8) in the strip with $m_A \lesssim 120$ GeV, as well as when $\tan\beta \lesssim 10$ and $m_A \lesssim 400$ GeV; for A production (figure 9) in the strip with $\tan\beta \lesssim 10$. In contrast, the scale uncertainty exceeds 20% in the regions where the bottom contribution is enhanced or downright dominant: at large $\tan\beta$ for H and A production, and at small m_A for h production.

The plots for H and A production in figures 8 and 9 show additional structures. In the case of H production, the scale uncertainty becomes very large for $8 \lesssim \tan\beta \lesssim 16$ and $m_A \gtrsim 460$ GeV. As appears from figure 5, this region is characterized by a significant cancellation between the top, bottom and stop contributions to the gluon-fusion amplitude, resulting in a very small NLO cross section and an enhanced sensitivity to higher-order effects. In the case of A production, the structure visible for $m_A \approx 350$ GeV is associated to the cusp-like behavior of the top contribution to the gluon-fusion amplitude around the threshold $m_A = 2\,m_t$. Another feature of H and A production, partially overshadowed by the structures described above, is a tendency towards smaller scale uncertainties for larger pseudoscalar (and hence scalar) masses. This is due to the fact that the strong gauge coupling – which controls the size of the higher-order effects that we are estimating – is evaluated at a scale proportional to the mass of the considered Higgs boson, and gets smaller when the scale increases.

The other scenarios were studied following the same procedure, and the results are qualitatively similar. For h production, the scale dependence in the decoupling region is similar to, or even bigger than, the one in the SM. For H production, due to the different interplay of quark and squark contributions, the cancellations that in the *light-stop* scenario cause the region of very large uncertainty for $8 \lesssim \tan\beta \lesssim 16$ and $m_A \gtrsim 460$ GeV occur at higher values of m_A.

Finally, a study of independent variations of the renormalization and factorization scales shows

that, in a large fraction of the parameter space, the former yield a much larger uncertainty than the latter. The factorization-scale uncertainty is smaller in size than the renormalization-scale uncertainty already at the LO, and it is further reduced by the inclusion of higher-order terms.

3.1.2 Bottom-quark annihilation

In `SusHi`, the cross section for Higgs production in bottom-quark annihilation is implemented at NNLO-QCD in the 5FS. Our default choice for the central scales is $\bar{\mu}_R = m_\phi$ and $\bar{\mu}_F = m_\phi/4$, following the observation that radiative corrections are particularly small for this value of the factorization scale [43, 44, 85]. To study the uncertainty associated to the variation of the scales, we consider seven combinations corresponding to all possible pairings of $\mu_R = \{m_\phi/2, m_\phi, 2\,m_\phi\}$ and $\mu_F = \{m_\phi/8, m_\phi/4, m_\phi/2\}$, with the additional constraint that $2 \leq \mu_R/\mu_F \leq 8$ (again, we discard the two pairs with the largest variation of μ_R/μ_F around its central value, which in this case is 4). We then determine the scale uncertainty Δ_μ in analogy to eqs. (2) and (3).

Differently from the case of gluon fusion, the scale uncertainty of bottom-quark annihilation depends very weakly on $\tan\beta$. This is due to the fact that, in eq. (3), the $\tan\beta$-dependence of the cross section via the effective Higgs-bottom coupling cancels out in the ratio, leaving only a mild, indirect dependence – only for scalar production – via the value of the Higgs mass that determines μ_R and μ_F.

In figures 10 and 11 we show the scale dependence of the cross section for scalar and pseudoscalar production, respectively, as a function of m_A in the *light-stop* scenario with $\tan\beta = 20$. In the upper part of each plot, the solid line denotes the cross section for bottom-quark annihilation computed with the central scale choice $(\bar{\mu}_R, \bar{\mu}_F)$, while the yellow band around the solid line is delimited by the maximal and minimal cross sections σ^+ and σ^-, defined in analogy to eq. (2). The lower part of each plot shows the relative variation of the cross section with respect to the central value (i.e., the total width of the yellow band corresponds to Δ_μ). While the values of the total cross section do of course depend on the chosen benchmark scenario, the relative scale variation is essentially the same in all scenarios, due to the above-mentioned cancellation of the dependence on the effective Higgs-bottom coupling.

The left plot in figure 10 shows that the relative scale uncertainty of the cross section for h production can be as large as 30% for low values of m_A, then it stabilizes to roughly 18% in the decoupling region where m_h becomes independent of m_A. In contrast, the relative scale uncertainty of the cross section for the production of H (right plot in figure 10) and A (figure 11) decreases as m_A (and hence m_H) increases. As already mentioned for the case of gluon fusion, this behavior is due to the fact that the higher-order effects that we are estimating are controlled by the strong gauge coupling, and the latter decreases when the scale at which it is computed, which is proportional to the Higgs mass, increases.

Finally, an independent variation of the renormalization and factorization scales shows that, in this case, the dominant uncertainty is given by the dependence on the factorization scale.

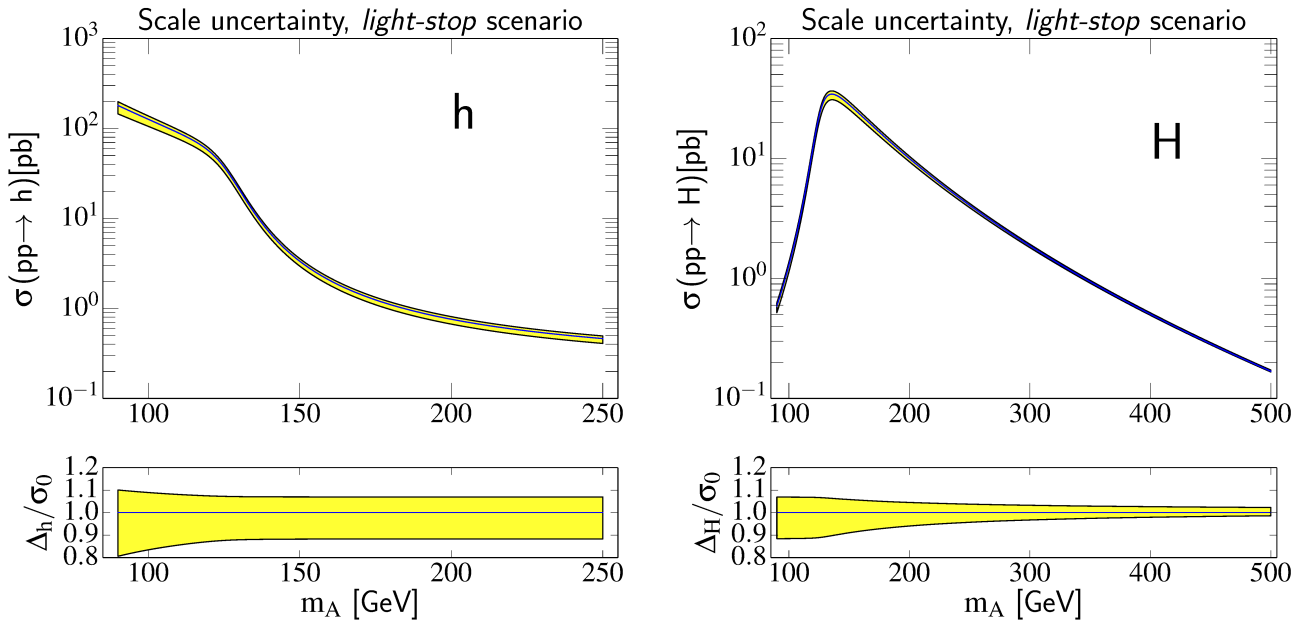

Figure 10: Scale uncertainty of the cross section for h production (left) and H production (right) in bottom-quark annihilation, in the *light-stop* scenario with $\tan\beta = 20$.

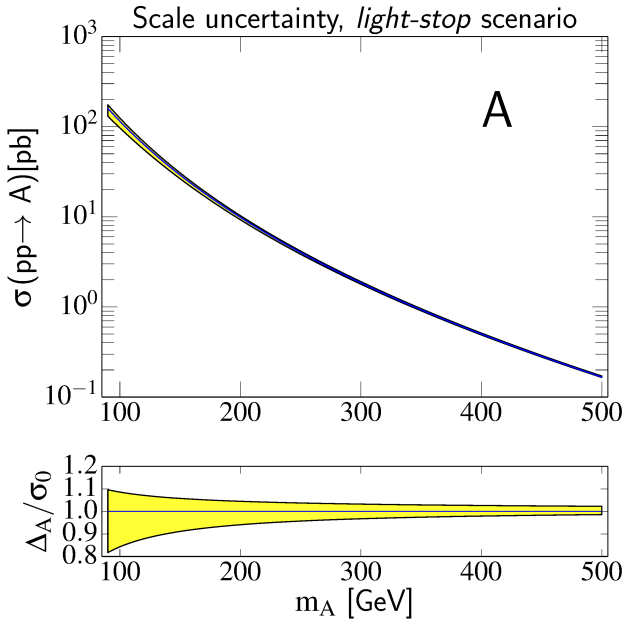

Figure 11: Same as figure 10 for the production of the pseudoscalar A.

3.2 Definition of the Higgs-bottom coupling

In the production of a SM-like Higgs boson, the contribution of bottom-quark annihilation and the effect of the bottom-quark loops in gluon fusion amount to a few percent of the total cross section. Therefore, in that case the theoretical uncertainty associated to the definition of the Higgs coupling to bottom quarks is negligible compared to other sources of uncertainty. On the other hand, this uncertainty becomes significant in scenarios where the Higgs-bottom coupling is enhanced with respect to its SM counterpart, $Y_b^{\rm SM} = \sqrt{2}\, m_b/v$ (here $v \approx 246$ GeV). In the MSSM the tree-level couplings of the neutral Higgs bosons to bottom quarks are modified as follows:

$$Y_b^h \;=\; -\,\frac{\sin\alpha}{\cos\beta}\; Y_b^{\rm SM}\;, \qquad Y_b^H \;=\; \frac{\cos\alpha}{\cos\beta}\; Y_b^{\rm SM}\;, \qquad Y_b^A \;=\; \tan\beta\; Y_b^{\rm SM}\;, \tag{4}$$

where α is the mixing angle in the CP-even Higgs sector. In the decoupling limit, $m_A \gg m_Z$, the mixing angle simplifies to $\alpha \approx \beta - \pi/2$, so that the coupling of h to bottom quarks is SM-like, while the couplings of H and A are both enhanced by $\tan\beta$.

In this section we discuss two issues that affect the precise definition of the Higgs-bottom couplings: the first concerns the choice of renormalization scheme – and scale – for the bottom mass from which the couplings are extracted; the second concerns higher-order effects in the procedure through which the $\tan\beta$-enhanced SUSY contributions are resummed in effective Higgs-bottom couplings.

3.2.1 Scheme and scale dependence of the bottom mass

The parameter m_b enters the expression for the gluon-fusion amplitude with two distinct roles: as the actual mass of the bottom quarks running in the loops, and as a proxy for the Higgs-bottom coupling Y_b^ϕ, where $\phi = \{h, H, A\}$. The numerical value of m_b depends strongly on the renormalization scheme and scale: an $\overline{\rm MS}$ mass $m_b(m_b) = 4.16$ GeV corresponds to a pole mass $M_b = 4.92$ GeV at three-loop level, whereas evolving $m_b(m_b)$ up to a scale of the order of the typical energy of the gluon-fusion process decreases significantly its value. For example, if we evolve at four-loop level the bottom mass up to the scale at which we express the strong gauge coupling, $\mu_R = m_\phi/2$, we obtain $m_b(m_\phi/2) = 2.93$ GeV for $m_\phi = 125$ GeV. While any change in the definition of the bottom mass and Yukawa coupling entering the one-loop part of the amplitude is formally compensated for, up to higher orders, by counterterm contributions in the two-loop part, the numerical impact of such strong variations on the prediction for the gluon-fusion cross section can be significant.

To illustrate this point, we identify the mass of the bottom quarks in the loops with the pole mass M_b, and consider the dependence of the gluon-fusion cross section on the prescription for the Higgs-bottom coupling Y_b^ϕ, focusing on $\phi = \{h, H\}$. In the *light-stop* scenario with $m_A = 130$ GeV and $\tan\beta = 40$, where both Higgs scalars are relatively light and have enhanced couplings to the bottom quark, the effect of extracting Y_b^ϕ from the $\overline{\rm MS}$ mass $m_b(m_b)$ instead of the pole mass M_b leads to a 17% decrease in the cross section for h production, and a 24% decrease in the cross section for H production. The use of $m_b(m_\phi/2)$ would instead decrease the cross section for h production by 34%,

and the one for H production by 51%, with respect to the values obtained with M_b. As a second example, we take the *light-stop* scenario with $m_A = 300$ GeV and $\tan\beta = 10$, where the lightest scalar h has SM-like couplings to quarks. In this case the cross section for h production varies by less than 2% when choosing among the three options discussed above for the definition of Y_b^h. For the heaviest scalar H, on the other hand, the changes in the cross section relative to the value derived with M_b amount to -22% and -50% when Y_b^H is extracted from $m_b(m_b)$ and $m_b(m_H/2)$, respectively.

The strong sensitivity of the production of non-standard Higgs bosons on the choice of renormalization scheme (and scale) for the bottom mass and Yukawa coupling has been discussed in the past, see e.g. refs. [8, 49, 88]. However, unlike many other processes for which there are theoretical arguments in favor of one or the other choice, for Higgs production in gluon fusion we are not aware of any such arguments that go beyond heuristic. As was already noted in ref. [8], the options of relating Y_b^ϕ to M_b or to $m_b(m_b)$ might seem preferable to the one of using $m_b(m_\phi/2)$, in that they lead to smaller two-loop contributions. If in the one-loop part of the amplitude for scalar production we identify the mass of the bottom quark with M_b and the bottom Yukawa coupling with $m_b(\mu_b)$, where μ_b is a generic renormalization scale, the contribution of diagrams with bottom quarks and gluons to the two-loop part of the amplitude reads

$$\mathcal{A}_b^{2\ell}(\tau) \;\propto\; C_F\left[\mathcal{F}_{C_F}(\tau) + \mathcal{F}_{1/2}^{1\ell}(\tau)\left(1 - \frac{3}{4}\ln\frac{m_b^2}{\mu_b^2}\right)\right] + C_A\,\mathcal{F}_{C_A}(\tau)\;, \tag{5}$$

where $C_F = 4/3$ and $C_A = 3$ are color factors, $\tau = 4\,m_b^2/m_\phi^2$, and we omit an overall multiplicative factor. Truncating the functions at the first order in an expansion in powers of τ, one finds [11]

$$\mathcal{F}_{1/2}^{1\ell}(\tau) = -2\,\tau\left(1 - \frac{1}{4}\,L_{b\phi}^2\right) + \mathcal{O}(\tau^2)\;, \tag{6}$$

$$\mathcal{F}_{C_F}(\tau) = -\tau\left[5 + \frac{9}{5}\,\zeta_2^2 - \zeta_3 - (3 + \zeta_2 + 4\,\zeta_3)\,L_{b\phi} + \zeta_2\,L_{b\phi}^2 + \frac{1}{4}\,L_{b\phi}^3 + \frac{1}{48}\,L_{b\phi}^4\right] + \mathcal{O}(\tau^2)\;, \tag{7}$$

$$\mathcal{F}_{C_A}(\tau) = -\tau\left[3 - \frac{8}{5}\,\zeta_2^2 - 3\,\zeta_3 + 3\,\zeta_3\,L_{b\phi} - \frac{1}{4}(1 + 2\,\zeta_2)\,L_{b\phi}^2 - \frac{1}{48}\,L_{b\phi}^4\right] + \mathcal{O}(\tau^2)\;, \tag{8}$$

with

$$L_{b\phi} \;\equiv\; \ln(-4/\tau) \;=\; \ln(m_\phi^2/m_b^2) - i\,\pi\;. \tag{9}$$

The equations above show that the two-loop bottom contribution to the gluon-fusion amplitude contains powers of $\ln(m_\phi^2/m_b^2)$, and that the choice $\mu_b = m_b$ does eliminate some of the logarithmically enhanced terms. Similarly, relating the coupling entering the one-loop part of the amplitude to the pole mass M_b eliminates the whole piece proportional to $\mathcal{F}_{1/2}^{1\ell}(\tau)$ in eq. (5). Each of the two remaining terms, $C_F\,\mathcal{F}_{C_F}(\tau)$ and $C_A\,\mathcal{F}_{C_A}(\tau)$, also contains powers of $\ln(m_\phi^2/m_b^2)$, but for realistic values of m_ϕ the two terms largely cancel out against each other, resulting in a small two-loop contribution from bottom quarks. However, such cancellation should be considered accidental: there is no argument suggesting that it persists at higher orders in QCD, or that it is motivated by some physical property of the bottom contribution to gluon fusion. To illustrate this point, we can consider the case of Higgs

decay to two photons: the one-loop bottom contribution to the amplitude has the same structure as the corresponding contribution to gluon fusion, but the two-loop bottom-gluon contribution is obtained from eq. (5) by dropping the term proportional to C_A, which originates from diagrams with three- and four-gluon interactions. In that case no significant cancellation occurs, and the amplitude is not minimized when Y_b^ϕ is extracted from $m_b(m_b)$ or M_b. In fact, it was also noted in ref. [8] that the two-loop bottom-gluon contribution to the amplitude for Higgs decay to photons is minimized when the one-loop contribution is fully expressed in terms of $m_b(m_\phi/2)$.

In the case of the Higgs coupling to photons, the problems related to the ambiguity in the definition of Y_b^ϕ have been solved with a resummation of the leading and next-to-leading logarithms of the ratio m_ϕ^2/m_b^2 [89]. Until a similar calculation is performed for the Higgs coupling to gluons, there is no obvious reason to favor one choice of renormalization scheme (and scale) for the bottom Yukawa coupling over the others. In our study we choose to relate the coupling to the pole mass M_b, and we consider the difference between the results obtained using M_b and those obtained using $m_b(m_\phi/2)$ as a measure of the uncertainty associated with the uncomputed higher-order QCD corrections. For the production of a SM-like Higgs with mass around 125.5 GeV, this procedure – also advocated by the LHC-HXSWG in ref. [3] – results in an uncertainty of $1-2\%$ in the gluon-fusion cross section. On the other hand, as we show in figures 12 and 13 for scalar and pseudoscalar production in the *light-stop* scenario, the cross section could be reduced by more than 60% in the regions of the m_A–$\tan\beta$ plane where the gluon-fusion process is dominated by the bottom-quark contribution. It is however worth recalling that, as shown in figures 3 and 4, in such regions the total cross section for Higgs production is dominated by bottom-quark annihilation. In the 5FS, the cross section for the latter process is known at the NNLO in QCD [43, 44], and it is free of large logarithms of the ratio m_ϕ^2/m_b^2 when Y_b^ϕ is related to $m_b(m_\phi)$. The theoretical uncertainty of the cross section for bottom-quark annihilation associated to reasonable variations around this scale choice is already included in the uncertainty bands shown in figures 10 and 11 in the previous section.

3.2.2 Resummation of $\tan\beta$-enhanced corrections

It is well known that, in the MSSM, loop diagrams involving superparticles induce $\tan\beta$-enhanced corrections to the couplings of the Higgs bosons to bottom quarks [90]. If all superparticles are considerably heavier than the Higgs bosons they can be integrated out of the MSSM Lagrangian, leaving behind a two-Higgs-doublet model with effective Higgs-bottom couplings

$$\widetilde{Y}_b^{\,h} \;=\; \frac{Y_b^h}{1+\Delta_b}\left(1-\Delta_b\,\frac{\cot\alpha}{\tan\beta}\right), \quad \widetilde{Y}_b^{\,H} \;=\; \frac{Y_b^H}{1+\Delta_b}\left(1+\Delta_b\,\frac{\tan\alpha}{\tan\beta}\right), \quad \widetilde{Y}_b^{\,A} \;=\; \frac{Y_b^A}{1+\Delta_b}\left(1-\Delta_b\,\cot^2\beta\right), \tag{10}$$

where Y_b^ϕ are the tree-level Higgs-bottom couplings defined in eq. (4), and, retaining only the $\mathcal{O}(\alpha_s)$ contribution from diagrams with sbottoms and gluinos, the $\tan\beta$-enhanced term Δ_b reads

$$\Delta_b \;=\; \frac{2\,\alpha_s}{3\,\pi}\;\frac{m_{\tilde g}\,\mu\,\tan\beta}{m^2_{\tilde b_1}-m^2_{\tilde b_2}}\left(\frac{m^2_{\tilde b_1}}{m^2_{\tilde b_1}-m^2_{\tilde g}}\ln\frac{m^2_{\tilde b_1}}{m^2_{\tilde g}}-\frac{m^2_{\tilde b_2}}{m^2_{\tilde b_2}-m^2_{\tilde g}}\ln\frac{m^2_{\tilde b_2}}{m^2_{\tilde g}}\right). \tag{11}$$

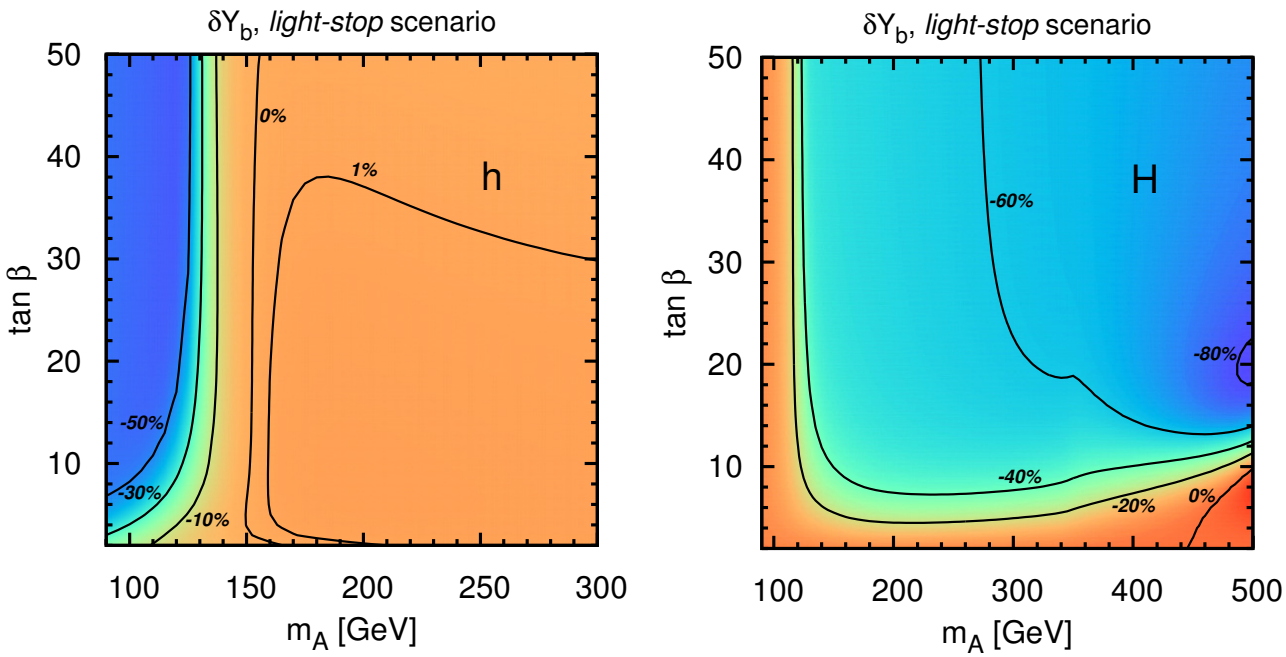

Figure 12: Variation (in percent) of the gluon-fusion cross section for the production of h (left) and H (right) when the Higgs-bottom coupling Y_b^ϕ is extracted from $m_b(m_\phi/2)$ instead of M_b, as a function of m_A and $\tan\beta$ in the *light-stop* scenario.

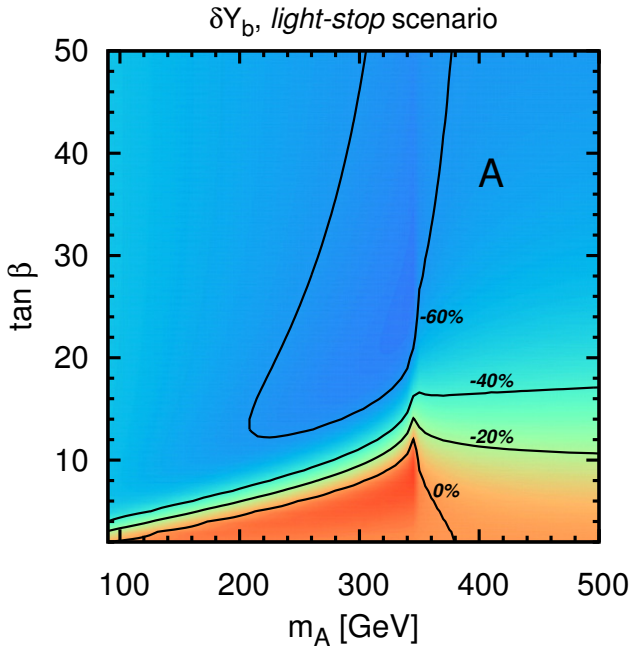

Figure 13: Same as figure 12 for the production of the pseudoscalar A.

In the limit $m_A \gg m_Z$, where $\cot\alpha \approx -\tan\beta$, the superparticle contributions encoded in Δ_b decouple from the coupling of the lightest scalar, while the couplings of the heaviest scalar and of the pseudoscalar are both rescaled by a factor $(1-\Delta_b \cot^2\beta)/(1+\Delta_b)$.

In refs. [39, 40] it was shown that, in the calculation of processes that involve the Higgs-bottom couplings, the $\tan\beta$-enhanced corrections can be resummed to all orders in the expansion in powers of Δ_b by inserting the effective couplings of eq. (10) in the lowest-order amplitude for the considered process. In the case of gluon fusion, this amounts to using $\widetilde{Y}_b^{\,\phi}$ in the bottom contribution to the one-loop part of the amplitude. However, when this resummation procedure is combined with the actual calculation of the superparticle contributions to the one- and two-loop amplitude for gluon fusion, care must be taken to avoid double counting. To this effect, we must subtract from the full result for the two-loop amplitude the contribution obtained by replacing $\widetilde{Y}_b^{\,\phi}$ in the resummed one-loop amplitude with the $\mathcal{O}(\Delta_b)$ term of the expansion of $\widetilde{Y}_b^{\,\phi}$ in powers of Δ_b. Depending on the choice of renormalization scheme for the parameters in the sbottom sector, additional $\tan\beta$-enhanced terms could be induced in the two-loop amplitude by the counterterm of the Higgs-sbottom coupling that enters the sbottom contribution to the one-loop amplitude. To avoid the occurrence of large two-loop corrections, which would put the validity of the perturbative expansion into question, we employ for the sbottom sector the OS renormalization scheme described in ref. [32].

An ambiguity in the procedure for the resummation of the Δ_b terms concerns the treatment of the Higgs-bottom couplings entering the two-loop part of the gluon-fusion amplitude. The difference between the results obtained using either Y_b^{ϕ} or $\widetilde{Y}_b^{\,\phi}$ in the two-loop part is formally of higher order, i.e., it amounts to three-loop terms that are suppressed by a factor $A_b/(\mu\tan\beta)$ with respect to the dominant three-loop terms of $\mathcal{O}(\Delta_b^2)$ accounted for by the resummation. Nevertheless, in our study we choose to identify the Higgs-bottom couplings in both the one- and two-loop parts of the amplitude with $\widetilde{Y}_b^{\,\phi}$. We found that this choice allows us to reproduce – after an expansion in powers of Δ_b – the three-loop result that can be inferred from ref. [40], where the sub-dominant terms proportional to A_b were also resummed in the effective couplings.

For large values of $\tan\beta$, the factor Δ_b can even become of order one, unless the superpotential parameter μ is suppressed with respect to the soft SUSY-breaking masses. The effect of the SUSY correction on the effective Higgs-bottom couplings depends crucially on the sign of Δ_b. For positive Δ_b the correction suppresses the couplings, reducing the overall relevance of the bottom contribution to gluon fusion. On the other hand, for negative Δ_b the correction enhances the couplings, which diverge as Δ_b approaches -1. As a consequence, when Δ_b is large and negative the result for the gluon-fusion cross section is extremely sensitive to the precise value of Δ_b, and a refined calculation of the latter becomes mandatory to reduce the uncertainty associated to the bottom contribution.

The first obvious step to improve the calculation of Δ_b consists in including other one-loop contributions that are not shown in eq. (11). In particular, the diagrams with stops and charginos induce a contribution, controlled by the top Yukawa coupling, that can be comparable in size with the $\mathcal{O}(\alpha_s)$ contribution in eq. (11). In our numerical analysis we use by default the full one-loop result for Δ_b as

computed by FeynHiggs, which allows us to resum in our prediction for the Higgs-production cross section also the $\tan\beta$-enhanced corrections of electroweak origin.

Another improvement in the calculation would come from the inclusion of the dominant two-loop contributions to Δ_b, which have been computed in ref. [41] but are not yet implemented in FeynHiggs. Indeed, it was shown in ref. [41] that the one-loop result for Δ_b is particularly sensitive to changes in the renormalization scales at which the strong-gauge and top-Yukawa couplings are expressed, and that the inclusion of the two-loop contributions stabilizes this scale dependence. In particular, both the one-loop sbottom-gluino and stop-chargino contributions to Δ_b vary by roughly $\pm 10\%$ when the renormalization scales are lowered or raised by a factor of two around their central values, which are chosen as the average of the masses of the relevant superparticles. We can therefore estimate the uncertainty of the gluon-fusion cross section associated to the one-loop computation of Δ_b by varying by $\pm 10\%$ the result provided by FeynHiggs.

In general, the impact of the uncertainty of Δ_b on the total uncertainty of the gluon-fusion cross section depends on the considered point in the MSSM parameter space. As was the case also for the scheme and scale dependence of Y_b^ϕ discussed in the previous section, the Δ_b uncertainty can be significant only if the bottom contribution to the cross section is substantially enhanced with respect to the SM case. For illustration, we consider again the *light-stop* scenario with $m_A = 130$ GeV and $\tan\beta = 40$, where both Higgs scalars have enhanced couplings to bottom quarks. The superpotential parameter μ has positive sign, and the Δ_b corrections suppress the effective couplings $\widetilde{Y}_b{}^\phi$. We find that the cross sections for h and H production in gluon fusion increase by 4% and 7%, respectively, if the value of Δ_b is reduced by 10%, while they decrease by 4% and 6%, respectively, if Δ_b is increased by 10%. The effect is larger if μ is taken negative, so that the Δ_b corrections enhance the effective couplings. In that case the dependence on Δ_b is reversed: if we consider the same point in the *light-stop* scenario but flip the sign of μ, the cross sections for h and H production in gluon fusion decrease by 17% and 16%, respectively, when $|\Delta_b|$ is reduced by 10%, while they increase by 23% and 21%, respectively, when $|\Delta_b|$ is increased by 10%.

Finally, we stress that a similar uncertainty affects the cross section for Higgs production via bottom-quark annihilation, where the tree-level amplitude is computed in terms of the effective couplings $\widetilde{Y}_b{}^\phi$. Also in this case, we can estimate the uncertainty by varying by $\pm 10\%$ the value of Δ_b provided by FeynHiggs.

3.3 Uncertainties from the PDFs and α_s

The prediction for the total cross section at hadron level is affected by our imperfect knowledge of the proton PDFs. This uncertainty has different sources: the PDFs cannot be computed from first principles but they rather have to be fitted from data, and the experimental error of the latter affects the outcome of the fit and propagates to the prediction of any observable. Also, the choices related to the fitting methodology and to the mathematical representation of the PDFs induce an ambiguity in the results, as can be appreciated by comparing the PDF parameterizations provided by three

collaborations that perform a global fit of low- and high-energy data: MSTW2008 [83], CT10 [91] and NNPDF2.3 [92]. These uncertainties will be discussed in section 3.3.1, together with the parametric dependence of the cross section on the value of the strong coupling constant. Another source of uncertainty is related to the available perturbative-QCD information on the scattering processes from which the PDFs are extracted. Among these perturbative effects, an issue that is particularly relevant in the case of Higgs production via bottom-quark annihilation is the consistent inclusion of the bottom-mass effects in the evolution of the PDFs according to the DGLAP equations. The transition between four and five active flavors in the proton occurs at a matching scale that is set equal to the bottom mass. The bottom density in the proton depends parametrically on this matching scale, which in turn affects the predictions for the cross section. The phenomenological implications of this issue will be discussed in detail in section 3.3.2. A systematic discussion of further sources of theoretical uncertainty – such as, e.g., the dependence of the PDFs on the choice of renormalization and factorization scale in the matrix elements that are used to perform the fit – is not yet available in the literature, and goes beyond the scope of this paper.

3.3.1 Combination of PDF and α_s uncertainties

The uncertainty associated to the experimental errors of the data from which the PDFs are extracted is represented by the PDF collaborations with the introduction of N_R different PDF sets (replicas), all equivalent from the statistical point of view in the description of the data. Any observable has to be computed N_R times with the different sets, and the spread of the results can be interpreted as the error induced by the PDF due to the data and to the fitting methodology. The replicas are determined by the PDF collaborations following the Hessian (for MSTW2008 and CT10) or the Monte Carlo (for NNPDF2.3) approaches, and the PDF error has to be computed accordingly. In QCD the cross sections are also affected by a parametric uncertainty associated to the input value of the strong coupling constant. This dependence is particularly relevant in the gluon-fusion cross section, which is proportional to α_s^2 at the LO and is subject to very large QCD corrections, of $\mathcal{O}(\alpha_s^3)$, at the NLO. Each PDF collaboration recommends a different central value for $\alpha_s(m_Z)$, generating a spread of the central predictions for the Higgs-production cross section. The combination of the PDF and α_s uncertainties (henceforth, PDF+α_s) and their correlation was first discussed in ref. [93]. A conservative approach to combine the different predictions obtained using the MSTW2008, CT10 and NNPDF2.3 PDF sets is known as PDF4LHC recipe, and it amounts to taking the envelope of the PDF+α_s uncertainty bands of the three collaborations, where for each group the preferred $\alpha_s(m_Z)$ central value is adopted [94]. Following this reference we take $\Delta\alpha_s = \pm 0.0012$ for the experimental error on the strong coupling constant.

Due to the very steep behavior of the PDFs for increasing values of the final-state invariant mass, the gluon-fusion process receives its dominant contribution from the threshold production region, with a very important role played by the virtual corrections and by the universal, factorizable, soft-gluon corrections. Consequently, the cross section is dominated by the LO-kinematics configurations also

at higher perturbative orders. At the LO, the gluon-fusion cross section depends on the rapidity of the Higgs boson only through the PDFs, therefore the relative size of the PDF+α_s uncertainty does not depend on the details of the partonic process, but only on the value of the Higgs-boson mass. As a consequence, the relative PDF+α_s uncertainty, for a given value of the Higgs mass, can be read directly from the tables of the SM predictions reported in the appendix B of the latest LHC-HXSWG report [5]. Differences with respect to the SM predictions may originate from hard, process-dependent radiative corrections, but their impact on the relative PDF+α_s uncertainty is at the sub-percent level.

To assess the PDF+α_s uncertainty of the cross section for Higgs production in bottom-quark annihilation we adopt again the PDF4LHC recipe. The bottom density in the proton does not have an intrinsic component, but it is generated dynamically, via gluon splittings, by the DGLAP evolution of the PDFs. Therefore, the uncertainties of the bottom and gluon PDFs are strongly correlated.

Similarly to the case of gluon fusion, for a given value of the Higgs mass the relative PDF+α_s uncertainty of the cross section for bottom-quark annihilation differs very little between the SM and the MSSM, because the radiative corrections involving SUSY particles affect the kinematics of the process only at higher orders.[6] We find that the uncertainty has an almost constant behavior when the mass m_ϕ of the produced Higgs boson is lighter than 300 GeV, and that it increases for larger mass values: for example, at the NNLO, the PDF+α_s uncertainty of the cross section for bottom-quark annihilation amounts to $\pm 6/6/8/21\%$ for $m_\phi = 124/300/500/1000$ GeV.

3.3.2 Bottom-mass dependence of the PDFs

The calculation of hadronic cross sections involves the convolution of the partonic cross sections with the PDFs, which have an intrinsic dependence on the bottom mass. For example, the central set of MSTW2008 [83], which we use as default for our analysis, assumes a pole mass $M_b = 4.75$ GeV. Converted to the $\overline{\rm MS}$ mass via a three-loop QCD calculation, this corresponds to $m_b(m_b) = 4.00$ GeV, which differs both from the value recommended by the LHC-HXSWG, $m_b(m_b) = 4.16$ GeV [57, 59], and from the current PDG value, $m_b(m_b) = 4.18$ GeV [95].

In addition to their dependence through the PDFs, the cross sections for Higgs production also depend on the bottom mass at the partonic level, i.e., through the bottom Yukawa coupling, the bottom-quark propagators and the phase space. In the regions of the MSSM parameter space where the bottom-quark contributions to Higgs production are enhanced, it becomes vital to evaluate the partonic cross sections with the correct input value for the bottom mass, which, as mentioned above, may not necessarily correspond to the value used in the PDFs. In this section we will examine the uncertainty that arises when we choose the bottom mass entering the partonic cross sections independently from the PDF set.

The MSTW2008 PDFs come in seven sets obtained with M_b ranging from 4 GeV to 5.5 GeV in steps of 0.25 GeV. In ref. [96] the MSTW collaboration studied the sensitivity of the PDFs on the

[6] In `SusHi` the SUSY corrections to bottom-quark annihilation enter only through the effective couplings $\widetilde{Y}_b^{\ \phi}$, therefore our estimate of the PDF+α_s uncertainty for a given Higgs mass is exactly the same in the SM and in the MSSM.

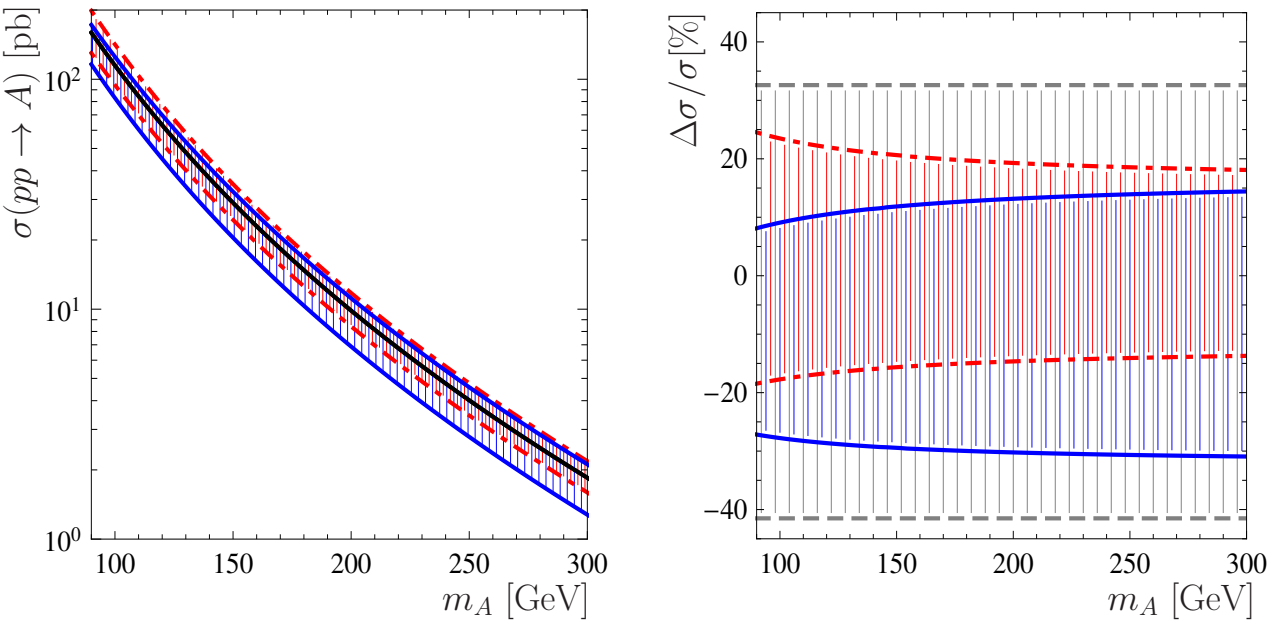

Figure 14: (Left) Cross section for pseudoscalar Higgs production in bottom-quark annihilation as a function of m_A for the *light-stop* scenario with $\tan\beta = 20$. (Right) Relative variation of the cross section for different choices of the pole bottom mass used in the PDFs and of the running mass used in the partonic cross section. Red: PDF variation, $\widetilde{Y}_b^{\,A}$ fixed; gray: PDF fixed, $\widetilde{Y}_b^{\,A}$ varies; blue: PDF and $\widetilde{Y}_b^{\,A}$ vary simultaneously.

value of the bottom mass, showing that the PDFs for the gluon and for the four lightest quarks are almost insensitive to M_b, whereas the bottom PDF exhibits quite a strong dependence. As shown in figure 6 of ref. [96], a variation by ± 0.5 GeV around the central value $M_b = 4.75$ GeV leads to changes in the bottom PDF that exceed the 90% C.L. uncertainty, even for the relatively large value of the factorization scale relevant to Higgs production, $\mu_F \approx 100$ GeV.

The cross section for Higgs production via gluon fusion is mostly sensitive to the gluon PDF, and receives only a small contribution, starting at the NLO, from diagrams with initial-state bottom quarks. As a result, when we evaluate the gluon-fusion cross section with the seven PDF sets – while fixing the bottom mass in the partonic cross section – we find that the result changes only at the per mil level, independently of the phenomenological scenario under consideration. We conclude that, for this process, the formal inconsistency of choosing different values for the bottom mass in the partonic cross section and in the PDFs induces only a negligible uncertainty.

In contrast, the hadronic cross section for Higgs production in bottom-quark annihilation, when computed in the 5FS, depends directly on the bottom PDF. As a result, we expect this process to show a significant dependence on the value of the bottom mass used in the PDFs, and the issue of consistency with the bottom mass used in the definition of the bottom Yukawa coupling becomes unavoidable.

In figure 14 we investigate the bottom-mass dependence of the hadronic cross section for pseudoscalar production in bottom-quark annihilation (we find similar behaviors for the production of the scalars, both light and heavy). The plot on the left shows the hadronic cross section as a function of the pseudoscalar mass m_A, in the *light-stop* scenario with $\tan\beta = 20$. As in section 2, the renormalization and factorization scales are set to $\mu_R = m_A$ and $\mu_F = m_A/4$. The central (black) solid line in the left plot is computed with our default settings, namely we use the PDF set with $M_b = 4.75$ GeV and we relate the Yukawa coupling $\widetilde{Y}_b^{\,A}$ to $m_b(m_A)$, which we obtain from the input $m_b(m_b) = 4.16$ GeV via renormalization-group evolution. The plot on the right of figure 14 represents the variation of the cross section relative to this default setting, when we change the bottom mass in the PDFs and/or in the Yukawa coupling.

In both plots, the red band between dot-dashed lines indicates the spread in the cross section obtained with the extreme PDF sets – corresponding to $M_b = 4$ GeV and $M_b = 5.5$ GeV, respectively – with $\widetilde{Y}_b^{\,A}$ fixed to the default value. As expected, the impact of the bottom mass used in the PDFs is significant: it amounts to about (+20/–15)% at large m_A, with larger values of M_b corresponding to smaller cross sections. This anti-correlation is a consequence of the fact that, for larger bottom masses, the reduced available phase space for the splitting of gluons into bottom pairs leads to a suppression of the bottom PDF. On the other hand, the bottom Yukawa coupling is directly correlated with the magnitude of the cross section. Simultaneously adjusting the bottom mass entering the bottom Yukawa coupling and the one entering the bottom PDF should therefore lead to some degree of compensation between these two effects.

Converting the pole-mass values $M_b = 4$ GeV and $M_b = 5.5$ GeV to the $\overline{\rm MS}$ scheme at three-loop level, one obtains $m_b(m_b) = 3.32$ GeV and $m_b(m_b) = 4.69$ GeV, respectively. Using these numbers to calculate $\widetilde{Y}_b^{\,A}$ while fixing the PDF set to the default (i.e., the set with $M_b = 4.75\,\text{GeV}$) results in the gray band between dashed lines in the right plot of figure 14. It turns out that this band is about twice as large as the red band arising from PDF variation. However, the gray band is rather asymmetric, because the pole mass $M_b = 4.75$ GeV for the default PDF set corresponds at the three-loop level to $m_b(m_b) = 4.00$ GeV, which is significantly smaller than our default input for $\widetilde{Y}_b^{\,A}$, i.e. $m_b(m_b) = 4.16$ GeV. The net effect on the cross section of a simultaneous variation of the bottom mass in the PDFs and in $\widetilde{Y}_b^{\,A}$, shown as a blue band between solid lines in both the left and the right plots, is thus also asymmetric, and it is of the order of (+15/–30)% at large m_A.

Our procedure to estimate the uncertainty of the cross section for bottom-quark annihilation arising from the bottom-mass dependence of the PDFs is similar to the one in ref. [88]. We fix the bottom Yukawa coupling to the value implied by $m_b(m_b) = 4.16$ GeV, as recommended by the LHC-HXSWG, and we use as uncertainty the spread in the cross section caused by the variation of M_b in the PDFs around the central value of 4.75 GeV. However, the full variation of ± 0.75 GeV allowed by the MSTW2008 PDFs, which would correspond to the red band in figure 14, seems overly conservative for our purposes. A variation of ± 0.25 GeV is in fact sufficient to encompass the value $M_b = 4.92$ GeV, which corresponds at the three-loop level to the recommended $\overline{\rm MS}$ mass $m_b(m_b) = 4.16$ GeV. This

variation finally leads to an estimate of the uncertainty of about ±6%. A similar estimate is obtained from NNPDF2.1 [97], which also provides PDF sets with different values of M_b.

3.4 Higher-order SUSY contributions to gluon fusion

In this section we discuss two sources of uncertainty affecting the SUSY contributions to the cross section for gluon fusion. The first is the validity of the expansion in the heavy superparticle masses of the two-loop SUSY contributions; the second is the impact of the three-loop SUSY contributions that are not included in `SusHi`.

3.4.1 Validity of the expansion in the SUSY masses

The results implemented in `SusHi` for the two-loop stop contributions to lightest-scalar production rely on the VHML, while the results for the remaining two-loop SUSY contributions rely on expansions in inverse powers of the superparticle masses. The latter include terms up to $\mathcal{O}(m_\phi^2/M^2)$, $\mathcal{O}(m_t^2/M^2)$, $\mathcal{O}(m_b/M)$ and $\mathcal{O}(m_Z^2/M^2)$, where m_ϕ denotes a Higgs mass and M denotes a generic superparticle mass. Therefore, the validity of the results for the two-loop SUSY contributions is limited to the region where the mass of the produced Higgs boson is smaller than the lowest-lying SUSY-particle threshold of the Feynman diagrams involved. In all of the six benchmark scenarios considered in our study, the lightest-scalar mass lies comfortably below this limit. Since we consider $m_A \leq 1$ TeV, the same applies also to the masses of the heaviest scalar and of the pseudoscalar in the five scenarios in which the squark masses are themselves of the order of 1 TeV. In the *light-stop* scenario, on the other hand, the lowest-lying SUSY threshold is at $2\,m_{\tilde{t}_1} \approx 650$ GeV, hence our need to limit our analysis to $m_A \leq 500$ GeV.

To assess the quality of our approximation in the vicinity of the threshold, we multiply the two-loop stop and sbottom contributions to the gluon-fusion amplitude by test factors $t_{\tilde{q}} \equiv \mathcal{A}^{1\ell}_{\tilde{q}_1}/\mathcal{A}^{1\ell,\,\mathrm{exp}}_{\tilde{q}_1}$, with $\tilde{q} = \{\tilde{t}, \tilde{b}\}$. Specifically, $\mathcal{A}^{1\ell}_{\tilde{q}_1}$ is the lightest-squark contribution to the one-loop part of the scalar-production amplitude including the full mass dependence, while $\mathcal{A}^{1\ell,\,\mathrm{exp}}_{\tilde{q}_1}$ includes only the leading $\mathcal{O}(m_{\tilde{q}_1}^{-2})$ terms in the expansion in the lightest-squark mass. Assuming that the expanded two-loop contributions deviate from the full ones by an amount comparable to that seen in the one-loop contributions, the variation in the gluon-fusion cross section resulting from the introduction of the test factors can be considered as an estimate of the uncertainty associated to the expansion in the SUSY masses.

The contour plots in figure 15 show the effect of introducing these test factors on the cross section for the production of the heaviest scalar (left plot) and of the pseudoscalar (right plot) in the *light-stop* scenario. In the case of H production, the variation of the cross section at large m_A amounts to a few percent when $\tan\beta$ is sufficiently large, but it can exceed 20% when $8 \lesssim \tan\beta \lesssim 16$. As can be seen in the right plot of figure 5, in this region the one-loop quark and squark contributions to the gluon-fusion amplitude largely cancel each other, with the result that the total cross section becomes small and particularly sensitive to variations in the two-loop contributions. This sensitivity to higher-order

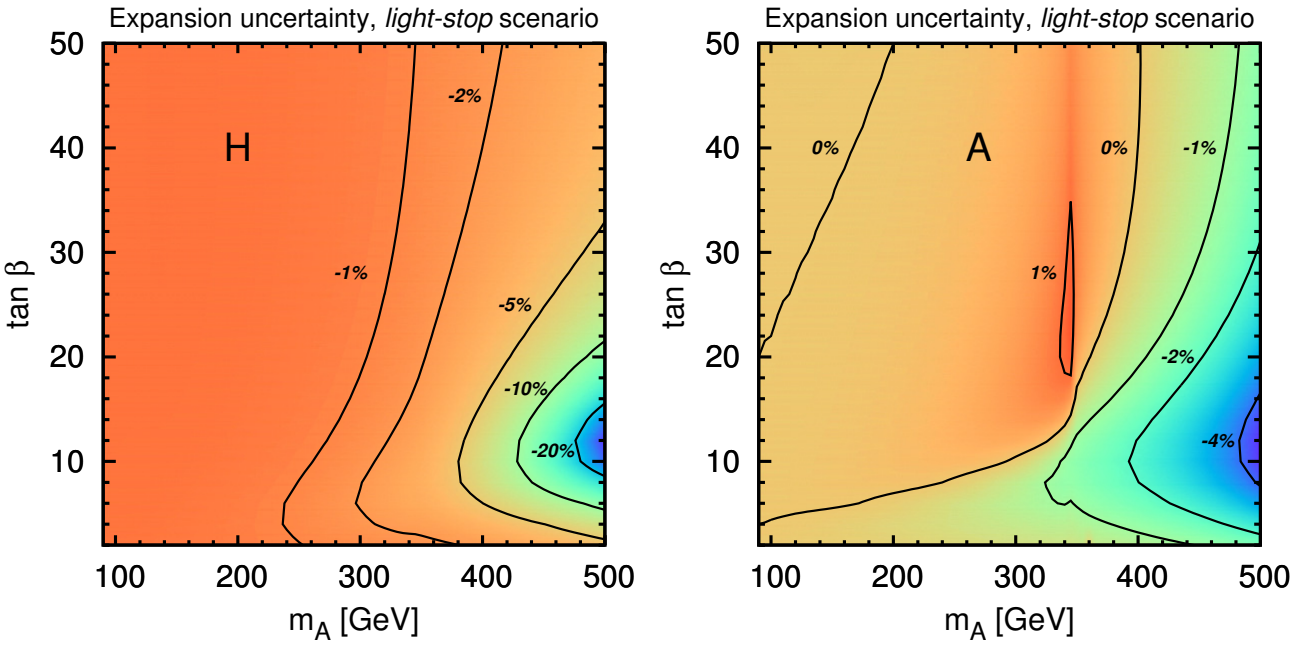

Figure 15: Variation of the gluon-fusion cross section for the production of H (left) and A (right) in the *light-stop* scenario when the two-loop SUSY contributions are rescaled by $t_{\tilde{q}} \equiv \mathcal{A}^{1\ell}_{\tilde{q}1}/\mathcal{A}^{1\ell,\,\mathrm{exp}}_{\tilde{q}1}$.

effects manifests also as the large scale uncertainty, up to 50%, visible in the right plot of figure 8. In the case of A production, on the other hand, no such cancellations occur, because the squarks do not contribute to the one-loop amplitude for gluon fusion.[7] The variation of the cross section at large m_A is therefore limited to a few percent even for moderate $\tan\beta$.

We performed the same analysis on the other five benchmark scenarios, where the squark masses are of the order of 1 TeV. As expected, we found that the effect of rescaling the two-loop SUSY contributions by test factors $t_{\tilde{q}}$ is much smaller than in the *light-stop* scenario, and it is certainly negligible when compared to the scale uncertainty of the cross section. In particular, in the *tau-phobic* scenario – where the squark contributions to the gluon-fusion amplitude are enhanced by the large value of the parameter μ – the effect on H production reaches the few-percent level only when m_A approaches 1 TeV, for moderate $\tan\beta$. In the remaining four scenarios the effect is even smaller.

3.4.2 The SUSY contributions at the NNLO

The QCD corrections to the gluon-fusion cross section are large, typically exceeding 100% at the energy of the LHC. In the SM, an excellent approximation to these corrections is obtained in the VHML (or heavy-top limit) [12, 13, 14], where a perturbative K-factor is calculated in the effective theory that results from neglecting the bottom Yukawa coupling and integrating out the top quark, leaving behind

[7] For the same reason, we cannot define test factors analogous to $t_{\tilde{q}}$ in terms of the pseudoscalar-production amplitude. To estimate the accuracy of the mass expansion for A production we use the same test factors $t_{\tilde{q}}$ as for H production.

a point-like Higgs-gluon interaction term $\mathcal{L}_{ggH} = -(1/4v)\, C(\alpha_s)\, H G_{\mu\nu} G^{\mu\nu}$, with $v \approx 246\,\text{GeV}$. The Wilson coefficient

$$C(\alpha_s) = C^{(0)} + \frac{\alpha_s}{\pi}\, C^{(1)} + \left(\frac{\alpha_s}{\pi}\right)^2 C^{(2)} \tag{12}$$

accounts for heavy particles that mediate the Higgs-gluon coupling in the underlying theory. In the SM, this is just the top quark; it is easy to see, though, that the inclusion of stop squarks (and gluinos) only affects $C(\alpha_s)$, while the form of $\mathcal{L}_{ggH}$ remains unchanged. A comparison with the full result at the NLO suggests that, within the SM, the VHML provides a decent approximation of the NNLO top contributions also for rather large Higgs masses [81, 82]. Therefore, `SusHi` includes the NNLO effects in the cross sections for the production of all three neutral Higgs bosons of the MSSM.

Within the effective theory, the K-factor at the NNLO takes the form

$$\begin{aligned} K &= 1 + \frac{\alpha_s}{\pi}\frac{1}{C^{(0)}\,\Sigma^{(0)}}\Big[C^{(0)}\,\Sigma^{(1)} + 2\,C^{(1)}\,\Sigma^{(0)} \\ &+ \frac{\alpha_s}{\pi}\left(C^{(0)}\,\Sigma^{(2)} + 2\,C^{(1)}\,\Sigma^{(1)} + (C^{(1)})^2\,\Sigma^{(0)} + 2\,C^{(2)}\,\Sigma^{(0)}\right)\Big], \end{aligned} \tag{13}$$

where $\Sigma^{(n)}$ is the n^{th}-order term in the perturbative expansion of the hadronic cross section based on $\mathcal{L}_{ggH}\big|_{C(\alpha_s)\equiv 1}$. Note that, in the NNLO part of the K-factor in eq. (13), the only genuine three-loop term that depends on the underlying theory is $C^{(2)}$. This observation was exploited in ref. [36] to derive an estimate of the NNLO top/stop contribution to the gluon-fusion cross section in the MSSM. In particular, it was shown that the final result depends only very weakly on the numerical value of $C^{(2)}$. Consequently, once the two-loop stop contributions are included in $C^{(1)}$, the unknown three-loop stop contributions to $C^{(2)}$ induce an uncertainty in the cross section much smaller than the residual uncertainty derived from scale variation. It was suggested to use the top contribution $C_t^{(2)}$ for the whole $C^{(2)}$, and to estimate the related uncertainty by varying that coefficient within the interval $[0, 2\,C_t^{(2)}]$.

In ref. [36] the hadronic cross section was obtained, in analogy to the SM NNLO result, by reweighting its exact LO expression with the K-factor of eq. (13):

$$\sigma^{\text{NNLO}} = K\,|\mathcal{A}_{t\tilde{t}}^{1\ell}|^2\,\Sigma_0\,, \tag{14}$$

where $\mathcal{A}_{t\tilde{t}}^{1\ell} \equiv \mathcal{A}_t^{1\ell} + \mathcal{A}_{\tilde{t}}^{1\ell}$ is the one-loop amplitude including both the top and stop contributions with the exact Higgs-mass dependence (in particular, $\mathcal{A}_{t\tilde{t}}^{1\ell} \to C^{(0)}$ in the VHML, i.e. for $m_\phi \to 0$). However, as was discussed also in the previous section, there exist so-called *gluophobic* regions of the MSSM parameter space in which the top and stop contributions to the amplitude can cancel each other to a large extent. Since the precise values of the MSSM parameters where this cancellation is maximal differ between the full calculation and the VHML, the ratio $|\mathcal{A}_{t\tilde{t}}^{1\ell}|/C^{(0)}$ entering the cross section – see eqs. (13) and (14) – can become spuriously large when $C^{(0)} \approx 0$. In order to evade this effect, we

replace $C^{(0)}$ in eq. (12) with $\mathcal{A}_{t\tilde{t}}^{1\ell}$. This leads to the following expression for the cross section:

$$\begin{aligned}\sigma^{\text{NNLO}} &= |\mathcal{A}_{t\tilde{t}}^{1\ell}|^2\,\Sigma^{(0)} + \frac{\alpha_s}{\pi}\left(|\mathcal{A}_{t\tilde{t}}^{1\ell}|^2\,\Sigma^{(1)} + 2\,C^{(1)}\,\Sigma^{(0)}\,\text{Re}\,\mathcal{A}_{t\tilde{t}}^{1\ell}\right) \\ &+ \left(\frac{\alpha_s}{\pi}\right)^2\left[|\mathcal{A}_{t\tilde{t}}^{1\ell}|^2\,\Sigma^{(2)} + 2\left(C^{(1)}\,\Sigma^{(1)} + C^{(2)}\,\Sigma^{(0)}\right)\text{Re}\,\mathcal{A}_{t\tilde{t}}^{1\ell} + (C^{(1)})^2\,\Sigma^{(0)}\right]. \qquad (15)\end{aligned}$$

This formula applies to both MSSM scalars. The effective Lagrangian for the gluonic interaction of the pseudoscalar involves an additional operator which contributes at the NNLO [35], but it can be treated in a completely analogous way.

In `SusHi`, the NNLO top and stop contributions to the gluon-fusion cross section in the VHML are isolated by subtracting from the σ^{NNLO} in eq. (15) the same quantity truncated at the NLO (and computed with NLO PDFs). The result is then added to the full NLO cross section, which accounts also for the bottom and sbottom contributions and for the known Higgs-mass dependence of the two-loop amplitude. The 6% suppression of the cross section for the production of a SM-like scalar induced by the NNLO stop contributions in the *light-stop* scenario – see section 2.2 – can be ascribed to the effect of the term $2\,C^{(1)}\,\Sigma^{(1)}\,\text{Re}\,\mathcal{A}_{t\tilde{t}}^{1\ell}$ in the second line of eq. (15). Indeed, the large value of the (normalized) NLO term of the cross section in the effective theory, $\Sigma^{(1)}/\Sigma^{(0)} \approx 26$, compensates for the suppression by α_s/π, with the result that the effect of the two-loop stop contribution to $C^{(1)}$ at the NNLO is roughly as large as the corresponding effect at the NLO.

To assess the uncertainty arising from the fact that we neglect the three-loop SUSY contributions to $C^{(2)}$, we make use of a recent calculation of those contributions in the VHML [37, 38]. The calculation is based on an expansion of the relevant Feynman diagrams in terms of certain hierarchies among the different masses, similar to the strategy that was pursued in ref. [70] for the calculation of the 3-loop corrections to the Higgs mass in the MSSM. The results of ref. [38] are available in the form of a `Mathematica` file, which provides the basis for the expansion of $C^{(2)}$ in various hierarchies of the masses $m_{\tilde{t}_1}$, $m_{\tilde{t}_2}$, $m_{\tilde{g}}$, m_t, and $m_{\tilde{q}}$, combined with expansions in differences of these masses. Following an algorithm suggested in ref. [38], these expansions should allow one to derive a numerical approximation for $C^{(2)}$ in any viable MSSM scenario.

Applying this approach to the scenarios defined in table 1, we find that the deviation of the whole $C^{(2)}$ from the top contribution $C_t^{(2)}$ is rather small, and the second-order coefficient certainly stays within the range $[\,0,\,2\,C_t^{(2)}]$. Varying $C^{(2)}$ within this interval, we estimate that the effect of the three-loop SUSY contributions to the gluon-fusion cross section does not exceed 1% in all of the scenarios considered in this paper. It is therefore a viable strategy to follow ref. [36] and set $C^{(2)} = C_t^{(2)}$, attributing an uncertainty of $\pm 1\%$ to the final result for the cross section.

4 Conclusions

A precise prediction of the cross sections for Higgs-boson production, as well as a detailed understanding of the associated uncertainties, are of vital importance to interpret the recent discovery of a Higgs boson in the context of the MSSM. In this paper we used the public code `SusHi` [53], which computes the cross sections for gluon fusion and bottom-quark annihilation, to study the production of scalar and pseudoscalar Higgs bosons in a set of MSSM scenarios compatible with the LHC results. We showed how the cross sections can substantially differ from the SM prediction, and how their qualitative behavior over the MSSM parameter space depends mainly on the relative importance of the contributions involving top and bottom quarks. We also emphasized that, in a scenario with relatively light squarks which is not yet constrained by the LHC, the contributions to the gluon-fusion process that involve superparticles can significantly suppress the cross section for scalar production.

Next, we studied the different sources of uncertainty that affect our predictions for the Higgs-production cross sections. Some of these uncertainties, namely the ones associated to the choice of renormalization and factorization scales, to the PDF parameterization and to the input value for the strong coupling constant, are relevant also for the production of the SM Higgs, although their size may differ in the case of the production of non-standard Higgs bosons. In contrast, the uncertainties associated to the definition of the bottom mass and Yukawa coupling are practically negligible in the SM – where the bottom-quark contributions amount only to a few percent of the total cross section – but they can become dominant in regions of the MSSM parameter space where the couplings of the Higgs bosons to bottom quarks are enhanced. In the particular case of heavy-scalar and pseudoscalar production at large $\tan\beta$, we found that legitimate variations in the renormalization scheme and scale of the bottom Yukawa coupling can suppress the gluon-fusion cross section by more than 60%, due to the presence of large QCD corrections enhanced by logarithms of the ratio m_ϕ^2/m_b^2. Luckily, in this case the total cross section is dominated by the contribution of bottom-quark annihilation, which is subject to a considerably smaller scale uncertainty. Finally, we studied the uncertainties associated to our implementation of the SUSY contributions to gluon fusion at the NLO and, partially, at the NNLO. With the exception of a gluophobic region in the *light-stop* scenario, these uncertainties are generally small, reflecting the sub-dominant nature of the SUSY contributions themselves for values of the squark masses compatible with the LHC bounds.

Future improvements in the accuracy of the predictions for the Higgs-production cross sections in the MSSM could come from different directions. First of all, any progress in the SM calculation will eventually trickle down to the MSSM calculation, at least where the production of a SM-like scalar is concerned. In addition, a resummation of the QCD corrections enhanced by $\ln(m_\phi^2/m_b^2)$, analogous to the one performed in ref. [89] for the Higgs decay to photons, will be necessary to reduce the large uncertainty in the production of non-standard Higgs bosons via gluon fusion (incidentally, such calculation would benefit all models with enhanced Higgs couplings to bottom quarks, whether they are supersymmetric or not). Implementing the existing results for the two-loop contributions to Δ_b [41], in both the Higgs mass and cross-section calculations, will also reduce the uncertainty in

scenarios where the bottom contributions are relevant. Finally, it could be worthwhile to improve the calculation of the gluon-fusion cross section by taking into account the full Higgs-mass dependence of the two-loop squark-gluon [8] contributions [10, 11, 24] – to cover scenarios in which the non-standard Higgs bosons are heavier than the third-generation squarks – and by including the genuine three-loop effects [37, 38].

For the time being, however, we believe that `SusHi` provides the most sophisticated calculation of the Higgs-production cross sections in the MSSM available to the physics community. Differently from the case of the SM, where all the relevant inputs are now known and a definite prediction for the total cross section can be made solely as a function of the collision energy, in the MSSM the predictions for the cross sections – and the relevance of the different sources of uncertainty – depend crucially on a number of yet-undetermined parameters. In the appendix we collect predictions for the Higgs-production cross sections via gluon fusion and bottom-quark annihilation, and their respective uncertainties, in a few representative points of the six benchmark scenarios described in section 2.1. However, the tables in the appendix should be regarded as having an illustrative purpose only: we encourage the readers to take both `SusHi` and our recipes for the uncertainties directly in their own hands, and use them to analyze their favorite corners of the MSSM parameter space. Our results should prove useful for ruling out scenarios that are incompatible with the current experimental bounds. We also hope that, when the time comes, they will help interpret within the MSSM the discovery of new particles at the LHC.

Acknowledgments

This work was initiated in the context of the activities of the LHC-HXSWG, and some of our preliminary findings were presented in section 14 of ref. [5]. We thank the authors of ref. [56] and the SUSY convenors of the ATLAS and CMS collaborations for helpful communication about the experimental constraints on the MSSM benchmark scenarios, and the authors of ref. [38] for helpful communication about their results. We also thank M. Spira for useful discussions about the uncertainties of the cross-section calculations.

This work was supported in part by the Research Executive Agency (REA) of the European Commission under the Grant Agreements PITN-GA-2010-264564 (LHCPhenoNet), PITN-GA-2012-315877 (MCnet) and PITN-GA-2012-316704 (HiggsTools), and by the European Research Council (ERC) under the Advanced Grant ERC-2012-ADG_20120216-321133 (Higgs@LHC). The work of E. B. and P. S. at LPTHE is supported in part by French state funds managed by the ANR (ANR-11-IDEX-0004-02) in the context of the ILP LABEX (ANR-10-LABX-63). S. L. acknowledges support by the DFG (SFB 676 "Particles, Strings and the Early Universe"). S. L., H. M. and R. H. were also supported by the DFG grant HA 2990/5-1. A. V. was supported in part by an Italian PRIN2009 grant and a European Investment Bank EIBURS grant.

[8] As well as the two-loop quark-squark-gluino contributions [25, 26], when they become available.

Appendix: Cross sections and uncertainties

In this appendix we include eighteen tables, listing the cross sections and uncertainties for the production at the LHC of the three neutral Higgs bosons in the six MSSM scenarios defined in table 1. We use version `1.3.0` of `SusHi`, and provide separate results for gluon fusion and bottom-quark annihilation. Input files for the six scenarios can be found on the code's website [53]. We set $\sqrt{s} = 8$ TeV, $m_t = 173.2$ GeV and $m_b(m_b) = 4.16$ GeV, and we choose thirty combinations of the parameters m_A and $\tan\beta$ for each scenario. The predictions for the scalar masses are obtained with version `2.10.0` of `FeynHiggs`. The uncertainties provided in the tables are computed as follows:

- The renormalization- and factorization-scale uncertainties are summarized in the quantities $\Delta^{\pm}_{\mu}$, defined as in section 3.1.1, eq. (3). For gluon fusion we consider the seven combinations obtained from $\mu_R = \{m_\phi/4,\, m_\phi/2,\, m_\phi\}$ and $\mu_F = \{m_\phi/4,\, m_\phi/2,\, m_\phi\}$, where we discard the two pairs with the largest variation of the ratio μ_R/μ_F with respect to the central choice. For bottom-quark annihilation we proceed accordingly, using $\mu_R = \{m_\phi/2, m_\phi, 2\,m_\phi\}$ and $\mu_F = \{m_\phi/8, m_\phi/4, m_\phi/2\}$.

- The uncertainty δY_b of the gluon-fusion process, related to the definition of the bottom Yukawa coupling and discussed in section 3.2.1, is computed as the relative difference between the cross section calculated with $Y_b^\phi \propto m_b(m_\phi/2)$ and the cross section calculated with $Y_b^\phi \propto M_b$. In the case of bottom-quark annihilation, the scale dependence of Y_b^ϕ is included in the computation of $\Delta^{\pm}_{\mu}$.

- The uncertainty $\delta\Delta_b$, stemming from the resummation of $\tan\beta$-enhanced corrections to Y_b^ϕ and described in section 3.2.2, is computed by adding an uncertainty of $\pm 10\%$ to the value of Δ_b obtained from `FeynHiggs`.

The PDF uncertainties are not included in the tables, but they were extensively discussed in section 3.3. In section 3.3.1 we pointed out that the relative size of the PDF+α_s uncertainty depends mainly on the value of the Higgs mass, thus it can be taken over directly from the existing estimates for the production of the SM Higgs. Apart from the PDF+α_s uncertainty, in the case of bottom-quark annihilation an additional uncertainty of $\pm 6\%$ has to be added due to the dependence of the bottom-quark PDF on the pole bottom mass (see section 3.3.2). The uncertainties associated to our incomplete knowledge of the SUSY contributions to the gluon-fusion cross section can become sizeable only in the *light-stop* scenario, especially in the case of H production at large m_A and moderate $\tan\beta$. We do not include them in the tables, pointing the reader to the discussion in section 3.4.

We show the results for the $m_h^{\rm max}$ scenario in tables 2−4. Rather similar results for the $m_h^{\rm mod+}$ and $m_h^{\rm mod-}$ scenarios are given in tables 5−7 and 8−10, respectively. The *light-stop* and *light-stau* scenarios are presented in tables 11−13 and 14−16, respectively. Finally, cross sections and uncertainties for the *tau-phobic* scenario are shown in tables 17−19, which are limited to $\tan\beta \leq 40$ due to a drop in the lightest-scalar mass for larger $\tan\beta$.

m_A [GeV]	$\tan\beta$	m_h [GeV]	σ_{ggh} [pb]	$\Delta_\mu^\pm$ [%]	δY_b [%]	$\delta\Delta_b$ [%]	σ_{bbh} [pb]	$\Delta_\mu^\pm$ [%]	$\delta\Delta_b$ [%]
100	5	92.2	15.08	$^{+17.3}_{-14.5}$	-41.6	$^{+0.3}_{-0.3}$	12.47	$^{+9.3}_{-17.6}$	$^{+0.3}_{-0.3}$
100	10	97.6	42.08	$^{+16.9}_{-14.2}$	-53.5	$^{+0.7}_{-0.7}$	42.73	$^{+8.8}_{-16.3}$	$^{+0.7}_{-0.7}$
100	15	98.9	90.51	$^{+16.4}_{-13.9}$	-53.8	$^{+1.1}_{-1.1}$	91.10	$^{+8.7}_{-16.0}$	$^{+1.1}_{-1.0}$
100	20	99.3	156.0	$^{+16.1}_{-13.8}$	-53.5	$^{+1.5}_{-1.4}$	155.5	$^{+8.6}_{-15.8}$	$^{+1.4}_{-1.4}$
100	30	99.7	329.5	$^{+15.9}_{-13.7}$	-53.2	$^{+2.1}_{-2.0}$	325.5	$^{+8.6}_{-15.8}$	$^{+2.0}_{-2.0}$
100	50	99.9	806.0	$^{+15.7}_{-13.6}$	-53.0	$^{+3.3}_{-3.2}$	792.8	$^{+8.6}_{-15.7}$	$^{+3.2}_{-3.1}$
120	5	105.6	10.69	$^{+13.9}_{-12.6}$	-16.3	$^{+0.1}_{-0.1}$	6.418	$^{+8.1}_{-14.5}$	$^{+0.3}_{-0.3}$
120	10	114.2	16.02	$^{+15.8}_{-13.5}$	-43.5	$^{+0.6}_{-0.6}$	20.57	$^{+7.5}_{-13.0}$	$^{+0.7}_{-0.7}$
120	15	116.9	30.90	$^{+15.9}_{-13.6}$	-53.0	$^{+1.1}_{-1.0}$	44.57	$^{+7.3}_{-12.6}$	$^{+1.0}_{-1.0}$
120	20	118.1	53.81	$^{+15.6}_{-13.4}$	-55.0	$^{+1.5}_{-1.4}$	77.88	$^{+7.2}_{-12.4}$	$^{+1.4}_{-1.4}$
120	30	119.1	119.3	$^{+15.1}_{-13.1}$	-55.3	$^{+2.1}_{-2.1}$	168.5	$^{+7.2}_{-12.2}$	$^{+2.0}_{-2.0}$
120	50	119.6	306.4	$^{+14.7}_{-12.9}$	-54.7	$^{+3.3}_{-3.2}$	421.7	$^{+7.1}_{-12.2}$	$^{+3.2}_{-3.1}$
150	5	116.7	14.16	$^{+10.6}_{-10.7}$	$+0.5$	—	2.299	$^{+7.3}_{-12.6}$	$^{+0.3}_{-0.3}$
150	10	125.2	14.61	$^{+10.7}_{-10.6}$	-0.1	—	3.556	$^{+6.8}_{-11.4}$	$^{+0.6}_{-0.6}$
150	15	127.5	15.20	$^{+10.8}_{-10.6}$	-0.5	—	4.206	$^{+6.7}_{-11.1}$	$^{+0.9}_{-0.8}$
150	20	128.5	15.53	$^{+10.8}_{-10.7}$	-0.6	—	4.498	$^{+6.7}_{-11.0}$	$^{+1.1}_{-1.1}$
150	30	129.3	15.81	$^{+10.8}_{-10.6}$	-0.6	—	4.640	$^{+6.6}_{-10.9}$	$^{+1.6}_{-1.6}$
150	50	130.0	15.91	$^{+10.7}_{-10.6}$	-0.3	—	4.426	$^{+6.6}_{-10.8}$	$^{+2.6}_{-2.5}$
200	5	122.0	17.30	$^{+9.3}_{-10.0}$	$+2.0$	—	0.780	$^{+7.0}_{-11.8}$	$^{+0.2}_{-0.2}$
200	10	127.6	16.89	$^{+9.2}_{-9.9}$	$+2.1$	—	0.787	$^{+6.7}_{-11.1}$	$^{+0.4}_{-0.4}$
200	15	128.8	16.84	$^{+9.1}_{-9.8}$	$+2.1$	—	0.785	$^{+6.6}_{-11.0}$	$^{+0.5}_{-0.5}$
200	20	129.2	16.82	$^{+9.1}_{-9.8}$	$+2.1$	—	0.779	$^{+6.6}_{-10.9}$	$^{+0.7}_{-0.7}$
200	30	129.6	16.79	$^{+9.1}_{-9.8}$	$+2.1$	—	0.766	$^{+6.6}_{-10.9}$	$^{+1.0}_{-1.0}$
200	50	130.0	16.75	$^{+9.0}_{-9.8}$	$+2.0$	—	0.737	$^{+6.6}_{-10.8}$	$^{+1.6}_{-1.5}$
300	5	124.2	18.36	$^{+8.9}_{-9.8}$	$+1.7$	—	0.369	$^{+6.9}_{-11.5}$	—
300	10	128.2	17.55	$^{+8.8}_{-9.7}$	$+1.7$	—	0.343	$^{+6.7}_{-11.0}$	$^{+0.2}_{-0.2}$
300	15	129.1	17.40	$^{+8.8}_{-9.7}$	$+1.7$	—	0.337	$^{+6.6}_{-10.9}$	$^{+0.3}_{-0.3}$
300	20	129.4	17.34	$^{+8.8}_{-9.7}$	$+1.7$	—	0.334	$^{+6.6}_{-10.9}$	$^{+0.3}_{-0.3}$
300	30	129.7	17.28	$^{+8.8}_{-9.7}$	$+1.7$	—	0.329	$^{+6.6}_{-10.9}$	$^{+0.5}_{-0.5}$
300	50	130.0	17.22	$^{+8.8}_{-9.7}$	$+1.6$	—	0.323	$^{+6.6}_{-10.8}$	$^{+0.8}_{-0.7}$

Table 2: Cross sections and uncertainties for lightest-scalar production in the $m_h^{\max}$ scenario for $\sqrt{s} = 8$ TeV. Uncertainties below 0.1% are not listed (—). For the PDF uncertainties see text.

m_A [GeV]	$\tan\beta$	m_H [GeV]	σ_{ggH} [pb]	$\Delta_\mu^\pm$ [%]	δY_b [%]	$\delta\Delta_b$ [%]	σ_{bbH} [pb]	$\Delta_\mu^\pm$ [%]	$\delta\Delta_b$ [%]
100	5	136.8	16.65	$^{+7.8}_{-9.3}$	-3.9	— —	0.530	$^{+6.3}_{-10.1}$	$^{+0.6}_{-0.6}$
100	10	131.9	19.86	$^{+8.0}_{-9.5}$	-5.0	— —	0.941	$^{+6.5}_{-10.6}$	$^{+1.0}_{-1.0}$
100	15	130.8	20.92	$^{+8.1}_{-9.5}$	-5.3	$^{+0.1}_{-0.1}$	1.077	$^{+6.5}_{-10.7}$	$^{+1.5}_{-1.5}$
100	20	130.4	21.33	$^{+8.1}_{-9.5}$	-5.4	$^{+0.2}_{-0.2}$	1.124	$^{+6.6}_{-10.8}$	$^{+2.0}_{-1.9}$
100	30	130.2	21.60	$^{+8.1}_{-9.5}$	-5.4	$^{+0.3}_{-0.3}$	1.143	$^{+6.6}_{-10.8}$	$^{+2.9}_{-2.8}$
100	50	130.3	21.62	$^{+8.1}_{-9.5}$	-5.4	$^{+0.4}_{-0.4}$	1.134	$^{+6.6}_{-10.8}$	$^{+4.6}_{-4.3}$
200	5	205.9	1.521	$^{+7.1}_{-8.8}$	-17.5	$^{+0.1}_{-0.1}$	0.743	$^{+4.4}_{-5.6}$	$^{+0.4}_{-0.4}$
200	10	201.7	1.838	$^{+9.7}_{-10.2}$	-41.9	$^{+0.5}_{-0.5}$	3.337	$^{+4.4}_{-5.8}$	$^{+0.7}_{-0.7}$
200	15	200.8	3.068	$^{+10.8}_{-10.9}$	-50.4	$^{+1.0}_{-1.0}$	7.497	$^{+4.5}_{-5.8}$	$^{+1.1}_{-1.1}$
200	20	200.5	4.826	$^{+11.2}_{-11.2}$	-53.3	$^{+1.4}_{-1.3}$	13.03	$^{+4.5}_{-5.8}$	$^{+1.4}_{-1.4}$
200	30	200.2	9.553	$^{+11.6}_{-11.4}$	-55.2	$^{+2.0}_{-2.0}$	27.64	$^{+4.5}_{-5.9}$	$^{+2.1}_{-2.0}$
200	50	200.1	22.60	$^{+11.8}_{-11.5}$	-56.2	$^{+3.3}_{-3.1}$	67.78	$^{+4.5}_{-5.9}$	$^{+3.2}_{-3.1}$
300	5	303.3	0.319	$^{+6.2}_{-8.8}$	-13.8	— —	0.160	$^{+3.2}_{-3.2}$	$^{+0.4}_{-0.4}$
300	10	301.0	0.252	$^{+8.3}_{-10.3}$	-37.9	$^{+0.5}_{-0.5}$	0.653	$^{+3.2}_{-3.2}$	$^{+0.7}_{-0.7}$
300	15	300.6	0.357	$^{+9.7}_{-11.1}$	-49.1	$^{+0.9}_{-0.9}$	1.432	$^{+3.2}_{-3.2}$	$^{+1.1}_{-1.1}$
300	20	300.4	0.526	$^{+10.3}_{-11.5}$	-53.5	$^{+1.3}_{-1.3}$	2.469	$^{+3.2}_{-3.2}$	$^{+1.4}_{-1.4}$
300	30	300.3	0.992	$^{+10.8}_{-11.7}$	-56.5	$^{+2.0}_{-2.0}$	5.202	$^{+3.2}_{-3.2}$	$^{+2.1}_{-2.0}$
300	50	300.2	2.292	$^{+11.0}_{-11.8}$	-58.0	$^{+3.3}_{-3.1}$	12.71	$^{+3.2}_{-3.2}$	$^{+3.2}_{-3.1}$
500	5	501.2	54.5×10^{-3}	$^{+1.5}_{-5.6}$	-0.7	— —	15.3×10^{-3}	$^{+2.3}_{-1.4}$	$^{+0.4}_{-0.4}$
500	10	500.1	18.0×10^{-3}	$^{+0.2}_{-4.6}$	-14.7	$^{+0.2}_{-0.2}$	60.3×10^{-3}	$^{+2.3}_{-1.4}$	$^{+0.7}_{-0.7}$
500	15	499.9	16.3×10^{-3}	$^{+2.0}_{-6.7}$	-38.3	$^{+0.7}_{-0.7}$	0.131	$^{+2.3}_{-1.4}$	$^{+1.1}_{-1.1}$
500	20	499.8	21.4×10^{-3}	$^{+4.6}_{-8.9}$	-51.4	$^{+1.3}_{-1.2}$	0.226	$^{+2.3}_{-1.4}$	$^{+1.4}_{-1.4}$
500	30	499.7	40.2×10^{-3}	$^{+7.6}_{-11.0}$	-58.9	$^{+2.1}_{-2.0}$	0.475	$^{+2.3}_{-1.4}$	$^{+2.1}_{-2.0}$
500	50	499.5	95.8×10^{-3}	$^{+9.6}_{-12.0}$	-60.9	$^{+3.3}_{-3.2}$	1.160	$^{+2.3}_{-1.4}$	$^{+3.2}_{-3.1}$
1000	5	1000.5	675×10^{-6}	$^{+0.1}_{-3.8}$	$+6.1$	— —	293×10^{-6}	$^{+1.4}_{-1.1}$	$^{+0.4}_{-0.4}$
1000	10	1000.0	117×10^{-6}	$^{+5.1}_{-19.1}$	$+19.7$	$^{+0.1}_{-0.1}$	1.14×10^{-3}	$^{+1.4}_{-1.1}$	$^{+0.7}_{-0.7}$
1000	15	999.9	53.1×10^{-6}	$^{+10.1}_{-30.5}$	-10.4	$^{+0.5}_{-0.5}$	2.47×10^{-3}	$^{+1.4}_{-1.1}$	$^{+1.1}_{-1.1}$
1000	20	999.9	74.2×10^{-6}	$^{+1.3}_{-11.9}$	-58.6	$^{+1.7}_{-1.6}$	4.24×10^{-3}	$^{+1.4}_{-1.1}$	$^{+1.4}_{-1.4}$
1000	30	999.7	203×10^{-6}	$^{+5.0}_{-10.7}$	-71.3	$^{+2.5}_{-2.4}$	8.92×10^{-3}	$^{+1.4}_{-1.1}$	$^{+2.1}_{-2.0}$
1000	50	999.3	615×10^{-6}	$^{+9.8}_{-13.2}$	-68.4	$^{+3.6}_{-3.4}$	21.8×10^{-3}	$^{+1.4}_{-1.1}$	$^{+3.2}_{-3.1}$

Table 3: Cross sections and uncertainties for heaviest-scalar production in the $m_h^{\max}$ scenario for $\sqrt{s} = 8$ TeV. Uncertainties below 0.1% are not listed (—). For the PDF uncertainties see text.

m_A [GeV]	$\tan\beta$	σ_{ggA} [pb]	$\Delta_\mu^\pm$ [%]	δY_b [%]	$\delta\Delta_b$ [%]	σ_{bbA} [pb]	$\Delta_\mu^\pm$ [%]	$\delta\Delta_b$ [%]
100	5	10.55	$^{+15.6}_{-13.5}$	-47.9	$^{+0.4}_{-0.4}$	10.74	$^{+8.6}_{-15.7}$	$^{+0.4}_{-0.4}$
100	10	43.02	$^{+15.4}_{-13.4}$	-53.9	$^{+0.8}_{-0.8}$	41.46	$^{+8.6}_{-15.7}$	$^{+0.7}_{-0.7}$
100	15	97.28	$^{+15.2}_{-13.3}$	-53.3	$^{+1.1}_{-1.1}$	90.03	$^{+8.6}_{-15.7}$	$^{+1.1}_{-1.1}$
100	20	169.6	$^{+15.0}_{-13.2}$	-53.0	$^{+1.5}_{-1.4}$	154.5	$^{+8.6}_{-15.7}$	$^{+1.4}_{-1.4}$
100	30	360.3	$^{+14.9}_{-13.2}$	-52.7	$^{+2.1}_{-2.0}$	324.7	$^{+8.6}_{-15.7}$	$^{+2.1}_{-2.0}$
100	50	881.7	$^{+14.8}_{-13.1}$	-52.6	$^{+3.3}_{-3.2}$	791.8	$^{+8.6}_{-15.7}$	$^{+3.2}_{-3.1}$
200	5	0.566	$^{+9.2}_{-9.9}$	-4.2	$^{—}_{—}$	0.922	$^{+4.5}_{-5.9}$	$^{+0.4}_{-0.4}$
200	10	0.951	$^{+12.3}_{-11.7}$	-57.7	$^{+0.8}_{-0.8}$	3.560	$^{+4.5}_{-5.9}$	$^{+0.7}_{-0.7}$
200	15	2.323	$^{+11.9}_{-11.5}$	-59.2	$^{+1.2}_{-1.2}$	7.732	$^{+4.5}_{-5.9}$	$^{+1.1}_{-1.1}$
200	20	4.237	$^{+11.6}_{-11.4}$	-58.3	$^{+1.5}_{-1.5}$	13.27	$^{+4.5}_{-5.9}$	$^{+1.4}_{-1.4}$
200	30	9.337	$^{+11.4}_{-11.3}$	-57.3	$^{+2.1}_{-2.1}$	27.89	$^{+4.5}_{-5.9}$	$^{+2.1}_{-2.0}$
200	50	23.32	$^{+11.2}_{-11.1}$	-56.8	$^{+3.3}_{-3.2}$	68.00	$^{+4.5}_{-5.9}$	$^{+3.2}_{-3.1}$
300	5	0.324	$^{+7.2}_{-8.9}$	$+8.3$	$^{—}_{—}$	0.173	$^{+3.2}_{-3.2}$	$^{+0.4}_{-0.4}$
300	10	99.5×10^{-3}	$^{+9.4}_{-10.1}$	-28.3	$^{+0.4}_{-0.4}$	0.668	$^{+3.2}_{-3.2}$	$^{+0.7}_{-0.7}$
300	15	0.189	$^{+11.1}_{-11.6}$	-60.3	$^{+1.2}_{-1.2}$	1.450	$^{+3.2}_{-3.2}$	$^{+1.1}_{-1.1}$
300	20	0.365	$^{+11.0}_{-11.8}$	-62.4	$^{+1.6}_{-1.6}$	2.489	$^{+3.2}_{-3.2}$	$^{+1.4}_{-1.4}$
300	30	0.864	$^{+10.8}_{-11.7}$	-60.9	$^{+2.2}_{-2.1}$	5.231	$^{+3.2}_{-3.2}$	$^{+2.1}_{-2.0}$
300	50	2.256	$^{+10.5}_{-11.6}$	-59.5	$^{+3.4}_{-3.2}$	12.75	$^{+3.2}_{-3.2}$	$^{+3.2}_{-3.1}$
500	5	0.102	$^{+4.8}_{-8.1}$	-4.0	$^{—}_{—}$	15.7×10^{-3}	$^{+2.3}_{-1.4}$	$^{+0.4}_{-0.4}$
500	10	35.6×10^{-3}	$^{+10.0}_{-11.1}$	-18.1	$^{+0.2}_{-0.2}$	60.4×10^{-3}	$^{+2.3}_{-1.4}$	$^{+0.7}_{-0.7}$
500	15	28.8×10^{-3}	$^{+13.5}_{-13.2}$	-35.2	$^{+0.6}_{-0.6}$	0.131	$^{+2.3}_{-1.4}$	$^{+1.1}_{-1.1}$
500	20	32.4×10^{-3}	$^{+14.2}_{-13.8}$	-46.5	$^{+1.0}_{-1.0}$	0.225	$^{+2.3}_{-1.4}$	$^{+1.4}_{-1.4}$
500	30	50.5×10^{-3}	$^{+13.0}_{-13.5}$	-55.6	$^{+1.9}_{-1.8}$	0.473	$^{+2.3}_{-1.4}$	$^{+2.1}_{-2.0}$
500	50	0.108	$^{+11.3}_{-12.8}$	-59.4	$^{+3.2}_{-3.0}$	1.154	$^{+2.3}_{-1.4}$	$^{+3.2}_{-3.1}$
1000	5	1.18×10^{-3}	$^{+3.0}_{-7.1}$	-5.6	$^{—}_{—}$	295×10^{-6}	$^{+1.4}_{-1.1}$	$^{+0.4}_{-0.4}$
1000	10	433×10^{-6}	$^{+6.3}_{-10.0}$	-19.2	$^{+0.2}_{-0.2}$	1.14×10^{-3}	$^{+1.4}_{-1.1}$	$^{+0.7}_{-0.7}$
1000	15	335×10^{-6}	$^{+9.8}_{-12.3}$	-33.4	$^{+0.5}_{-0.5}$	2.47×10^{-3}	$^{+1.4}_{-1.1}$	$^{+1.1}_{-1.1}$
1000	20	344×10^{-6}	$^{+11.4}_{-13.4}$	-43.5	$^{+0.9}_{-0.9}$	4.24×10^{-3}	$^{+1.4}_{-1.1}$	$^{+1.4}_{-1.4}$
1000	30	465×10^{-6}	$^{+11.9}_{-14.0}$	-54.0	$^{+1.7}_{-1.6}$	8.91×10^{-3}	$^{+1.4}_{-1.1}$	$^{+2.1}_{-2.0}$
1000	50	880×10^{-6}	$^{+11.2}_{-13.9}$	-60.2	$^{+3.0}_{-2.9}$	21.7×10^{-3}	$^{+1.4}_{-1.1}$	$^{+3.2}_{-3.1}$

Table 4: Cross sections and uncertainties for pseudoscalar production in the $m_h^{\max}$ scenario for $\sqrt{s} =$ 8 TeV. Uncertainties below 0.1% are not listed (—). For the PDF uncertainties see text.

m_A [GeV]	$\tan\beta$	m_h [GeV]	σ_{ggh} [pb]	$\Delta_\mu^\pm$ [%]	δY_b [%]	$\delta\Delta_b$ [%]	σ_{bbh} [pb]	$\Delta_\mu^\pm$ [%]	$\delta\Delta_b$ [%]
100	5	91.0	16.46	$^{+17.2}_{-14.4}$	-38.3	$^{+0.2}_{-0.2}$	12.60	$^{+9.5}_{-18.0}$	$^{+0.3}_{-0.3}$
100	10	97.0	42.48	$^{+17.1}_{-14.3}$	-52.8	$^{+0.6}_{-0.6}$	42.91	$^{+8.8}_{-16.4}$	$^{+0.6}_{-0.6}$
100	15	98.5	91.10	$^{+16.5}_{-14.0}$	-53.6	$^{+0.9}_{-0.9}$	91.98	$^{+8.7}_{-16.0}$	$^{+0.9}_{-0.9}$
100	20	99.1	157.8	$^{+16.2}_{-13.8}$	-53.4	$^{+1.3}_{-1.2}$	157.9	$^{+8.6}_{-15.9}$	$^{+1.2}_{-1.2}$
100	30	99.6	337.2	$^{+16.0}_{-13.7}$	-53.1	$^{+1.8}_{-1.8}$	333.8	$^{+8.6}_{-15.8}$	$^{+1.8}_{-1.7}$
100	50	99.8	841.1	$^{+15.8}_{-13.6}$	-52.8	$^{+2.9}_{-2.8}$	827.2	$^{+8.6}_{-15.7}$	$^{+2.8}_{-2.7}$
120	5	103.5	12.56	$^{+13.8}_{-12.5}$	-13.4	$^{—}_{—}$	6.377	$^{+8.2}_{-14.9}$	$^{+0.3}_{-0.3}$
120	10	112.7	16.82	$^{+15.5}_{-13.4}$	-37.5	$^{+0.4}_{-0.4}$	19.42	$^{+7.6}_{-13.2}$	$^{+0.6}_{-0.6}$
120	15	115.7	29.60	$^{+16.0}_{-13.6}$	-49.5	$^{+0.9}_{-0.8}$	41.30	$^{+7.4}_{-12.8}$	$^{+0.9}_{-0.9}$
120	20	117.1	49.77	$^{+15.9}_{-13.5}$	-53.5	$^{+1.2}_{-1.2}$	71.97	$^{+7.3}_{-12.5}$	$^{+1.2}_{-1.2}$
120	30	118.4	109.6	$^{+15.4}_{-13.3}$	-55.0	$^{+1.8}_{-1.8}$	157.5	$^{+7.2}_{-12.3}$	$^{+1.8}_{-1.7}$
120	50	119.3	289.0	$^{+15.0}_{-13.1}$	-54.9	$^{+2.9}_{-2.8}$	404.7	$^{+7.2}_{-12.2}$	$^{+2.8}_{-2.7}$
150	5	113.6	16.12	$^{+10.8}_{-10.8}$	$+0.6$	$^{—}_{—}$	2.319	$^{+7.5}_{-13.1}$	$^{+0.2}_{-0.2}$
150	10	122.1	16.33	$^{+10.8}_{-10.6}$	$+0.1$	$^{—}_{—}$	3.432	$^{+7.0}_{-11.8}$	$^{+0.5}_{-0.5}$
150	15	124.4	16.80	$^{+10.9}_{-10.7}$	-0.2	$^{—}_{—}$	4.049	$^{+6.9}_{-11.5}$	$^{+0.7}_{-0.7}$
150	20	125.3	17.07	$^{+10.9}_{-10.7}$	-0.4	$^{—}_{—}$	4.401	$^{+6.8}_{-11.4}$	$^{+1.0}_{-0.9}$
150	30	126.1	17.30	$^{+11.0}_{-10.7}$	-0.7	$^{—}_{—}$	4.780	$^{+6.8}_{-11.3}$	$^{+1.4}_{-1.4}$
150	50	126.7	17.40	$^{+11.0}_{-10.8}$	-1.0	$^{—}_{—}$	5.097	$^{+6.7}_{-11.2}$	$^{+2.3}_{-2.2}$
200	5	118.6	19.05	$^{+9.6}_{-10.2}$	$+1.9$	$^{—}_{—}$	0.830	$^{+7.2}_{-12.3}$	$^{+0.2}_{-0.2}$
200	10	124.3	18.41	$^{+9.4}_{-10.0}$	$+2.0$	$^{—}_{—}$	0.846	$^{+6.9}_{-11.5}$	$^{+0.3}_{-0.3}$
200	15	125.5	18.31	$^{+9.4}_{-10.0}$	$+2.0$	$^{—}_{—}$	0.861	$^{+6.8}_{-11.4}$	$^{+0.5}_{-0.5}$
200	20	126.0	18.26	$^{+9.4}_{-10.0}$	$+2.0$	$^{—}_{—}$	0.873	$^{+6.8}_{-11.3}$	$^{+0.6}_{-0.6}$
200	30	126.4	18.20	$^{+9.4}_{-10.0}$	$+2.0$	$^{—}_{—}$	0.895	$^{+6.8}_{-11.3}$	$^{+0.9}_{-0.9}$
200	50	126.8	18.10	$^{+9.4}_{-10.0}$	$+1.9$	$^{—}_{—}$	0.928	$^{+6.7}_{-11.2}$	$^{+1.5}_{-1.4}$
300	5	120.7	20.09	$^{+9.2}_{-10.0}$	$+1.7$	$^{—}_{—}$	0.403	$^{+7.1}_{-12.0}$	$^{—}_{—}$
300	10	125.0	19.10	$^{+9.1}_{-9.9}$	$+1.7$	$^{—}_{—}$	0.376	$^{+6.8}_{-11.4}$	$^{+0.2}_{-0.2}$
300	15	125.9	18.90	$^{+9.0}_{-9.9}$	$+1.7$	$^{—}_{—}$	0.373	$^{+6.8}_{-11.3}$	$^{+0.2}_{-0.2}$
300	20	126.2	18.82	$^{+9.0}_{-9.9}$	$+1.7$	$^{—}_{—}$	0.373	$^{+6.8}_{-11.3}$	$^{+0.3}_{-0.3}$
300	30	126.5	18.75	$^{+9.0}_{-9.9}$	$+1.7$	$^{—}_{—}$	0.376	$^{+6.8}_{-11.2}$	$^{+0.5}_{-0.5}$
300	50	126.8	18.65	$^{+9.0}_{-9.9}$	$+1.6$	$^{—}_{—}$	0.383	$^{+6.7}_{-11.2}$	$^{+0.8}_{-0.7}$

Table 5: Cross sections and uncertainties for lightest-scalar production in the $m_h^{\text{mod+}}$ scenario for $\sqrt{s} = 8$ TeV. Uncertainties below 0.1% are not listed (—). For the PDF uncertainties see text.

m_A [GeV]	$\tan\beta$	m_H [GeV]	σ_{ggH} [pb]	$\Delta_\mu^\pm$ [%]	δY_b [%]	$\delta\Delta_b$ [%]	σ_{bbH} [pb]	$\Delta_\mu^\pm$ [%]	$\delta\Delta_b$ [%]
100	5	134.7	17.43	$^{+8.0}_{-9.4}$	-4.5	— —	0.693	$^{+6.4}_{-10.3}$	$^{+0.5}_{-0.5}$
100	10	129.3	21.67	$^{+8.3}_{-9.6}$	-6.3	— —	1.428	$^{+6.6}_{-10.9}$	$^{+0.9}_{-0.8}$
100	15	128.0	23.41	$^{+8.3}_{-9.7}$	-7.0	$^{+0.2}_{-0.2}$	1.806	$^{+6.7}_{-11.1}$	$^{+1.2}_{-1.2}$
100	20	127.5	24.27	$^{+8.4}_{-9.7}$	-7.4	$^{+0.2}_{-0.2}$	2.039	$^{+6.7}_{-11.1}$	$^{+1.6}_{-1.6}$
100	30	127.2	25.16	$^{+8.4}_{-9.7}$	-8.0	$^{+0.3}_{-0.3}$	2.361	$^{+6.7}_{-11.2}$	$^{+2.3}_{-2.2}$
100	50	127.3	26.08	$^{+8.5}_{-9.7}$	-9.0	$^{+0.6}_{-0.6}$	2.889	$^{+6.7}_{-11.1}$	$^{+3.6}_{-3.4}$
200	5	206.0	1.526	$^{+7.2}_{-8.9}$	-17.4	$^{+0.1}_{-0.1}$	0.750	$^{+4.4}_{-5.6}$	$^{+0.3}_{-0.3}$
200	10	201.8	1.860	$^{+9.7}_{-10.3}$	-41.6	$^{+0.5}_{-0.5}$	3.369	$^{+4.4}_{-5.8}$	$^{+0.6}_{-0.6}$
200	15	200.9	3.122	$^{+10.8}_{-10.9}$	-50.1	$^{+0.8}_{-0.8}$	7.601	$^{+4.5}_{-5.8}$	$^{+0.9}_{-0.9}$
200	20	200.6	4.934	$^{+11.3}_{-11.2}$	-53.0	$^{+1.2}_{-1.1}$	13.28	$^{+4.5}_{-5.8}$	$^{+1.2}_{-1.2}$
200	30	200.3	9.857	$^{+11.6}_{-11.4}$	-54.9	$^{+1.8}_{-1.7}$	28.42	$^{+4.5}_{-5.9}$	$^{+1.8}_{-1.7}$
200	50	200.1	23.73	$^{+11.8}_{-11.5}$	-55.9	$^{+2.8}_{-2.7}$	70.88	$^{+4.5}_{-5.9}$	$^{+2.8}_{-2.7}$
300	5	303.4	0.325	$^{+6.3}_{-8.9}$	-13.6	— —	0.161	$^{+3.2}_{-3.2}$	$^{+0.3}_{-0.3}$
300	10	301.1	0.257	$^{+8.4}_{-10.3}$	-37.5	$^{+0.4}_{-0.4}$	0.659	$^{+3.2}_{-3.2}$	$^{+0.6}_{-0.6}$
300	15	300.6	0.365	$^{+9.7}_{-11.1}$	-48.7	$^{+0.8}_{-0.8}$	1.454	$^{+3.2}_{-3.2}$	$^{+0.9}_{-0.9}$
300	20	300.5	0.540	$^{+10.4}_{-11.5}$	-53.1	$^{+1.1}_{-1.1}$	2.517	$^{+3.2}_{-3.2}$	$^{+1.2}_{-1.2}$
300	30	300.3	1.026	$^{+10.8}_{-11.7}$	-56.2	$^{+1.7}_{-1.7}$	5.353	$^{+3.2}_{-3.2}$	$^{+1.8}_{-1.7}$
300	50	300.2	2.410	$^{+11.1}_{-11.9}$	-57.7	$^{+2.8}_{-2.7}$	13.31	$^{+3.2}_{-3.2}$	$^{+2.8}_{-2.7}$
500	5	501.2	55.8×10^{-3}	$^{+1.6}_{-5.7}$	-0.7	— —	15.4×10^{-3}	$^{+2.3}_{-1.4}$	$^{+0.3}_{-0.3}$
500	10	500.1	18.6×10^{-3}	$^{+0.1}_{-4.8}$	-14.6	$^{+0.2}_{-0.2}$	60.9×10^{-3}	$^{+2.3}_{-1.4}$	$^{+0.6}_{-0.6}$
500	15	499.9	16.9×10^{-3}	$^{+2.2}_{-6.8}$	-37.8	$^{+0.6}_{-0.6}$	0.133	$^{+2.3}_{-1.4}$	$^{+0.9}_{-0.9}$
500	20	499.8	22.2×10^{-3}	$^{+4.7}_{-9.0}$	-50.8	$^{+1.1}_{-1.0}$	0.230	$^{+2.3}_{-1.4}$	$^{+1.2}_{-1.2}$
500	30	499.7	41.8×10^{-3}	$^{+7.7}_{-11.0}$	-58.4	$^{+1.8}_{-1.7}$	0.489	$^{+2.3}_{-1.4}$	$^{+1.8}_{-1.7}$
500	50	499.5	0.101	$^{+9.7}_{-12.0}$	-60.6	$^{+2.9}_{-2.8}$	1.214	$^{+2.3}_{-1.4}$	$^{+2.8}_{-2.7}$
1000	5	1000.6	687×10^{-6}	— -3.6	$+5.7$	— —	295×10^{-6}	$^{+1.4}_{-1.1}$	$^{+0.3}_{-0.3}$
1000	10	1000.1	124×10^{-6}	$^{+4.1}_{-17.5}$	$+17.0$	— —	1.15×10^{-3}	$^{+1.4}_{-1.1}$	$^{+0.6}_{-0.6}$
1000	15	999.9	60.1×10^{-6}	$^{+7.5}_{-26.1}$	-13.9	$^{+0.5}_{-0.5}$	2.51×10^{-3}	$^{+1.4}_{-1.1}$	$^{+0.9}_{-0.9}$
1000	20	999.9	83.0×10^{-6}	$^{+0.7}_{-9.7}$	-57.2	$^{+1.4}_{-1.3}$	4.33×10^{-3}	$^{+1.4}_{-1.1}$	$^{+1.2}_{-1.2}$
1000	30	999.8	219×10^{-6}	$^{+5.3}_{-10.9}$	-69.7	$^{+2.1}_{-2.0}$	9.19×10^{-3}	$^{+1.4}_{-1.1}$	$^{+1.8}_{-1.7}$
1000	50	999.3	660×10^{-6}	$^{+9.9}_{-13.3}$	-67.5	$^{+3.1}_{-3.0}$	22.9×10^{-3}	$^{+1.4}_{-1.1}$	$^{+2.8}_{-2.7}$

Table 6: Cross sections and uncertainties for heaviest-scalar production in the $m_h^{\text{mod+}}$ scenario for $\sqrt{s} = 8$ TeV. Uncertainties below 0.1% are not listed (—). For the PDF uncertainties see text.

m_A [GeV]	$\tan\beta$	σ_{ggA} [pb]	$\Delta_\mu^\pm$ [%]	δY_b [%]	$\delta\Delta_b$ [%]	σ_{bbA} [pb]	$\Delta_\mu^\pm$ [%]	$\delta\Delta_b$ [%]
100	5	10.61	$^{+15.6}_{-13.5}$	-47.8	$^{+0.3}_{-0.3}$	10.80	$^{+8.6}_{-15.7}$	$^{+0.3}_{-0.3}$
100	10	43.51	$^{+15.4}_{-13.4}$	-53.7	$^{+0.7}_{-0.7}$	41.90	$^{+8.6}_{-15.7}$	$^{+0.6}_{-0.6}$
100	15	98.90	$^{+15.2}_{-13.3}$	-53.1	$^{+1.0}_{-1.0}$	91.44	$^{+8.6}_{-15.7}$	$^{+0.9}_{-0.9}$
100	20	173.3	$^{+15.1}_{-13.3}$	-52.7	$^{+1.3}_{-1.2}$	157.7	$^{+8.6}_{-15.7}$	$^{+1.2}_{-1.2}$
100	30	371.6	$^{+15.0}_{-13.2}$	-52.5	$^{+1.8}_{-1.8}$	334.4	$^{+8.6}_{-15.7}$	$^{+1.8}_{-1.7}$
100	50	925.5	$^{+14.9}_{-13.2}$	-52.4	$^{+2.9}_{-2.8}$	829.0	$^{+8.6}_{-15.7}$	$^{+2.8}_{-2.7}$
200	5	0.567	$^{+9.2}_{-9.9}$	-4.3	$^{—}_{—}$	0.927	$^{+4.5}_{-5.9}$	$^{+0.3}_{-0.3}$
200	10	0.962	$^{+12.4}_{-11.7}$	-57.5	$^{+0.7}_{-0.7}$	3.598	$^{+4.5}_{-5.9}$	$^{+0.6}_{-0.6}$
200	15	2.363	$^{+11.9}_{-11.5}$	-59.0	$^{+1.0}_{-1.0}$	7.852	$^{+4.5}_{-5.9}$	$^{+0.9}_{-0.9}$
200	20	4.332	$^{+11.7}_{-11.4}$	-58.1	$^{+1.3}_{-1.3}$	13.54	$^{+4.5}_{-5.9}$	$^{+1.2}_{-1.2}$
200	30	9.635	$^{+11.4}_{-11.3}$	-57.1	$^{+1.8}_{-1.8}$	28.72	$^{+4.5}_{-5.9}$	$^{+1.8}_{-1.7}$
200	50	24.48	$^{+11.3}_{-11.2}$	-56.5	$^{+2.9}_{-2.8}$	71.19	$^{+4.5}_{-5.9}$	$^{+2.8}_{-2.7}$
300	5	0.324	$^{+7.2}_{-8.9}$	$+8.2$	$^{—}_{—}$	0.174	$^{+3.2}_{-3.2}$	$^{+0.3}_{-0.3}$
300	10	0.100	$^{+9.4}_{-10.2}$	-28.6	$^{+0.4}_{-0.4}$	0.675	$^{+3.2}_{-3.2}$	$^{+0.6}_{-0.6}$
300	15	0.193	$^{+11.1}_{-11.6}$	-60.2	$^{+1.0}_{-1.0}$	1.473	$^{+3.2}_{-3.2}$	$^{+0.9}_{-0.9}$
300	20	0.373	$^{+11.1}_{-11.8}$	-62.2	$^{+1.4}_{-1.3}$	2.540	$^{+3.2}_{-3.2}$	$^{+1.2}_{-1.2}$
300	30	0.892	$^{+10.8}_{-11.7}$	-60.7	$^{+1.9}_{-1.9}$	5.386	$^{+3.2}_{-3.2}$	$^{+1.8}_{-1.7}$
300	50	2.370	$^{+10.6}_{-11.6}$	-59.2	$^{+2.9}_{-2.8}$	13.35	$^{+3.2}_{-3.2}$	$^{+2.8}_{-2.7}$
500	5	0.102	$^{+4.8}_{-8.1}$	-4.1	$^{—}_{—}$	15.7×10^{-3}	$^{+2.3}_{-1.4}$	$^{+0.3}_{-0.3}$
500	10	35.7×10^{-3}	$^{+10.1}_{-11.1}$	-18.1	$^{+0.2}_{-0.2}$	61.1×10^{-3}	$^{+2.3}_{-1.4}$	$^{+0.6}_{-0.6}$
500	15	29.0×10^{-3}	$^{+13.5}_{-13.2}$	-35.3	$^{+0.5}_{-0.5}$	0.133	$^{+2.3}_{-1.4}$	$^{+0.9}_{-0.9}$
500	20	32.9×10^{-3}	$^{+14.2}_{-13.8}$	-46.6	$^{+0.9}_{-0.9}$	0.230	$^{+2.3}_{-1.4}$	$^{+1.2}_{-1.2}$
500	30	51.9×10^{-3}	$^{+13.0}_{-13.5}$	-55.5	$^{+1.6}_{-1.6}$	0.487	$^{+2.3}_{-1.4}$	$^{+1.8}_{-1.7}$
500	50	0.113	$^{+11.4}_{-12.8}$	-59.2	$^{+2.8}_{-2.7}$	1.208	$^{+2.3}_{-1.4}$	$^{+2.8}_{-2.7}$
1000	5	1.18×10^{-3}	$^{+3.0}_{-7.1}$	-5.6	$^{—}_{—}$	296×10^{-6}	$^{+1.4}_{-1.1}$	$^{+0.3}_{-0.3}$
1000	10	435×10^{-6}	$^{+6.3}_{-10.0}$	-19.3	$^{+0.2}_{-0.2}$	1.15×10^{-3}	$^{+1.4}_{-1.1}$	$^{+0.6}_{-0.6}$
1000	15	337×10^{-6}	$^{+9.9}_{-12.3}$	-33.4	$^{+0.4}_{-0.4}$	2.51×10^{-3}	$^{+1.4}_{-1.1}$	$^{+0.9}_{-0.9}$
1000	20	348×10^{-6}	$^{+11.5}_{-13.5}$	-43.6	$^{+0.8}_{-0.8}$	4.33×10^{-3}	$^{+1.4}_{-1.1}$	$^{+1.2}_{-1.2}$
1000	30	476×10^{-6}	$^{+12.0}_{-14.0}$	-53.9	$^{+1.5}_{-1.4}$	9.17×10^{-3}	$^{+1.4}_{-1.1}$	$^{+1.8}_{-1.7}$
1000	50	920×10^{-6}	$^{+11.3}_{-13.9}$	-60.1	$^{+2.7}_{-2.5}$	22.7×10^{-3}	$^{+1.4}_{-1.1}$	$^{+2.8}_{-2.7}$

Table 7: Cross sections and uncertainties for pseudoscalar production in the $m_h^{\text{mod+}}$ scenario for $\sqrt{s} = 8$ TeV. Uncertainties below 0.1% are not listed (—). For the PDF uncertainties see text.

m_A [GeV]	$\tan\beta$	m_h [GeV]	σ_{ggh} [pb]	$\Delta_\mu^\pm$ [%]	δY_b [%]	$\delta\Delta_b$ [%]	σ_{bbh} [pb]	$\Delta_\mu^\pm$ [%]	$\delta\Delta_b$ [%]
100	5	91.5	16.24	$^{+17.3}_{-14.5}$	-38.9	— —	12.92	$^{+9.4}_{-17.8}$	— —
100	10	97.3	45.45	$^{+17.0}_{-14.2}$	-51.6	— —	45.95	$^{+8.8}_{-16.3}$	— —
100	15	98.7	101.7	$^{+16.4}_{-13.9}$	-52.0	— —	102.1	$^{+8.7}_{-16.0}$	— —
100	20	99.3	182.6	$^{+16.2}_{-13.8}$	-51.7	$^{+0.1}_{-0.1}$	181.3	$^{+8.6}_{-15.9}$	$^{+0.1}_{-0.1}$
100	30	99.7	416.8	$^{+16.0}_{-13.7}$	-51.4	$^{+0.2}_{-0.2}$	409.6	$^{+8.6}_{-15.8}$	$^{+0.2}_{-0.2}$
100	50	99.9	1182.	$^{+15.9}_{-13.6}$	-51.1	$^{+0.3}_{-0.3}$	1153.	$^{+8.6}_{-15.7}$	$^{+0.3}_{-0.3}$
120	5	104.1	12.11	$^{+13.9}_{-12.6}$	-14.3	— —	6.521	$^{+8.2}_{-14.8}$	— —
120	10	113.1	17.34	$^{+15.7}_{-13.5}$	-38.9	— —	20.88	$^{+7.5}_{-13.2}$	— —
120	15	116.0	32.84	$^{+16.0}_{-13.6}$	-49.7	— —	46.46	$^{+7.4}_{-12.7}$	— —
120	20	117.4	58.48	$^{+15.8}_{-13.5}$	-52.7	$^{+0.1}_{-0.1}$	84.37	$^{+7.3}_{-12.5}$	$^{+0.1}_{-0.1}$
120	30	118.7	140.5	$^{+15.3}_{-13.3}$	-53.4	$^{+0.2}_{-0.2}$	198.9	$^{+7.2}_{-12.3}$	$^{+0.2}_{-0.2}$
120	50	119.5	426.0	$^{+14.9}_{-13.1}$	-52.9	$^{+0.3}_{-0.3}$	584.9	$^{+7.1}_{-12.2}$	$^{+0.3}_{-0.3}$
150	5	114.0	15.70	$^{+10.9}_{-10.8}$	$+0.3$	— —	2.329	$^{+7.5}_{-13.0}$	— —
150	10	122.4	16.02	$^{+10.9}_{-10.7}$	-0.3	— —	3.473	$^{+7.0}_{-11.8}$	— —
150	15	124.5	16.52	$^{+11.0}_{-10.7}$	-0.6	— —	4.087	$^{+6.9}_{-11.5}$	— —
150	20	125.5	16.79	$^{+11.0}_{-10.8}$	-0.9	— —	4.421	$^{+6.8}_{-11.4}$	$^{+0.1}_{-0.1}$
150	30	126.2	17.01	$^{+11.1}_{-10.8}$	-1.1	— —	4.737	$^{+6.8}_{-11.3}$	$^{+0.2}_{-0.2}$
150	50	127.0	17.03	$^{+11.0}_{-10.8}$	-1.3	— —	4.830	$^{+6.7}_{-11.2}$	$^{+0.3}_{-0.3}$
200	5	118.8	18.64	$^{+9.7}_{-10.3}$	$+1.7$	— —	0.824	$^{+7.2}_{-12.3}$	— —
200	10	124.4	18.07	$^{+9.5}_{-10.1}$	$+1.7$	— —	0.839	$^{+6.9}_{-11.5}$	— —
200	15	125.6	17.97	$^{+9.5}_{-10.1}$	$+1.7$	— —	0.852	$^{+6.8}_{-11.4}$	— —
200	20	126.1	17.92	$^{+9.5}_{-10.0}$	$+1.6$	— —	0.861	$^{+6.8}_{-11.3}$	— —
200	30	126.5	17.86	$^{+9.5}_{-10.0}$	$+1.5$	— —	0.875	$^{+6.8}_{-11.2}$	— —
200	50	127.1	17.74	$^{+9.4}_{-10.0}$	$+1.3$	— —	0.882	$^{+6.7}_{-11.2}$	$^{+0.2}_{-0.2}$
300	5	120.9	19.68	$^{+9.3}_{-10.1}$	$+1.5$	— —	0.400	$^{+7.1}_{-12.0}$	— —
300	10	125.1	18.74	$^{+9.2}_{-10.0}$	$+1.4$	— —	0.374	$^{+6.8}_{-11.4}$	— —
300	15	125.9	18.55	$^{+9.1}_{-9.9}$	$+1.4$	— —	0.370	$^{+6.8}_{-11.3}$	— —
300	20	126.3	18.47	$^{+9.1}_{-9.9}$	$+1.3$	— —	0.370	$^{+6.8}_{-11.3}$	— —
300	30	126.6	18.39	$^{+9.1}_{-9.9}$	$+1.2$	— —	0.371	$^{+6.7}_{-11.2}$	— —
300	50	127.0	18.27	$^{+9.1}_{-9.9}$	$+0.9$	— —	0.372	$^{+6.7}_{-11.2}$	— —

Table 8: Cross sections and uncertainties for lightest-scalar production in the $m_h^{\text{mod}-}$ scenario for $\sqrt{s} = 8$ TeV. Uncertainties below 0.1% are not listed (—). For the PDF uncertainties see text.

m_A [GeV]	$\tan\beta$	m_H [GeV]	σ_{ggH} [pb]	$\Delta_\mu^\pm$ [%]	δY_b [%]	$\delta\Delta_b$ [%]	σ_{bbH} [pb]	$\Delta_\mu^\pm$ [%]	$\delta\Delta_b$ [%]
100	5	134.3	17.53	$^{+8.1}_{-9.5}$	-4.4	— —	0.704	$^{+6.4}_{-10.3}$	— —
100	10	129.1	21.64	$^{+8.4}_{-9.7}$	-6.1	— —	1.410	$^{+6.6}_{-10.9}$	— —
100	15	127.8	23.23	$^{+8.4}_{-9.7}$	-6.8	— —	1.747	$^{+6.7}_{-11.1}$	$^{+0.1}_{-0.1}$
100	20	127.4	23.97	$^{+8.5}_{-9.8}$	-7.3	— —	1.941	$^{+6.7}_{-11.1}$	$^{+0.2}_{-0.2}$
100	30	127.2	24.67	$^{+8.5}_{-9.8}$	-7.9	— —	2.187	$^{+6.7}_{-11.2}$	$^{+0.3}_{-0.3}$
100	50	127.5	25.20	$^{+8.5}_{-9.8}$	-8.8	— —	2.512	$^{+6.7}_{-11.1}$	$^{+0.4}_{-0.4}$
200	5	205.8	1.541	$^{+7.3}_{-9.0}$	-17.2	— —	0.784	$^{+4.4}_{-5.6}$	— —
200	10	201.7	1.963	$^{+9.8}_{-10.3}$	-41.0	— —	3.631	$^{+4.4}_{-5.8}$	— —
200	15	200.8	3.436	$^{+10.9}_{-11.0}$	-49.0	— —	8.463	$^{+4.5}_{-5.8}$	— —
200	20	200.5	5.636	$^{+11.4}_{-11.3}$	-51.8	$^{+0.1}_{-0.1}$	15.27	$^{+4.5}_{-5.8}$	$^{+0.1}_{-0.1}$
200	30	200.3	12.07	$^{+11.8}_{-11.5}$	-53.6	$^{+0.2}_{-0.2}$	34.89	$^{+4.5}_{-5.9}$	$^{+0.2}_{-0.2}$
200	50	200.1	33.11	$^{+12.0}_{-11.6}$	-54.4	$^{+0.3}_{-0.3}$	98.75	$^{+4.5}_{-5.9}$	$^{+0.3}_{-0.3}$
300	5	303.3	0.331	$^{+6.3}_{-8.9}$	-13.3	— —	0.168	$^{+3.2}_{-3.2}$	— —
300	10	301.1	0.272	$^{+8.5}_{-10.4}$	-36.7	— —	0.708	$^{+3.2}_{-3.2}$	— —
300	15	300.6	0.402	$^{+9.8}_{-11.2}$	-47.6	— —	1.615	$^{+3.2}_{-3.2}$	— —
300	20	300.5	0.617	$^{+10.5}_{-11.5}$	-51.8	$^{+0.1}_{-0.1}$	2.891	$^{+3.2}_{-3.2}$	$^{+0.1}_{-0.1}$
300	30	300.3	1.258	$^{+11.0}_{-11.8}$	-54.8	$^{+0.2}_{-0.2}$	6.565	$^{+3.2}_{-3.2}$	$^{+0.2}_{-0.2}$
300	50	300.1	3.368	$^{+11.2}_{-11.9}$	-56.2	$^{+0.3}_{-0.3}$	18.53	$^{+3.2}_{-3.2}$	$^{+0.3}_{-0.3}$
500	5	501.2	56.6×10^{-3}	$^{+1.7}_{-5.8}$	-0.7	— —	16.0×10^{-3}	$^{+2.3}_{-1.4}$	— —
500	10	500.1	19.7×10^{-3}	$^{+0.4}_{-5.1}$	-14.8	— —	65.4×10^{-3}	$^{+2.3}_{-1.4}$	— —
500	15	499.9	18.9×10^{-3}	$^{+2.6}_{-7.2}$	-37.3	— —	0.148	$^{+2.3}_{-1.4}$	— —
500	20	499.8	26.0×10^{-3}	$^{+5.1}_{-9.3}$	-49.6	$^{+0.1}_{-0.1}$	0.264	$^{+2.3}_{-1.4}$	$^{+0.1}_{-0.1}$
500	30	499.7	52.3×10^{-3}	$^{+8.1}_{-11.2}$	-56.7	$^{+0.2}_{-0.2}$	0.599	$^{+2.3}_{-1.4}$	$^{+0.2}_{-0.2}$
500	50	499.4	0.144	$^{+10.0}_{-12.2}$	-58.7	$^{+0.3}_{-0.3}$	1.691	$^{+2.3}_{-1.4}$	$^{+0.3}_{-0.3}$
1000	5	1000.6	698×10^{-6}	— -3.8	$+5.4$	— —	306×10^{-6}	$^{+1.4}_{-1.1}$	— —
1000	10	1000.1	136×10^{-6}	$^{+3.2}_{-15.5}$	$+12.5$	— —	1.23×10^{-3}	$^{+1.4}_{-1.1}$	— —
1000	15	999.9	80.7×10^{-6}	$^{+3.3}_{-18.1}$	-21.5	— —	2.79×10^{-3}	$^{+1.4}_{-1.1}$	— —
1000	20	999.9	120×10^{-6}	— -5.5	-54.3	$^{+0.1}_{-0.1}$	4.97×10^{-3}	$^{+1.4}_{-1.1}$	$^{+0.1}_{-0.1}$
1000	30	999.7	314×10^{-6}	$^{+6.6}_{-11.6}$	-64.0	$^{+0.2}_{-0.2}$	11.3×10^{-3}	$^{+1.4}_{-1.1}$	$^{+0.2}_{-0.2}$
1000	50	999.1	1.02×10^{-3}	$^{+10.3}_{-13.4}$	-63.3	$^{+0.3}_{-0.3}$	31.8×10^{-3}	$^{+1.4}_{-1.1}$	$^{+0.3}_{-0.3}$

Table 9: Cross sections and uncertainties for heaviest-scalar production in the $m_h^{\text{mod}-}$ scenario for $\sqrt{s} = 8$ TeV. Uncertainties below 0.1% are not listed (—). For the PDF uncertainties see text.

m_A [GeV]	$\tan\beta$	σ_{ggA} [pb]	$\Delta_\mu^\pm$ [%]	δY_b [%]	$\delta\Delta_b$ [%]	σ_{bbA} [pb]	$\Delta_\mu^\pm$ [%]	$\delta\Delta_b$ [%]
100	5	11.00	$^{+15.6}_{-13.6}$	-47.0	$^{—}_{—}$	11.22	$^{+8.6}_{-15.7}$	$^{—}_{—}$
100	10	46.87	$^{+15.4}_{-13.4}$	-52.2	$^{—}_{—}$	44.98	$^{+8.6}_{-15.7}$	$^{—}_{—}$
100	15	110.1	$^{+15.2}_{-13.3}$	-51.5	$^{—}_{—}$	101.5	$^{+8.6}_{-15.7}$	$^{—}_{—}$
100	20	199.6	$^{+15.1}_{-13.3}$	-51.2	$^{+0.1}_{-0.1}$	181.0	$^{+8.6}_{-15.7}$	$^{+0.1}_{-0.1}$
100	30	457.1	$^{+15.0}_{-13.2}$	-50.9	$^{+0.2}_{-0.2}$	409.9	$^{+8.6}_{-15.7}$	$^{+0.2}_{-0.2}$
100	50	1294.	$^{+15.0}_{-13.2}$	-50.7	$^{+0.3}_{-0.3}$	1153.	$^{+8.6}_{-15.7}$	$^{+0.3}_{-0.3}$
200	5	0.570	$^{+9.3}_{-9.9}$	-5.4	$^{—}_{—}$	0.963	$^{+4.5}_{-5.9}$	$^{—}_{—}$
200	10	1.039	$^{+12.4}_{-11.7}$	-56.6	$^{—}_{—}$	3.863	$^{+4.5}_{-5.9}$	$^{—}_{—}$
200	15	2.645	$^{+11.9}_{-11.5}$	-57.4	$^{+0.1}_{-0.1}$	8.718	$^{+4.5}_{-5.9}$	$^{—}_{—}$
200	20	5.009	$^{+11.7}_{-11.4}$	-56.4	$^{+0.1}_{-0.1}$	15.55	$^{+4.5}_{-5.9}$	$^{+0.1}_{-0.1}$
200	30	11.89	$^{+11.5}_{-11.3}$	-55.4	$^{+0.2}_{-0.2}$	35.20	$^{+4.5}_{-5.9}$	$^{+0.2}_{-0.2}$
200	50	34.28	$^{+11.4}_{-11.2}$	-54.9	$^{+0.3}_{-0.3}$	99.04	$^{+4.5}_{-5.9}$	$^{+0.3}_{-0.3}$
300	5	0.323	$^{+7.2}_{-8.9}$	$+7.9$	$^{—}_{—}$	0.181	$^{+3.2}_{-3.2}$	$^{—}_{—}$
300	10	0.105	$^{+9.6}_{-10.3}$	-30.9	$^{—}_{—}$	0.725	$^{+3.2}_{-3.2}$	$^{—}_{—}$
300	15	0.216	$^{+11.2}_{-11.7}$	-59.6	$^{+0.1}_{-0.1}$	1.635	$^{+3.2}_{-3.2}$	$^{—}_{—}$
300	20	0.435	$^{+11.1}_{-11.8}$	-60.7	$^{+0.1}_{-0.1}$	2.916	$^{+3.2}_{-3.2}$	$^{+0.1}_{-0.1}$
300	30	1.108	$^{+10.9}_{-11.7}$	-58.9	$^{+0.2}_{-0.2}$	6.603	$^{+3.2}_{-3.2}$	$^{+0.2}_{-0.2}$
300	50	3.331	$^{+10.7}_{-11.7}$	-57.5	$^{+0.3}_{-0.3}$	18.58	$^{+3.2}_{-3.2}$	$^{+0.3}_{-0.3}$
500	5	0.102	$^{+4.9}_{-8.1}$	-4.1	$^{—}_{—}$	16.4×10^{-3}	$^{+2.3}_{-1.4}$	$^{—}_{—}$
500	10	36.4×10^{-3}	$^{+10.3}_{-11.2}$	-18.5	$^{—}_{—}$	65.6×10^{-3}	$^{+2.3}_{-1.4}$	$^{—}_{—}$
500	15	30.7×10^{-3}	$^{+13.7}_{-13.4}$	-35.7	$^{—}_{—}$	0.148	$^{+2.3}_{-1.4}$	$^{—}_{—}$
500	20	36.4×10^{-3}	$^{+14.2}_{-13.9}$	-46.7	$^{—}_{—}$	0.264	$^{+2.3}_{-1.4}$	$^{+0.1}_{-0.1}$
500	30	62.4×10^{-3}	$^{+12.9}_{-13.5}$	-54.9	$^{+0.2}_{-0.2}$	0.598	$^{+2.3}_{-1.4}$	$^{+0.2}_{-0.2}$
500	50	0.156	$^{+11.3}_{-12.8}$	-58.0	$^{+0.3}_{-0.3}$	1.681	$^{+2.3}_{-1.4}$	$^{+0.3}_{-0.3}$
1000	5	1.19×10^{-3}	$^{+3.1}_{-7.2}$	-5.6	$^{—}_{—}$	308×10^{-6}	$^{+1.4}_{-1.1}$	$^{—}_{—}$
1000	10	444×10^{-6}	$^{+6.6}_{-10.2}$	-19.3	$^{—}_{—}$	1.23×10^{-3}	$^{+1.4}_{-1.1}$	$^{—}_{—}$
1000	15	355×10^{-6}	$^{+10.2}_{-12.5}$	-33.6	$^{—}_{—}$	2.79×10^{-3}	$^{+1.4}_{-1.1}$	$^{—}_{—}$
1000	20	381×10^{-6}	$^{+11.7}_{-13.6}$	-43.7	$^{—}_{—}$	4.97×10^{-3}	$^{+1.4}_{-1.1}$	$^{+0.1}_{-0.1}$
1000	30	564×10^{-6}	$^{+12.0}_{-14.1}$	-53.7	$^{+0.2}_{-0.2}$	11.2×10^{-3}	$^{+1.4}_{-1.1}$	$^{+0.2}_{-0.2}$
1000	50	1.26×10^{-3}	$^{+11.4}_{-13.9}$	-59.4	$^{+0.3}_{-0.3}$	31.6×10^{-3}	$^{+1.4}_{-1.1}$	$^{+0.3}_{-0.3}$

Table 10: Cross sections and uncertainties for pseudoscalar production in the $m_h^{\text{mod}-}$ scenario for $\sqrt{s} = 8$ TeV. Uncertainties below 0.1% are not listed (—). For the PDF uncertainties see text.

m_A [GeV]	$\tan\beta$	m_h [GeV]	σ_{ggh} [pb]	$\Delta_\mu^\pm$ [%]	δY_b [%]	$\delta\Delta_b$ [%]	σ_{bbh} [pb]	$\Delta_\mu^\pm$ [%]	$\delta\Delta_b$ [%]
100	5	88.1	18.27	$^{+17.4}_{-14.6}$	-37.3	$^{+0.8}_{-0.8}$	12.88	$^{+9.8}_{-18.8}$	$^{+1.1}_{-1.1}$
100	10	94.3	41.55	$^{+17.3}_{-14.4}$	-52.2	$^{+2.2}_{-2.1}$	39.99	$^{+9.1}_{-17.1}$	$^{+2.2}_{-2.1}$
100	15	95.8	81.16	$^{+16.7}_{-14.1}$	-53.6	$^{+3.3}_{-3.1}$	79.26	$^{+9.0}_{-16.7}$	$^{+3.1}_{-3.0}$
100	20	96.4	130.2	$^{+16.3}_{-13.9}$	-53.7	$^{+4.2}_{-4.0}$	126.6	$^{+8.9}_{-16.6}$	$^{+4.0}_{-3.8}$
100	30	96.8	243.2	$^{+15.9}_{-13.7}$	-53.5	$^{+5.8}_{-5.4}$	235.0	$^{+8.9}_{-16.4}$	$^{+5.6}_{-5.2}$
100	50	97.0	484.8	$^{+15.5}_{-13.5}$	-53.4	$^{+8.4}_{-7.5}$	468.1	$^{+8.8}_{-16.4}$	$^{+8.1}_{-7.2}$
120	5	101.2	12.97	$^{+13.5}_{-12.4}$	-13.9	$^{+0.3}_{-0.3}$	6.357	$^{+8.4}_{-15.4}$	$^{+1.0}_{-1.0}$
120	10	110.5	16.39	$^{+15.3}_{-13.3}$	-35.5	$^{+1.5}_{-1.4}$	17.64	$^{+7.7}_{-13.6}$	$^{+2.1}_{-2.0}$
120	15	113.6	26.08	$^{+15.9}_{-13.6}$	-47.5	$^{+2.8}_{-2.7}$	34.69	$^{+7.5}_{-13.1}$	$^{+3.0}_{-2.9}$
120	20	115.0	40.03	$^{+15.9}_{-13.6}$	-52.3	$^{+4.0}_{-3.7}$	56.34	$^{+7.4}_{-12.9}$	$^{+3.9}_{-3.7}$
120	30	116.3	76.24	$^{+15.4}_{-13.3}$	-54.9	$^{+5.8}_{-5.4}$	108.8	$^{+7.3}_{-12.7}$	$^{+5.5}_{-5.1}$
120	50	117.1	161.4	$^{+14.7}_{-13.0}$	-55.3	$^{+8.5}_{-7.6}$	227.6	$^{+7.3}_{-12.5}$	$^{+8.0}_{-7.1}$
150	5	111.2	15.00	$^{+9.8}_{-10.3}$	—	—	2.282	$^{+7.7}_{-13.5}$	$^{+0.8}_{-0.8}$
150	10	119.6	14.84	$^{+9.7}_{-10.1}$	-0.3	—	3.057	$^{+7.1}_{-12.2}$	$^{+1.6}_{-1.6}$
150	15	121.7	15.04	$^{+9.6}_{-10.0}$	-0.4	—	3.313	$^{+7.0}_{-11.9}$	$^{+2.4}_{-2.3}$
150	20	122.6	15.13	$^{+9.5}_{-9.9}$	-0.4	—	3.345	$^{+7.0}_{-11.8}$	$^{+3.0}_{-2.9}$
150	30	123.2	15.16	$^{+9.3}_{-9.9}$	-0.5	—	3.210	$^{+6.9}_{-11.7}$	$^{+4.1}_{-3.8}$
150	50	123.7	15.11	$^{+9.0}_{-9.7}$	-0.7	—	2.843	$^{+6.9}_{-11.6}$	$^{+5.8}_{-5.2}$
200	5	115.9	16.78	$^{+8.3}_{-9.5}$	$+1.8$	—	0.837	$^{+7.4}_{-12.7}$	$^{+0.5}_{-0.5}$
200	10	121.5	15.99	$^{+8.0}_{-9.3}$	$+1.8$	—	0.805	$^{+7.0}_{-11.9}$	$^{+1.0}_{-1.0}$
200	15	122.7	15.83	$^{+7.9}_{-9.3}$	$+1.7$	—	0.781	$^{+7.0}_{-11.7}$	$^{+1.5}_{-1.4}$
200	20	123.1	15.76	$^{+7.8}_{-9.2}$	$+1.6$	—	0.759	$^{+6.9}_{-11.7}$	$^{+1.9}_{-1.8}$
200	30	123.5	15.70	$^{+7.8}_{-9.2}$	$+1.3$	—	0.720	$^{+6.9}_{-11.6}$	$^{+2.5}_{-2.3}$
200	50	123.8	15.63	$^{+7.7}_{-9.1}$	$+0.5$	$^{+0.1}_{-0.1}$	0.663	$^{+6.9}_{-11.6}$	$^{+3.4}_{-3.1}$
300	5	117.8	17.32	$^{+7.7}_{-9.3}$	$+1.7$	—	0.421	$^{+7.2}_{-12.4}$	$^{+0.3}_{-0.3}$
300	10	122.1	16.36	$^{+7.5}_{-9.1}$	$+1.6$	—	0.383	$^{+7.0}_{-11.8}$	$^{+0.5}_{-0.5}$
300	15	123.0	16.14	$^{+7.6}_{-9.1}$	$+1.6$	—	0.371	$^{+6.9}_{-11.7}$	$^{+0.7}_{-0.7}$
300	20	123.3	16.08	$^{+7.5}_{-9.1}$	$+1.4$	—	0.364	$^{+6.9}_{-11.7}$	$^{+0.9}_{-0.8}$
300	30	123.6	16.00	$^{+7.5}_{-9.1}$	$+1.0$	—	0.354	$^{+6.9}_{-11.6}$	$^{+1.2}_{-1.1}$
300	50	123.8	15.92	$^{+7.4}_{-9.0}$	$+0.2$	—	0.340	$^{+6.9}_{-11.6}$	$^{+1.5}_{-1.4}$

Table 11: Cross sections and uncertainties for lightest-scalar production in the *light-stop* scenario for $\sqrt{s} = 8$ TeV. Uncertainties below 0.1% are not listed (—). For the PDF uncertainties see text.

m_A [GeV]	$\tan\beta$	m_H [GeV]	σ_{ggH} [pb]	$\Delta_\mu^\pm$ [%]	δY_b [%]	$\delta\Delta_b$ [%]	σ_{bbH} [pb]	$\Delta_\mu^\pm$ [%]	$\delta\Delta_b$ [%]
100	5	130.9	13.85	$^{+5.9}_{-8.4}$	-5.0	$^{+0.2}_{-0.2}$	0.650	$^{+6.5}_{-10.7}$	$^{+1.8}_{-1.7}$
100	10	125.9	17.64	$^{+6.4}_{-8.7}$	-6.5	$^{+0.4}_{-0.4}$	1.163	$^{+6.8}_{-11.3}$	$^{+3.2}_{-3.0}$
100	15	124.7	19.01	$^{+6.6}_{-8.8}$	-6.7	$^{+0.5}_{-0.5}$	1.287	$^{+6.9}_{-11.5}$	$^{+4.5}_{-4.3}$
100	20	124.3	19.53	$^{+6.6}_{-8.8}$	-6.7	$^{+0.7}_{-0.6}$	1.283	$^{+6.9}_{-11.5}$	$^{+5.8}_{-5.4}$
100	30	124.0	19.79	$^{+6.6}_{-8.8}$	-6.7	$^{+0.9}_{-0.8}$	1.184	$^{+6.9}_{-11.6}$	$^{+8.1}_{-7.4}$
100	50	123.9	19.64	$^{+6.6}_{-8.8}$	-6.8	$^{+1.2}_{-1.1}$	0.982	$^{+6.9}_{-11.6}$	$^{+12.0}_{-10.5}$
200	5	203.7	0.919	$^{+4.6}_{-7.3}$	-23.8	$^{+0.5}_{-0.5}$	0.715	$^{+4.4}_{-5.7}$	$^{+1.3}_{-1.3}$
200	10	199.9	1.266	$^{+8.9}_{-9.7}$	-48.9	$^{+2.0}_{-1.9}$	2.943	$^{+4.5}_{-5.9}$	$^{+2.3}_{-2.2}$
200	15	199.1	2.178	$^{+10.4}_{-10.7}$	-54.6	$^{+3.2}_{-3.0}$	6.144	$^{+4.5}_{-5.9}$	$^{+3.2}_{-3.1}$
200	20	198.9	3.341	$^{+10.9}_{-11.0}$	-56.2	$^{+4.2}_{-3.9}$	9.987	$^{+4.5}_{-5.9}$	$^{+4.1}_{-3.9}$
200	30	198.7	6.051	$^{+11.2}_{-11.2}$	-57.1	$^{+5.8}_{-5.4}$	18.77	$^{+4.5}_{-5.9}$	$^{+5.6}_{-5.2}$
200	50	198.5	11.88	$^{+11.2}_{-11.1}$	-57.5	$^{+8.5}_{-7.6}$	37.63	$^{+4.5}_{-5.9}$	$^{+8.1}_{-7.2}$
300	5	301.7	0.161	$^{+2.9}_{-6.7}$	-20.3	$^{+0.4}_{-0.4}$	0.150	$^{+3.2}_{-3.2}$	$^{+1.3}_{-1.2}$
300	10	299.6	0.137	$^{+6.6}_{-9.3}$	-50.1	$^{+1.9}_{-1.9}$	0.567	$^{+3.2}_{-3.2}$	$^{+2.3}_{-2.2}$
300	15	299.2	0.211	$^{+8.6}_{-10.6}$	-57.7	$^{+3.2}_{-3.1}$	1.159	$^{+3.3}_{-3.2}$	$^{+3.2}_{-3.1}$
300	20	299.1	0.315	$^{+9.5}_{-11.0}$	-59.6	$^{+4.3}_{-4.0}$	1.869	$^{+3.3}_{-3.2}$	$^{+4.1}_{-3.9}$
300	30	299.0	0.564	$^{+10.1}_{-11.3}$	-60.5	$^{+6.0}_{-5.5}$	3.493	$^{+3.3}_{-3.2}$	$^{+5.6}_{-5.2}$
300	50	298.9	1.107	$^{+10.2}_{-11.4}$	-60.9	$^{+8.7}_{-7.7}$	6.979	$^{+3.3}_{-3.2}$	$^{+8.1}_{-7.2}$
400	5	401.0	80.4×10^{-3}	$^{\text{—}}_{-4.2}$	-6.6	$^{+0.1}_{-0.1}$	41.8×10^{-3}	$^{+2.6}_{-2.0}$	$^{+1.2}_{-1.2}$
400	10	399.6	27.0×10^{-3}	$^{+0.6}_{-5.1}$	-39.5	$^{+1.6}_{-1.5}$	0.154	$^{+2.6}_{-2.0}$	$^{+2.3}_{-2.2}$
400	15	399.3	31.4×10^{-3}	$^{+2.5}_{-7.1}$	-61.0	$^{+3.4}_{-3.3}$	0.313	$^{+2.6}_{-2.0}$	$^{+3.2}_{-3.1}$
400	20	399.2	45.9×10^{-3}	$^{+5.2}_{-9.1}$	-65.4	$^{+4.7}_{-4.4}$	0.504	$^{+2.6}_{-2.0}$	$^{+4.1}_{-3.9}$
400	30	399.1	84.9×10^{-3}	$^{+7.5}_{-10.6}$	-65.7	$^{+6.5}_{-6.0}$	0.941	$^{+2.6}_{-2.0}$	$^{+5.6}_{-5.2}$
400	50	399.1	0.173	$^{+8.8}_{-11.2}$	-64.9	$^{+9.2}_{-8.1}$	1.878	$^{+2.6}_{-2.0}$	$^{+8.1}_{-7.2}$
500	5	500.4	23.6×10^{-3}	$^{+1.3}_{-9.1}$	$+4.4$	$^{\text{—}}_{\text{—}}$	14.2×10^{-3}	$^{+2.3}_{-1.4}$	$^{+1.2}_{-1.2}$
500	10	499.4	2.81×10^{-3}	$^{+18.6}_{-46.2}$	-1.3	$^{+0.9}_{-0.9}$	51.6×10^{-3}	$^{+2.3}_{-1.4}$	$^{+2.3}_{-2.2}$
500	15	499.3	2.47×10^{-3}	$^{+9.8}_{-32.2}$	-69.4	$^{+5.2}_{-4.9}$	0.105	$^{+2.3}_{-1.4}$	$^{+3.2}_{-3.1}$
500	20	499.2	5.12×10^{-3}	$^{+1.2}_{-7.5}$	-80.8	$^{+6.6}_{-6.1}$	0.169	$^{+2.3}_{-1.4}$	$^{+4.1}_{-3.9}$
500	30	499.2	13.4×10^{-3}	$^{+5.2}_{-9.3}$	-75.8	$^{+7.8}_{-7.1}$	0.315	$^{+2.3}_{-1.4}$	$^{+5.6}_{-5.2}$
500	50	499.1	33.2×10^{-3}	$^{+8.3}_{-11.3}$	-70.6	$^{+10.1}_{-8.9}$	0.628	$^{+2.3}_{-1.4}$	$^{+8.1}_{-7.2}$

Table 12: Cross sections and uncertainties for heaviest-scalar production in the *light-stop* scenario for $\sqrt{s} = 8$ TeV. Uncertainties below 0.1% are not listed (—). For the PDF uncertainties see text.

m_A [GeV]	$\tan\beta$	σ_{ggA} [pb]	$\Delta_\mu^\pm$ [%]	δY_b [%]	$\delta\Delta_b$ [%]	σ_{bbA} [pb]	$\Delta_\mu^\pm$ [%]	$\delta\Delta_b$ [%]
100	5	9.685	$^{+15.5}_{-13.5}$	-47.8	$^{+1.2}_{-1.2}$	9.841	$^{+8.6}_{-15.7}$	$^{+1.2}_{-1.2}$
100	10	36.48	$^{+15.5}_{-13.5}$	-54.1	$^{+2.4}_{-2.3}$	35.29	$^{+8.6}_{-15.7}$	$^{+2.3}_{-2.2}$
100	15	76.79	$^{+15.2}_{-13.3}$	-53.4	$^{+3.4}_{-3.2}$	71.44	$^{+8.6}_{-15.7}$	$^{+3.2}_{-3.1}$
100	20	125.2	$^{+15.0}_{-13.2}$	-53.1	$^{+4.2}_{-4.0}$	114.8	$^{+8.6}_{-15.7}$	$^{+4.1}_{-3.9}$
100	30	235.2	$^{+14.7}_{-13.1}$	-52.9	$^{+5.8}_{-5.4}$	214.0	$^{+8.6}_{-15.7}$	$^{+5.6}_{-5.2}$
100	50	467.6	$^{+14.3}_{-12.9}$	-52.9	$^{+8.4}_{-7.5}$	426.8	$^{+8.6}_{-15.7}$	$^{+8.1}_{-7.2}$
200	5	0.534	$^{+7.8}_{-9.1}$	-4.0	$^{+0.2}_{-0.2}$	0.845	$^{+4.5}_{-5.9}$	$^{+1.2}_{-1.2}$
200	10	0.808	$^{+12.7}_{-11.9}$	-57.8	$^{+2.4}_{-2.4}$	3.030	$^{+4.5}_{-5.9}$	$^{+2.3}_{-2.2}$
200	15	1.831	$^{+12.3}_{-11.7}$	-59.5	$^{+3.5}_{-3.3}$	6.135	$^{+4.5}_{-5.9}$	$^{+3.2}_{-3.1}$
200	20	3.125	$^{+11.9}_{-11.5}$	-58.6	$^{+4.4}_{-4.1}$	9.859	$^{+4.5}_{-5.9}$	$^{+4.1}_{-3.9}$
200	30	6.097	$^{+11.5}_{-11.3}$	-57.6	$^{+5.9}_{-5.4}$	18.38	$^{+4.5}_{-5.9}$	$^{+5.6}_{-5.2}$
200	50	12.39	$^{+11.0}_{-11.0}$	-57.0	$^{+8.4}_{-7.5}$	36.65	$^{+4.5}_{-5.9}$	$^{+8.1}_{-7.2}$
300	5	0.310	$^{+5.5}_{-8.0}$	$+8.0$	$^{+0.1}_{-0.1}$	0.159	$^{+3.2}_{-3.2}$	$^{+1.2}_{-1.2}$
300	10	87.7×10^{-3}	$^{+8.5}_{-9.6}$	-27.2	$^{+1.3}_{-1.2}$	0.568	$^{+3.2}_{-3.2}$	$^{+2.3}_{-2.2}$
300	15	0.150	$^{+11.9}_{-12.0}$	-60.4	$^{+3.6}_{-3.4}$	1.151	$^{+3.2}_{-3.2}$	$^{+3.2}_{-3.1}$
300	20	0.269	$^{+12.0}_{-12.2}$	-62.9	$^{+4.6}_{-4.3}$	1.849	$^{+3.2}_{-3.2}$	$^{+4.1}_{-3.9}$
300	30	0.564	$^{+11.5}_{-12.0}$	-61.4	$^{+6.1}_{-5.6}$	3.447	$^{+3.2}_{-3.2}$	$^{+5.6}_{-5.2}$
300	50	1.201	$^{+10.7}_{-11.7}$	-59.8	$^{+8.5}_{-7.6}$	6.874	$^{+3.2}_{-3.2}$	$^{+8.1}_{-7.2}$
400	5	0.334	$^{+4.8}_{-7.8}$	-1.9	— —	42.8×10^{-3}	$^{+2.6}_{-2.0}$	$^{+1.2}_{-1.2}$
400	10	98.9×10^{-3}	$^{+9.0}_{-10.2}$	-14.5	$^{+0.5}_{-0.5}$	0.154	$^{+2.6}_{-2.0}$	$^{+2.3}_{-2.2}$
400	15	73.4×10^{-3}	$^{+13.5}_{-12.8}$	-35.0	$^{+1.8}_{-1.7}$	0.311	$^{+2.6}_{-2.0}$	$^{+3.2}_{-3.1}$
400	20	81.1×10^{-3}	$^{+14.7}_{-13.7}$	-48.4	$^{+3.2}_{-3.0}$	0.500	$^{+2.6}_{-2.0}$	$^{+4.1}_{-3.9}$
400	30	0.123	$^{+13.7}_{-13.5}$	-57.2	$^{+5.4}_{-4.9}$	0.932	$^{+2.6}_{-2.0}$	$^{+5.6}_{-5.2}$
400	50	0.227	$^{+11.7}_{-12.6}$	-59.7	$^{+8.2}_{-7.3}$	1.858	$^{+2.6}_{-2.0}$	$^{+8.1}_{-7.2}$
500	5	96.7×10^{-3}	$^{+3.5}_{-7.0}$	-4.0	— —	14.3×10^{-3}	$^{+2.3}_{-1.4}$	$^{+1.2}_{-1.2}$
500	10	31.9×10^{-3}	$^{+7.1}_{-9.5}$	-17.7	$^{+0.6}_{-0.5}$	51.4×10^{-3}	$^{+2.3}_{-1.4}$	$^{+2.3}_{-2.2}$
500	15	23.9×10^{-3}	$^{+11.0}_{-11.9}$	-34.4	$^{+1.7}_{-1.6}$	0.104	$^{+2.3}_{-1.4}$	$^{+3.2}_{-3.1}$
500	20	24.9×10^{-3}	$^{+12.4}_{-12.9}$	-45.8	$^{+2.9}_{-2.8}$	0.167	$^{+2.3}_{-1.4}$	$^{+4.1}_{-3.9}$
500	30	33.9×10^{-3}	$^{+12.2}_{-13.1}$	-55.2	$^{+5.0}_{-4.6}$	0.312	$^{+2.3}_{-1.4}$	$^{+5.6}_{-5.2}$
500	50	58.0×10^{-3}	$^{+10.8}_{-12.5}$	-59.3	$^{+8.0}_{-7.1}$	0.622	$^{+2.3}_{-1.4}$	$^{+8.1}_{-7.2}$

Table 13: Cross sections and uncertainties for pseudoscalar production in the *light-stop* scenario for $\sqrt{s} = 8$ TeV. Uncertainties below 0.1% are not listed (—). For the PDF uncertainties see text.

m_A [GeV]	$\tan\beta$	m_h [GeV]	σ_{ggh} [pb]	$\Delta_\mu^\pm$ [%]	δY_b [%]	$\delta\Delta_b$ [%]	σ_{bbh} [pb]	$\Delta_\mu^\pm$ [%]	$\delta\Delta_b$ [%]
100	5	90.2	16.60	$^{+17.4}_{-14.5}$	-38.3	$^{+0.5}_{-0.5}$	12.49	$^{+9.5}_{-18.2}$	$^{+0.7}_{-0.7}$
100	10	96.3	40.47	$^{+17.1}_{-14.3}$	-52.7	$^{+1.5}_{-1.4}$	40.40	$^{+8.9}_{-16.6}$	$^{+1.4}_{-1.4}$
100	15	97.8	82.65	$^{+16.5}_{-14.0}$	-53.6	$^{+2.2}_{-2.1}$	82.90	$^{+8.8}_{-16.2}$	$^{+2.1}_{-2.0}$
100	20	98.4	137.3	$^{+16.2}_{-13.8}$	-53.5	$^{+2.8}_{-2.7}$	136.7	$^{+8.7}_{-16.1}$	$^{+2.7}_{-2.6}$
100	30	98.9	272.2	$^{+15.9}_{-13.7}$	-53.2	$^{+4.0}_{-3.8}$	268.7	$^{+8.7}_{-15.9}$	$^{+3.9}_{-3.7}$
100	50	99.2	596.9	$^{+15.6}_{-13.5}$	-53.0	$^{+6.0}_{-5.5}$	587.1	$^{+8.6}_{-15.9}$	$^{+5.9}_{-5.4}$
120	5	103.2	12.37	$^{+14.0}_{-12.6}$	-13.9	$^{+0.2}_{-0.2}$	6.361	$^{+8.3}_{-15.0}$	$^{+0.7}_{-0.6}$
120	10	112.3	16.25	$^{+15.6}_{-13.5}$	-37.6	$^{+1.0}_{-1.0}$	18.67	$^{+7.6}_{-13.3}$	$^{+1.4}_{-1.3}$
120	15	115.2	27.55	$^{+16.0}_{-13.6}$	-49.4	$^{+2.0}_{-1.9}$	38.16	$^{+7.4}_{-12.8}$	$^{+2.0}_{-2.0}$
120	20	116.6	44.40	$^{+15.8}_{-13.5}$	-53.3	$^{+2.8}_{-2.6}$	63.89	$^{+7.3}_{-12.6}$	$^{+2.7}_{-2.6}$
120	30	117.9	90.25	$^{+15.4}_{-13.3}$	-55.0	$^{+4.1}_{-3.8}$	129.6	$^{+7.2}_{-12.4}$	$^{+3.8}_{-3.6}$
120	50	118.7	207.2	$^{+14.8}_{-13.0}$	-55.1	$^{+6.1}_{-5.6}$	291.8	$^{+7.2}_{-12.3}$	$^{+5.8}_{-5.3}$
150	5	113.8	15.76	$^{+10.9}_{-10.8}$	$+0.5$	—	2.339	$^{+7.5}_{-13.1}$	$^{+0.5}_{-0.5}$
150	10	122.4	15.96	$^{+10.9}_{-10.7}$	—	—	3.479	$^{+7.0}_{-11.8}$	$^{+1.1}_{-1.1}$
150	15	124.7	16.45	$^{+10.9}_{-10.7}$	-0.4	—	4.112	$^{+6.8}_{-11.5}$	$^{+1.7}_{-1.6}$
150	20	125.7	16.74	$^{+11.0}_{-10.7}$	-0.7	—	4.466	$^{+6.8}_{-11.3}$	$^{+2.2}_{-2.1}$
150	30	126.5	17.01	$^{+11.0}_{-10.7}$	-1.0	—	4.824	$^{+6.8}_{-11.2}$	$^{+3.1}_{-3.0}$
150	50	126.8	17.24	$^{+11.0}_{-10.8}$	-1.4	$^{+0.1}_{-0.1}$	5.028	$^{+6.7}_{-11.2}$	$^{+4.7}_{-4.3}$
200	5	119.1	18.73	$^{+9.6}_{-10.2}$	$+1.9$	—	0.829	$^{+7.2}_{-12.2}$	$^{+0.4}_{-0.4}$
200	10	124.8	18.14	$^{+9.4}_{-10.0}$	$+2.0$	—	0.842	$^{+6.8}_{-11.5}$	$^{+0.7}_{-0.7}$
200	15	126.1	18.05	$^{+9.3}_{-10.0}$	$+2.0$	—	0.852	$^{+6.8}_{-11.3}$	$^{+1.1}_{-1.1}$
200	20	126.6	18.01	$^{+9.3}_{-10.0}$	$+1.9$	—	0.860	$^{+6.8}_{-11.2}$	$^{+1.4}_{-1.4}$
200	30	126.9	17.96	$^{+9.3}_{-10.0}$	$+1.8$	—	0.872	$^{+6.7}_{-11.2}$	$^{+2.0}_{-1.9}$
200	50	126.9	17.99	$^{+9.3}_{-10.0}$	$+1.5$	$^{+0.1}_{-0.1}$	0.890	$^{+6.7}_{-11.2}$	$^{+3.1}_{-2.8}$
300	5	121.3	19.77	$^{+9.2}_{-10.0}$	$+1.7$	—	0.398	$^{+7.0}_{-11.9}$	$^{+0.2}_{-0.2}$
300	10	125.6	18.82	$^{+9.0}_{-9.9}$	$+1.6$	—	0.371	$^{+6.8}_{-11.4}$	$^{+0.4}_{-0.4}$
300	15	126.4	18.63	$^{+9.0}_{-9.9}$	$+1.6$	—	0.367	$^{+6.8}_{-11.3}$	$^{+0.5}_{-0.5}$
300	20	126.8	18.56	$^{+9.0}_{-9.8}$	$+1.5$	—	0.367	$^{+6.7}_{-11.2}$	$^{+0.7}_{-0.7}$
300	30	127.0	18.50	$^{+9.0}_{-9.8}$	$+1.4$	—	0.368	$^{+6.7}_{-11.2}$	$^{+1.0}_{-1.0}$
300	50	127.0	18.52	$^{+9.0}_{-9.8}$	$+1.1$	—	0.373	$^{+6.7}_{-11.2}$	$^{+1.5}_{-1.4}$

Table 14: Cross sections and uncertainties for lightest-scalar production in the *light-stau* scenario for $\sqrt{s} = 8$ TeV. Uncertainties below 0.1% are not listed (—). For the PDF uncertainties see text.

m_A [GeV]	$\tan\beta$	m_H [GeV]	σ_{ggH} [pb]	$\Delta_\mu^\pm$ [%]	δY_b [%]	$\delta\Delta_b$ [%]	σ_{bbH} [pb]	$\Delta_\mu^\pm$ [%]	$\delta\Delta_b$ [%]
100	5	135.4	16.97	$^{+7.9}_{-9.3}$	-4.2	— —	0.614	$^{+6.3}_{-10.2}$	$^{+1.1}_{-1.1}$
100	10	130.0	20.91	$^{+8.1}_{-9.5}$	-5.8	$^{+0.2}_{-0.2}$	1.228	$^{+6.6}_{-10.8}$	$^{+2.0}_{-2.0}$
100	15	128.6	22.49	$^{+8.2}_{-9.6}$	-6.5	$^{+0.3}_{-0.3}$	1.523	$^{+6.6}_{-11.0}$	$^{+2.9}_{-2.8}$
100	20	128.1	23.25	$^{+8.2}_{-9.6}$	-6.8	$^{+0.5}_{-0.4}$	1.689	$^{+6.7}_{-11.0}$	$^{+3.7}_{-3.5}$
100	30	127.7	23.98	$^{+8.3}_{-9.6}$	-7.3	$^{+0.7}_{-0.6}$	1.890	$^{+6.7}_{-11.1}$	$^{+5.2}_{-4.9}$
100	50	127.4	24.77	$^{+8.3}_{-9.7}$	-8.2	$^{+1.1}_{-1.0}$	2.199	$^{+6.7}_{-11.1}$	$^{+7.7}_{-7.0}$
200	5	205.7	1.494	$^{+6.7}_{-8.6}$	-17.1	$^{+0.2}_{-0.2}$	0.713	$^{+4.4}_{-5.6}$	$^{+0.8}_{-0.8}$
200	10	201.5	1.739	$^{+9.3}_{-10.0}$	-41.2	$^{+1.1}_{-1.1}$	3.090	$^{+4.5}_{-5.8}$	$^{+1.5}_{-1.5}$
200	15	200.6	2.786	$^{+10.5}_{-10.7}$	-49.8	$^{+1.9}_{-1.9}$	6.709	$^{+4.5}_{-5.8}$	$^{+2.2}_{-2.1}$
200	20	200.2	4.223	$^{+11.0}_{-11.0}$	-52.8	$^{+2.6}_{-2.5}$	11.28	$^{+4.5}_{-5.9}$	$^{+2.8}_{-2.7}$
200	30	200.0	7.826	$^{+11.4}_{-11.3}$	-54.9	$^{+3.9}_{-3.7}$	22.50	$^{+4.5}_{-5.9}$	$^{+3.9}_{-3.7}$
200	50	199.8	16.54	$^{+11.5}_{-11.3}$	-56.0	$^{+5.9}_{-5.5}$	49.55	$^{+4.5}_{-5.9}$	$^{+5.9}_{-5.4}$
300	5	303.1	0.313	$^{+5.7}_{-8.5}$	-13.6	$^{+0.2}_{-0.2}$	0.154	$^{+3.2}_{-3.2}$	$^{+0.8}_{-0.8}$
300	10	300.7	0.237	$^{+7.6}_{-9.9}$	-37.4	$^{+0.9}_{-0.9}$	0.606	$^{+3.2}_{-3.2}$	$^{+1.5}_{-1.5}$
300	15	300.3	0.323	$^{+9.1}_{-10.8}$	-48.6	$^{+1.8}_{-1.7}$	1.284	$^{+3.2}_{-3.2}$	$^{+2.2}_{-2.1}$
300	20	300.1	0.458	$^{+9.8}_{-11.2}$	-53.1	$^{+2.5}_{-2.4}$	2.141	$^{+3.2}_{-3.2}$	$^{+2.8}_{-2.7}$
300	30	300.0	0.810	$^{+10.4}_{-11.5}$	-56.2	$^{+3.8}_{-3.6}$	4.240	$^{+3.2}_{-3.2}$	$^{+3.9}_{-3.7}$
300	50	299.8	1.672	$^{+10.6}_{-11.6}$	-57.8	$^{+5.9}_{-5.4}$	9.297	$^{+3.2}_{-3.2}$	$^{+5.9}_{-5.4}$
500	5	501.6	53.0×10^{-3}	$^{+0.8}_{-5.1}$	-0.6	— —	14.6×10^{-3}	$^{+2.3}_{-1.4}$	$^{+0.8}_{-0.8}$
500	10	500.4	16.7×10^{-3}	$^{+0.5}_{-4.9}$	-14.0	$^{+0.4}_{-0.4}$	55.5×10^{-3}	$^{+2.3}_{-1.4}$	$^{+1.5}_{-1.5}$
500	15	500.1	14.3×10^{-3}	$^{+0.5}_{-5.5}$	-37.7	$^{+1.4}_{-1.4}$	0.117	$^{+2.3}_{-1.4}$	$^{+2.2}_{-2.1}$
500	20	500.0	18.0×10^{-3}	$^{+3.4}_{-8.0}$	-51.3	$^{+2.5}_{-2.4}$	0.194	$^{+2.3}_{-1.4}$	$^{+2.8}_{-2.7}$
500	30	499.9	31.7×10^{-3}	$^{+6.5}_{-10.4}$	-59.1	$^{+4.0}_{-3.7}$	0.384	$^{+2.3}_{-1.4}$	$^{+3.9}_{-3.7}$
500	50	499.8	68.0×10^{-3}	$^{+8.9}_{-11.6}$	-61.2	$^{+6.1}_{-5.6}$	0.841	$^{+2.3}_{-1.4}$	$^{+5.9}_{-5.4}$
1000	5	1000.5	660×10^{-6}	$^{+0.4}_{-5.1}$	$+6.0$	— —	281×10^{-6}	$^{+1.4}_{-1.1}$	$^{+0.8}_{-0.8}$
1000	10	1000.	108×10^{-6}	$^{+7.5}_{-23.4}$	$+21.6$	$^{+0.3}_{-0.3}$	1.05×10^{-3}	$^{+1.4}_{-1.1}$	$^{+1.5}_{-1.5}$
1000	15	999.9	42.4×10^{-6}	$^{+16.6}_{-42.2}$	-3.0	$^{+1.0}_{-0.9}$	2.21×10^{-3}	$^{+1.4}_{-1.1}$	$^{+2.2}_{-2.1}$
1000	20	999.8	54.3×10^{-6}	$^{+3.3}_{-19.5}$	-58.8	$^{+3.5}_{-3.3}$	3.66×10^{-3}	$^{+1.4}_{-1.1}$	$^{+2.8}_{-2.7}$
1000	30	999.8	146×10^{-6}	$^{+4.2}_{-10.0}$	-74.4	$^{+5.0}_{-4.7}$	7.24×10^{-3}	$^{+1.4}_{-1.1}$	$^{+3.9}_{-3.7}$
1000	50	999.5	415×10^{-6}	$^{+9.7}_{-13.1}$	-70.4	$^{+6.8}_{-6.2}$	15.9×10^{-3}	$^{+1.4}_{-1.1}$	$^{+5.9}_{-5.4}$

Table 15: Cross sections and uncertainties for heaviest-scalar production in the *light-stau* scenario for $\sqrt{s} = 8$ TeV. Uncertainties below 0.1% are not listed (—). For the PDF uncertainties see text.

m_A [GeV]	$\tan\beta$	σ_{ggA} [pb]	$\Delta_\mu^\pm$ [%]	δY_b [%]	$\delta\Delta_b$ [%]	σ_{bbA} [pb]	$\Delta_\mu^\pm$ [%]	$\delta\Delta_b$ [%]
100	5	10.13	$^{+15.6}_{-13.5}$	-47.7	$^{+0.8}_{-0.8}$	10.30	$^{+8.6}_{-15.7}$	$^{+0.8}_{-0.8}$
100	10	39.73	$^{+15.5}_{-13.5}$	-53.8	$^{+1.6}_{-1.5}$	38.34	$^{+8.6}_{-15.7}$	$^{+1.5}_{-1.5}$
100	15	86.71	$^{+15.2}_{-13.3}$	-53.2	$^{+2.2}_{-2.2}$	80.38	$^{+8.6}_{-15.7}$	$^{+2.2}_{-2.1}$
100	20	146.1	$^{+15.0}_{-13.2}$	-52.9	$^{+2.9}_{-2.7}$	133.4	$^{+8.6}_{-15.7}$	$^{+2.8}_{-2.7}$
100	30	291.4	$^{+14.9}_{-13.2}$	-52.6	$^{+4.0}_{-3.8}$	263.4	$^{+8.6}_{-15.7}$	$^{+3.9}_{-3.7}$
100	50	638.7	$^{+14.7}_{-13.1}$	-52.5	$^{+6.0}_{-5.5}$	576.3	$^{+8.6}_{-15.7}$	$^{+5.9}_{-5.4}$
200	5	0.550	$^{+8.5}_{-9.5}$	-4.2	$^{+0.1}_{-0.1}$	0.884	$^{+4.5}_{-5.9}$	$^{+0.8}_{-0.8}$
200	10	0.879	$^{+12.5}_{-11.8}$	-57.6	$^{+1.6}_{-1.6}$	3.292	$^{+4.5}_{-5.9}$	$^{+1.5}_{-1.5}$
200	15	2.069	$^{+12.1}_{-11.6}$	-59.2	$^{+2.3}_{-2.3}$	6.902	$^{+4.5}_{-5.9}$	$^{+2.2}_{-2.1}$
200	20	3.649	$^{+11.8}_{-11.5}$	-58.2	$^{+2.9}_{-2.8}$	11.46	$^{+4.5}_{-5.9}$	$^{+2.8}_{-2.7}$
200	30	7.552	$^{+11.5}_{-11.3}$	-57.2	$^{+4.1}_{-3.9}$	22.62	$^{+4.5}_{-5.9}$	$^{+3.9}_{-3.7}$
200	50	16.90	$^{+11.2}_{-11.1}$	-56.7	$^{+6.1}_{-5.6}$	49.49	$^{+4.5}_{-5.9}$	$^{+5.9}_{-5.4}$
300	5	0.317	$^{+6.4}_{-8.5}$	$+8.1$	— —	0.166	$^{+3.2}_{-3.2}$	$^{+0.8}_{-0.8}$
300	10	93.6×10^{-3}	$^{+9.0}_{-9.9}$	-27.8	$^{+0.9}_{-0.9}$	0.617	$^{+3.2}_{-3.2}$	$^{+1.5}_{-1.5}$
300	15	0.169	$^{+11.5}_{-11.8}$	-60.2	$^{+2.4}_{-2.3}$	1.295	$^{+3.2}_{-3.2}$	$^{+2.2}_{-2.1}$
300	20	0.314	$^{+11.5}_{-12.0}$	-62.5	$^{+3.1}_{-3.0}$	2.149	$^{+3.2}_{-3.2}$	$^{+2.8}_{-2.7}$
300	30	0.698	$^{+11.1}_{-11.9}$	-60.9	$^{+4.2}_{-4.0}$	4.243	$^{+3.2}_{-3.2}$	$^{+3.9}_{-3.7}$
300	50	1.635	$^{+10.7}_{-11.6}$	-59.4	$^{+6.1}_{-5.6}$	9.283	$^{+3.2}_{-3.2}$	$^{+5.9}_{-5.4}$
500	5	99.4×10^{-3}	$^{+4.2}_{-7.6}$	-4.0	— —	15.0×10^{-3}	$^{+2.3}_{-1.4}$	$^{+0.8}_{-0.8}$
500	10	33.8×10^{-3}	$^{+8.7}_{-10.4}$	-17.8	$^{+0.4}_{-0.4}$	55.9×10^{-3}	$^{+2.3}_{-1.4}$	$^{+1.5}_{-1.5}$
500	15	26.4×10^{-3}	$^{+12.4}_{-12.6}$	-34.7	$^{+1.1}_{-1.1}$	0.117	$^{+2.3}_{-1.4}$	$^{+2.2}_{-2.1}$
500	20	28.5×10^{-3}	$^{+13.5}_{-13.5}$	-46.0	$^{+2.0}_{-1.9}$	0.195	$^{+2.3}_{-1.4}$	$^{+2.8}_{-2.7}$
500	30	41.5×10^{-3}	$^{+12.8}_{-13.4}$	-55.1	$^{+3.5}_{-3.3}$	0.384	$^{+2.3}_{-1.4}$	$^{+3.9}_{-3.7}$
500	50	78.6×10^{-3}	$^{+11.2}_{-12.7}$	-59.1	$^{+5.7}_{-5.3}$	0.840	$^{+2.3}_{-1.4}$	$^{+5.9}_{-5.4}$
1000	5	1.15×10^{-3}	$^{+2.4}_{-6.6}$	-5.5	— —	283×10^{-6}	$^{+1.4}_{-1.1}$	$^{+0.8}_{-0.8}$
1000	10	413×10^{-6}	$^{+4.7}_{-9.2}$	-18.8	$^{+0.4}_{-0.4}$	1.05×10^{-3}	$^{+1.4}_{-1.1}$	$^{+1.5}_{-1.5}$
1000	15	308×10^{-6}	$^{+8.2}_{-11.4}$	-32.6	$^{+1.0}_{-1.0}$	2.21×10^{-3}	$^{+1.4}_{-1.1}$	$^{+2.2}_{-2.1}$
1000	20	305×10^{-6}	$^{+9.9}_{-12.7}$	-42.7	$^{+1.7}_{-1.7}$	3.66×10^{-3}	$^{+1.4}_{-1.1}$	$^{+2.8}_{-2.7}$
1000	30	384×10^{-6}	$^{+10.8}_{-13.5}$	-53.2	$^{+3.2}_{-3.0}$	7.23×10^{-3}	$^{+1.4}_{-1.1}$	$^{+3.9}_{-3.7}$
1000	50	644×10^{-6}	$^{+10.4}_{-13.5}$	-59.8	$^{+5.5}_{-5.1}$	15.8×10^{-3}	$^{+1.4}_{-1.1}$	$^{+5.9}_{-5.4}$

Table 16: Cross sections and uncertainties for pseudoscalar production in the *light-stau* scenario for $\sqrt{s} = 8$ TeV. Uncertainties below 0.1% are not listed (—). For the PDF uncertainties see text.

m_A [GeV]	$\tan\beta$	m_h [GeV]	σ_{ggh} [pb]	$\Delta_\mu^\pm$ [%]	δY_b [%]	$\delta\Delta_b$ [%]	σ_{bbh} [pb]	$\Delta_\mu^\pm$ [%]	$\delta\Delta_b$ [%]
100	5	85.5	19.70	$^{+17.4}_{-14.5}$	-52.8	$^{+1.9}_{-1.8}$	15.57	$^{+10.1}_{-19.7}$	$^{+1.8}_{-1.7}$
100	10	86.5	62.66	$^{+16.9}_{-14.3}$	-52.9	$^{+3.4}_{-3.3}$	49.53	$^{+10.0}_{-19.3}$	$^{+3.3}_{-3.1}$
100	15	86.0	121.0	$^{+16.9}_{-14.3}$	-52.9	$^{+4.8}_{-4.5}$	95.38	$^{+10.0}_{-19.5}$	$^{+4.6}_{-4.3}$
100	20	85.7	187.9	$^{+16.8}_{-14.2}$	-52.9	$^{+6.0}_{-5.5}$	147.3	$^{+10.1}_{-19.6}$	$^{+5.7}_{-5.3}$
100	30	85.2	329.9	$^{+16.6}_{-14.1}$	-52.8	$^{+8.1}_{-7.2}$	257.0	$^{+10.2}_{-19.8}$	$^{+7.7}_{-6.9}$
100	40	84.9	468.4	$^{+16.3}_{-14.0}$	-52.8	$^{+9.7}_{-8.5}$	364.3	$^{+10.2}_{-19.9}$	$^{+9.2}_{-8.1}$
120	5	105.6	7.186	$^{+16.4}_{-13.9}$	-37.7	$^{+1.3}_{-1.2}$	7.355	$^{+8.1}_{-14.5}$	$^{+1.7}_{-1.6}$
120	10	109.0	20.00	$^{+15.1}_{-13.2}$	-54.5	$^{+3.5}_{-3.3}$	23.99	$^{+7.8}_{-13.9}$	$^{+3.3}_{-3.1}$
120	15	108.3	36.59	$^{+15.6}_{-13.5}$	-54.7	$^{+4.8}_{-4.5}$	45.27	$^{+7.9}_{-14.0}$	$^{+4.6}_{-4.3}$
120	20	107.6	55.96	$^{+15.6}_{-13.5}$	-54.6	$^{+6.0}_{-5.5}$	68.82	$^{+7.9}_{-14.1}$	$^{+5.7}_{-5.2}$
120	30	106.7	97.06	$^{+15.4}_{-13.4}$	-54.6	$^{+8.1}_{-7.2}$	117.9	$^{+8.0}_{-14.3}$	$^{+7.6}_{-6.8}$
120	40	105.9	136.0	$^{+15.2}_{-13.3}$	-54.6	$^{+9.8}_{-8.5}$	164.1	$^{+8.1}_{-14.5}$	$^{+9.1}_{-8.0}$
150	5	119.2	15.61	$^{+10.3}_{-10.5}$	$+1.7$	$^{—}_{—}$	1.476	$^{+7.2}_{-12.2}$	$^{+1.1}_{-1.1}$
150	10	125.0	18.67	$^{+9.0}_{-9.9}$	$+1.5$	$^{—}_{—}$	0.349	$^{+6.8}_{-11.4}$	$^{+0.7}_{-0.7}$
150	15	125.0	20.74	$^{+8.1}_{-9.6}$	-1.6	$^{+0.3}_{-0.3}$	95.1×10^{-3}	$^{+6.8}_{-11.4}$	$^{+11.8}_{-10.7}$
150	20	124.5	22.86	$^{+8.0}_{-9.5}$	-5.8	$^{+0.8}_{-0.7}$	1.098	$^{+6.9}_{-11.5}$	$^{+8.4}_{-7.6}$
150	30	123.4	27.52	$^{+8.2}_{-9.7}$	-13.0	$^{+2.1}_{-1.9}$	4.544	$^{+6.9}_{-11.6}$	$^{+9.5}_{-8.4}$
150	40	121.6	32.10	$^{+8.4}_{-9.8}$	-17.8	$^{+3.3}_{-2.9}$	7.936	$^{+7.0}_{-11.9}$	$^{+10.9}_{-9.5}$
200	5	121.2	19.02	$^{+9.2}_{-10.0}$	$+1.7$	$^{—}_{—}$	0.475	$^{+7.0}_{-11.9}$	$^{+0.6}_{-0.5}$
200	10	125.0	18.95	$^{+8.8}_{-9.8}$	$+1.3$	$^{—}_{—}$	0.237	$^{+6.8}_{-11.4}$	$^{+0.2}_{-0.2}$
200	15	125.5	19.21	$^{+8.6}_{-9.7}$	$+0.7$	$^{—}_{—}$	95.0×10^{-3}	$^{+6.8}_{-11.4}$	$^{+2.2}_{-2.3}$
200	20	125.5	19.52	$^{+8.5}_{-9.7}$	—	$^{+0.1}_{-0.1}$	23.5×10^{-3}	$^{+6.8}_{-11.4}$	$^{+11.1}_{-11.1}$
200	30	125.0	20.25	$^{+8.3}_{-9.6}$	-1.5	$^{+0.3}_{-0.3}$	10.4×10^{-3}	$^{+6.8}_{-11.4}$	$^{+46.6}_{-35.4}$
200	40	123.4	21.28	$^{+8.2}_{-9.6}$	-3.0	$^{+0.5}_{-0.5}$	89.8×10^{-3}	$^{+6.9}_{-11.6}$	$^{+24.8}_{-20.3}$
300	5	121.7	19.70	$^{+9.0}_{-9.9}$	$+1.5$	$^{—}_{—}$	0.301	$^{+7.0}_{-11.9}$	$^{+0.2}_{-0.2}$
300	10	125.0	18.99	$^{+8.8}_{-9.8}$	$+1.2$	$^{—}_{—}$	0.221	$^{+6.8}_{-11.4}$	$^{—}_{—}$
300	15	125.5	18.94	$^{+8.8}_{-9.8}$	$+0.9$	$^{—}_{—}$	0.171	$^{+6.8}_{-11.4}$	$^{+0.5}_{-0.5}$
300	20	125.7	19.00	$^{+8.7}_{-9.8}$	$+0.6$	$^{—}_{—}$	0.134	$^{+6.8}_{-11.4}$	$^{+1.4}_{-1.4}$
300	30	125.3	19.25	$^{+8.6}_{-9.7}$	-0.1	$^{—}_{—}$	84.2×10^{-3}	$^{+6.8}_{-11.4}$	$^{+4.2}_{-4.4}$
300	40	123.9	19.83	$^{+8.6}_{-9.8}$	-1.0	$^{+0.1}_{-0.1}$	54.8×10^{-3}	$^{+6.9}_{-11.6}$	$^{+8.6}_{-9.0}$

Table 17: Cross sections and uncertainties for lightest-scalar production in the *tau-phobic* scenario for $\sqrt{s} = 8$ TeV. Uncertainties below 0.1% are not listed (—). For the PDF uncertainties see text.

m_A [GeV]	$\tan\beta$	m_H [GeV]	σ_{ggH} [pb]	$\Delta_\mu^\pm$ [%]	δY_b [%]	$\delta\Delta_b$ [%]	σ_{bbH} [pb]	$\Delta_\mu^\pm$ [%]	$\delta\Delta_b$ [%]
100	5	124.1	21.05	$^{+8.1}_{-9.6}$	−0.6	— —	20.5×10^{-3}	$^{+6.9}_{-11.6}$	$^{+7.9}_{-7.5}$
100	10	124.9	20.60	$^{+8.1}_{-9.6}$	−1.1	$^{+0.2}_{-0.2}$	55.1×10^{-3}	$^{+6.8}_{-11.4}$	$^{+10.1}_{-9.3}$
100	15	125.8	21.16	$^{+8.0}_{-9.5}$	−3.2	$^{+0.4}_{-0.4}$	0.394	$^{+6.8}_{-11.3}$	$^{+8.1}_{-7.4}$
100	20	126.3	21.94	$^{+8.0}_{-9.5}$	−5.3	$^{+0.7}_{-0.7}$	0.913	$^{+6.8}_{-11.3}$	$^{+8.6}_{-7.8}$
100	30	126.6	23.85	$^{+8.0}_{-9.5}$	−9.1	$^{+1.5}_{-1.3}$	2.251	$^{+6.8}_{-11.2}$	$^{+10.1}_{-9.0}$
100	40	125.5	26.57	$^{+8.1}_{-9.6}$	−13.0	$^{+2.4}_{-2.1}$	4.121	$^{+6.8}_{-11.4}$	$^{+11.4}_{-9.9}$
200	5	194.9	1.152	$^{+6.0}_{-8.0}$	−23.5	$^{+0.8}_{-0.8}$	0.831	$^{+4.6}_{-6.1}$	$^{+1.9}_{-1.9}$
200	10	193.5	1.303	$^{+9.6}_{-10.1}$	−50.4	$^{+3.1}_{-2.9}$	3.044	$^{+4.6}_{-6.2}$	$^{+3.4}_{-3.2}$
200	15	193.6	2.074	$^{+10.8}_{-10.8}$	−55.8	$^{+4.7}_{-4.4}$	5.898	$^{+4.6}_{-6.2}$	$^{+4.7}_{-4.4}$
200	20	193.8	3.008	$^{+11.2}_{-11.1}$	−57.1	$^{+6.1}_{-5.6}$	9.059	$^{+4.6}_{-6.1}$	$^{+5.8}_{-5.3}$
200	30	194.0	4.996	$^{+11.3}_{-11.1}$	−57.9	$^{+8.2}_{-7.3}$	15.62	$^{+4.6}_{-6.1}$	$^{+7.7}_{-6.9}$
200	40	194.1	6.924	$^{+11.2}_{-11.1}$	−58.1	$^{+9.9}_{-8.7}$	21.97	$^{+4.6}_{-6.1}$	$^{+9.3}_{-8.2}$
300	5	296.5	0.234	$^{+4.1}_{-7.4}$	−16.4	$^{+0.5}_{-0.5}$	0.154	$^{+3.3}_{-3.3}$	$^{+1.9}_{-1.8}$
300	10	295.7	0.164	$^{+6.4}_{-9.1}$	−43.8	$^{+2.5}_{-2.4}$	0.535	$^{+3.3}_{-3.3}$	$^{+3.4}_{-3.2}$
300	15	295.7	0.218	$^{+8.0}_{-10.2}$	−53.9	$^{+4.4}_{-4.1}$	1.035	$^{+3.3}_{-3.3}$	$^{+4.7}_{-4.4}$
300	20	295.8	0.297	$^{+8.8}_{-10.7}$	−57.2	$^{+5.8}_{-5.4}$	1.594	$^{+3.3}_{-3.3}$	$^{+5.8}_{-5.4}$
300	30	295.9	0.475	$^{+9.4}_{-11.0}$	−59.2	$^{+8.1}_{-7.3}$	2.762	$^{+3.3}_{-3.3}$	$^{+7.8}_{-7.0}$
300	40	295.9	0.650	$^{+9.4}_{-11.0}$	−59.9	$^{+9.9}_{-8.6}$	3.896	$^{+3.3}_{-3.3}$	$^{+9.3}_{-8.2}$
500	5	497.8	44.4×10^{-3}	$^{+0.4}_{-4.2}$	−0.5	— —	13.6×10^{-3}	$^{+2.3}_{-1.4}$	$^{+1.9}_{-1.8}$
500	10	497.4	11.3×10^{-3}	$^{+1.8}_{-12.5}$	−15.9	$^{+1.1}_{-1.0}$	46.7×10^{-3}	$^{+2.3}_{-1.4}$	$^{+3.4}_{-3.2}$
500	15	497.4	8.91×10^{-3}	$^{+1.1}_{-9.0}$	−44.0	$^{+3.7}_{-3.5}$	90.3×10^{-3}	$^{+2.3}_{-1.4}$	$^{+4.7}_{-4.4}$
500	20	497.4	11.0×10^{-3}	$^{+0.8}_{-6.1}$	−57.4	$^{+5.9}_{-5.4}$	0.139	$^{+2.3}_{-1.4}$	$^{+5.8}_{-5.4}$
500	30	497.5	18.0×10^{-3}	$^{+5.2}_{-9.5}$	−62.8	$^{+8.4}_{-7.5}$	0.241	$^{+2.3}_{-1.4}$	$^{+7.8}_{-7.0}$
500	40	497.5	25.5×10^{-3}	$^{+6.7}_{-10.6}$	−63.3	$^{+10.1}_{-8.9}$	0.341	$^{+2.3}_{-1.4}$	$^{+9.3}_{-8.2}$
1000	5	998.6	609×10^{-6}	$^{+1.3}_{-8.7}$	+6.4	$^{+0.1}_{-0.1}$	254×10^{-6}	$^{+1.4}_{-1.1}$	$^{+1.9}_{-1.8}$
1000	10	998.5	87.3×10^{-6}	$^{+14.3}_{-36.1}$	+26.8	$^{+0.8}_{-0.8}$	865×10^{-6}	$^{+1.4}_{-1.1}$	$^{+3.4}_{-3.2}$
1000	15	998.6	24.8×10^{-6}	$^{+37.6}_{-79.9}$	+16.6	$^{+1.4}_{-1.2}$	1.67×10^{-3}	$^{+1.4}_{-1.1}$	$^{+4.7}_{-4.4}$
1000	20	998.6	27.5×10^{-6}	$^{+15.3}_{-42.3}$	−57.9	$^{+8.3}_{-7.3}$	2.57×10^{-3}	$^{+1.4}_{-1.1}$	$^{+5.8}_{-5.4}$
1000	30	998.6	75.0×10^{-6}	$^{+3.4}_{-8.6}$	−78.1	$^{+11.0}_{-9.6}$	4.46×10^{-3}	$^{+1.4}_{-1.1}$	$^{+7.8}_{-7.0}$
1000	40	998.6	133×10^{-6}	$^{+8.4}_{-12.3}$	−75.1	$^{+11.9}_{-10.3}$	6.30×10^{-3}	$^{+1.4}_{-1.1}$	$^{+9.3}_{-8.2}$

Table 18: Cross sections and uncertainties for heaviest-scalar production in the *tau-phobic* scenario for $\sqrt{s} = 8$ TeV. Uncertainties below 0.1% are not listed (—). For the PDF uncertainties see text.

m_A [GeV]	$\tan\beta$	σ_{ggA} [pb]	$\Delta_\mu^\pm$ [%]	δY_b [%]	$\delta\Delta_b$ [%]	σ_{bbA} [pb]	$\Delta_\mu^\pm$ [%]	$\delta\Delta_b$ [%]
100	5	9.055	$^{+15.4}_{-13.4}$	-47.8	$^{+1.8}_{-1.7}$	9.194	$^{+8.6}_{-15.7}$	$^{+1.9}_{-1.8}$
100	10	32.17	$^{+15.5}_{-13.5}$	-54.3	$^{+3.6}_{-3.4}$	31.25	$^{+8.6}_{-15.7}$	$^{+3.4}_{-3.2}$
100	15	64.46	$^{+15.1}_{-13.3}$	-53.7	$^{+4.9}_{-4.6}$	60.29	$^{+8.6}_{-15.7}$	$^{+4.7}_{-4.4}$
100	20	100.6	$^{+14.9}_{-13.2}$	-53.4	$^{+6.1}_{-5.6}$	92.87	$^{+8.6}_{-15.7}$	$^{+5.8}_{-5.4}$
100	30	175.3	$^{+14.5}_{-13.0}$	-53.2	$^{+8.1}_{-7.2}$	161.2	$^{+8.6}_{-15.7}$	$^{+7.8}_{-7.0}$
100	40	246.7	$^{+14.1}_{-12.8}$	-53.2	$^{+9.7}_{-8.5}$	227.6	$^{+8.6}_{-15.7}$	$^{+9.3}_{-8.2}$
200	5	0.510	$^{+6.7}_{-8.5}$	-3.7	$^{+0.2}_{-0.2}$	0.790	$^{+4.5}_{-5.9}$	$^{+1.9}_{-1.8}$
200	10	0.712	$^{+12.9}_{-12.0}$	-58.0	$^{+3.6}_{-3.4}$	2.683	$^{+4.5}_{-5.9}$	$^{+3.4}_{-3.2}$
200	15	1.536	$^{+12.6}_{-11.9}$	-59.9	$^{+5.1}_{-4.8}$	5.178	$^{+4.5}_{-5.9}$	$^{+4.7}_{-4.4}$
200	20	2.510	$^{+12.1}_{-11.6}$	-58.9	$^{+6.3}_{-5.7}$	7.976	$^{+4.5}_{-5.9}$	$^{+5.8}_{-5.4}$
200	30	4.552	$^{+11.5}_{-11.3}$	-57.9	$^{+8.2}_{-7.3}$	13.84	$^{+4.5}_{-5.9}$	$^{+7.8}_{-7.0}$
200	40	6.504	$^{+11.1}_{-11.1}$	-57.5	$^{+9.8}_{-8.6}$	19.55	$^{+4.5}_{-5.9}$	$^{+9.3}_{-8.2}$
300	5	0.300	$^{+4.3}_{-7.3}$	$+7.8$	$^{+0.2}_{-0.2}$	0.148	$^{+3.2}_{-3.2}$	$^{+1.9}_{-1.8}$
300	10	79.5×10^{-3}	$^{+7.5}_{-8.9}$	-26.2	$^{+1.9}_{-1.7}$	0.503	$^{+3.2}_{-3.2}$	$^{+3.4}_{-3.2}$
300	15	0.126	$^{+12.4}_{-12.2}$	-60.6	$^{+5.2}_{-4.8}$	0.971	$^{+3.2}_{-3.2}$	$^{+4.7}_{-4.4}$
300	20	0.216	$^{+12.7}_{-12.5}$	-63.4	$^{+6.6}_{-6.0}$	1.496	$^{+3.2}_{-3.2}$	$^{+5.8}_{-5.4}$
300	30	0.421	$^{+12.0}_{-12.3}$	-61.9	$^{+8.5}_{-7.5}$	2.596	$^{+3.2}_{-3.2}$	$^{+7.8}_{-7.0}$
300	40	0.622	$^{+11.4}_{-12.0}$	-60.8	$^{+10.0}_{-8.7}$	3.666	$^{+3.2}_{-3.2}$	$^{+9.3}_{-8.2}$
500	5	93.8×10^{-3}	$^{+2.7}_{-6.4}$	-3.9	— —	13.4×10^{-3}	$^{+2.3}_{-1.4}$	$^{+1.9}_{-1.8}$
500	10	29.7×10^{-3}	$^{+5.1}_{-8.4}$	-17.3	$^{+0.8}_{-0.8}$	45.5×10^{-3}	$^{+2.3}_{-1.4}$	$^{+3.4}_{-3.2}$
500	15	21.1×10^{-3}	$^{+9.0}_{-10.8}$	-33.8	$^{+2.4}_{-2.2}$	87.9×10^{-3}	$^{+2.3}_{-1.4}$	$^{+4.7}_{-4.4}$
500	20	20.8×10^{-3}	$^{+11.0}_{-12.1}$	-45.3	$^{+4.1}_{-3.8}$	0.135	$^{+2.3}_{-1.4}$	$^{+5.8}_{-5.4}$
500	30	25.8×10^{-3}	$^{+11.4}_{-12.6}$	-55.1	$^{+6.9}_{-6.2}$	0.235	$^{+2.3}_{-1.4}$	$^{+7.8}_{-7.0}$
500	40	32.5×10^{-3}	$^{+10.7}_{-12.4}$	-58.3	$^{+8.9}_{-7.8}$	0.332	$^{+2.3}_{-1.4}$	$^{+9.3}_{-8.2}$
1000	5	1.10×10^{-3}	$^{+1.2}_{-5.4}$	-5.3	$^{+0.1}_{-0.1}$	252×10^{-6}	$^{+1.4}_{-1.1}$	$^{+1.9}_{-1.8}$
1000	10	369×10^{-6}	$^{+2.7}_{-7.2}$	-17.9	$^{+0.8}_{-0.8}$	857×10^{-6}	$^{+1.4}_{-1.1}$	$^{+3.4}_{-3.2}$
1000	15	252×10^{-6}	$^{+4.4}_{-9.2}$	-31.0	$^{+2.0}_{-1.9}$	1.65×10^{-3}	$^{+1.4}_{-1.1}$	$^{+4.7}_{-4.4}$
1000	20	228×10^{-6}	$^{+5.6}_{-10.6}$	-40.8	$^{+3.5}_{-3.2}$	2.55×10^{-3}	$^{+1.4}_{-1.1}$	$^{+5.8}_{-5.4}$
1000	30	244×10^{-6}	$^{+7.1}_{-11.7}$	-51.8	$^{+6.1}_{-5.5}$	4.42×10^{-3}	$^{+1.4}_{-1.1}$	$^{+7.8}_{-7.0}$
1000	40	281×10^{-6}	$^{+7.3}_{-12.0}$	-56.8	$^{+8.3}_{-7.3}$	6.25×10^{-3}	$^{+1.4}_{-1.1}$	$^{+9.3}_{-8.2}$

Table 19: Cross sections and uncertainties for pseudoscalar production in the *tau-phobic* scenario for $\sqrt{s} = 8$ TeV. Uncertainties below 0.1% are not listed (—). For the PDF uncertainties see text.

References

[1] G. Aad *et al.* [ATLAS Collaboration], Phys. Lett. B **716** (2012) 1 [arXiv:1207.7214 [hep-ex]].

[2] S. Chatrchyan *et al.* [CMS Collaboration], Phys. Lett. B **716** (2012) 30 [arXiv:1207.7235 [hep-ex]].

[3] LHC Higgs Cross Section Working Group, S. Dittmaier, C. Mariotti, G. Passarino and R. Tanaka (Eds.), CERN-2011-002 (CERN, Geneva, 2011), [arXiv:1101.0593 [hep-ph]].

[4] LHC Higgs Cross Section Working Group, S. Dittmaier, C. Mariotti, G. Passarino and R. Tanaka (Eds.), CERN-2012-002 (CERN, Geneva, 2012), [arXiv:1201.3084 [hep-ph]].

[5] LHC Higgs Cross Section Working Group, S. Heinemeyer, C. Mariotti, G. Passarino and R. Tanaka (Eds.), CERN-2013-004 (CERN, Geneva, 2013), [arXiv:1307.1347 [hep-ph]].

[6] H. M. Georgi, S. L. Glashow, M. E. Machacek and D. V. Nanopoulos, Phys. Rev. Lett. **40** (1978) 692.

[7] S. Dawson, Nucl. Phys. B **359** (1991) 283; A. Djouadi, M. Spira and P. M. Zerwas, Phys. Lett. B **264** (1991) 440.

[8] M. Spira, A. Djouadi, D. Graudenz and P. M. Zerwas, Nucl. Phys. B **453** (1995) 17 [arXiv:hep-ph/9504378].

[9] R. Harlander and P. Kant, JHEP **0512** (2005) 015 [arXiv:hep-ph/0509189].

[10] C. Anastasiou, S. Beerli, S. Bucherer, A. Daleo and Z. Kunszt, JHEP **0701** (2007) 082 [arXiv:hep-ph/0611236].

[11] U. Aglietti, R. Bonciani, G. Degrassi and A. Vicini, JHEP **0701** (2007) 021 [arXiv:hep-ph/0611266]; R. Bonciani, G. Degrassi and A. Vicini, JHEP **0711** (2007) 095 [arXiv:0709.4227 [hep-ph]].

[12] R. V. Harlander, Phys. Lett. B **492** (2000) 74. [arXiv:hep-ph/0007289]; S. Catani, D. de Florian and M. Grazzini, JHEP **0105** (2001) 025 [arXiv:hep-ph/0102227]; R. V. Harlander and W. B. Kilgore, Phys. Rev. D **64** (2001) 013015 [arXiv:hep-ph/0102241], Phys. Rev. Lett. **88** (2002) 201801 [arXiv:hep-ph/0201206]; V. Ravindran, J. Smith and W. L. van Neerven, Nucl. Phys. B **665** (2003) 325 [arXiv:hep-ph/0302135].

[13] C. Anastasiou and K. Melnikov, Nucl. Phys. B **646**, 220 (2002) [hep-ph/0207004].

[14] S. Marzani, R. D. Ball, V. Del Duca, S. Forte and A. Vicini, Nucl. Phys. B **800** (2008) 127 [arXiv:0801.2544 [hep-ph]]; R. V. Harlander and K. J. Ozeren, Phys. Lett. B **679** (2009) 467 [arXiv:0907.2997 [hep-ph]], JHEP **0911** (2009) 088 [arXiv:0909.3420 [hep-ph]]; A. Pak, M. Rogal and M. Steinhauser, Phys. Lett. B **679** (2009) 473 [arXiv:0907.2998 [hep-ph]], JHEP **1002** (2010)

025 [arXiv:0911.4662 [hep-ph]]; R. V. Harlander, H. Mantler, S. Marzani and K. J. Ozeren, Eur. Phys. J. C **66** (2010) 359 [arXiv:0912.2104 [hep-ph]].

[15] M. Krämer, E. Laenen and M. Spira, Nucl. Phys. B **511**, 523 (1998) [arXiv:hep-ph/9611272]; S. Catani, D. de Florian, M. Grazzini and P. Nason, JHEP **0307** (2003) 028 [arXiv:hep-ph/0306211]; A. Idilbi, X. -d. Ji, J. -P. Ma and F. Yuan, Phys. Rev. D **73** (2006) 077501 [hep-ph/0509294]; A. Idilbi, X. -d. Ji and F. Yuan, Nucl. Phys. B **753** (2006) 42 [hep-ph/0605068]; V. Ahrens, T. Becher, M. Neubert and L. L. Yang, Eur. Phys. J. C **62** (2009) 333 [arXiv:0809.4283 [hep-ph]].

[16] S. Moch and A. Vogt, Phys. Lett. B **631** (2005) 48 [arXiv:hep-ph/0508265]; V. Ravindran, Nucl. Phys. B **752** (2006) 173 [arXiv:hep-ph/0603041]; R. D. Ball, M. Bonvini, S. Forte, S. Marzani and G. Ridolfi, arXiv:1303.3590 [hep-ph]; S. Buehler and A. Lazopoulos, arXiv:1306.2223 [hep-ph]; C. Anastasiou, C. Duhr, F. Dulat, E. Furlan, T. Gehrmann, F. Herzog and B. Mistlberger, arXiv:1403.4616 [hep-ph].

[17] A. Djouadi and P. Gambino, Phys. Rev. Lett. **73** (1994) 2528 [arXiv:hep-ph/9406432]; A. Djouadi, P. Gambino and B. A. Kniehl, Nucl. Phys. B **523** (1998) 17 [arXiv:hep-ph/9712330].

[18] U. Aglietti, R. Bonciani, G. Degrassi and A. Vicini, Phys. Lett. B **595** (2004) 432 [arXiv:hep-ph/0404071], Phys. Lett. B **600** (2004) 57 [arXiv:hep-ph/0407162].

[19] G. Degrassi and F. Maltoni, Phys. Lett. B **600** (2004) 255 [arXiv:hep-ph/0407249].

[20] S. Actis, G. Passarino, C. Sturm and S. Uccirati, Phys. Lett. B **670** (2008) 12 [arXiv:0809.1301 [hep-ph]], Nucl. Phys. B **811** (2009) 182 [arXiv:0809.3667 [hep-ph]].

[21] R. Bonciani, G. Degrassi and A. Vicini, Comput. Phys. Commun. **182** (2011) 1253 [arXiv:1007.1891 [hep-ph]].

[22] C. Anastasiou, R. Boughezal and F. Petriello, JHEP **0904** (2009) 003 [arXiv:0811.3458 [hep-ph]].

[23] S. Dawson, A. Djouadi and M. Spira, Phys. Rev. Lett. **77** (1996) 16 [arXiv:hep-ph/9603423].

[24] M. Mühlleitner and M. Spira, Nucl. Phys. B **790** (2008) 1 [arXiv:hep-ph/0612254].

[25] C. Anastasiou, S. Beerli and A. Daleo, Phys. Rev. Lett. **100** (2008) 241806 [arXiv:0803.3065 [hep-ph]].

[26] M. Mühlleitner, H. Rzehak and M. Spira, PoS RADCOR **2009** (2010) 043 [arXiv:1001.3214 [hep-ph]].

[27] R. V. Harlander and M. Steinhauser, Phys. Lett. B **574** (2003) 258 [hep-ph/0307346].

[28] R. V. Harlander and M. Steinhauser, JHEP **0409** (2004) 066 [hep-ph/0409010].

[29] G. Degrassi and P. Slavich, Nucl. Phys. B **805** (2008) 267 [arXiv:0806.1495 [hep-ph]].

[30] R. V. Harlander and F. Hofmann, JHEP **0603** (2006) 050 [hep-ph/0507041].

[31] G. Degrassi, S. Di Vita and P. Slavich, JHEP **1108** (2011) 128 [arXiv:1107.0914 [hep-ph]].

[32] G. Degrassi and P. Slavich, JHEP **1011** (2010) 044 [arXiv:1007.3465 [hep-ph]].

[33] R. V. Harlander, F. Hofmann and H. Mantler, JHEP **1102** (2011) 055 [arXiv:1012.3361 [hep-ph]].

[34] G. Degrassi, S. Di Vita and P. Slavich, Eur. Phys. J. C **72** (2012) 2032 [arXiv:1204.1016 [hep-ph]].

[35] K. G. Chetyrkin, B. A. Kniehl, M. Steinhauser and W. A. Bardeen, Nucl. Phys. B **535** (1998) 3 [hep-ph/9807241]; R. V. Harlander and W. B. Kilgore, JHEP **0210** (2002) 017 [hep-ph/0208096]; C. Anastasiou and K. Melnikov, Phys. Rev. D **67** (2003) 037501 [hep-ph/0208115]; F. Caola and S. Marzani, Phys. Lett. B **698** (2011) 275 [arXiv:1101.3975 [hep-ph]]; A. Pak, M. Rogal and M. Steinhauser, JHEP **1109** (2011) 088 [arXiv:1107.3391 [hep-ph]].

[36] R. Harlander and M. Steinhauser, Phys. Rev. D **68** (2003) 111701 [hep-ph/0308210].

[37] A. Pak, M. Steinhauser and N. Zerf, Eur. Phys. J. C **71** (2011) 1602 [Erratum-ibid. C **72** (2012) 2182] [arXiv:1012.0639 [hep-ph]].

[38] A. Pak, M. Steinhauser and N. Zerf, JHEP **1209** (2012) 118 [arXiv:1208.1588 [hep-ph]].

[39] M. S. Carena, D. Garcia, U. Nierste and C. E. M. Wagner, Nucl. Phys. B **577** (2000) 88 [arXiv:hep-ph/9912516].

[40] J. Guasch, P. Häfliger and M. Spira, Phys. Rev. D **68** (2003) 115001 [arXiv:hep-ph/0305101].

[41] D. Noth and M. Spira, Phys. Rev. Lett. **101** (2008) 181801 [arXiv:0808.0087 [hep-ph]], JHEP **1106** (2011) 084 [arXiv:1001.1935 [hep-ph]]; L. Mihaila and C. Reisser, JHEP **1008** (2010) 021 [arXiv:1007.0693 [hep-ph]].

[42] S. Dittmaier, M. Krämer and M. Spira, Phys. Rev. D **70** (2004) 074010 [hep-ph/0309204]; S. Dawson, C. B. Jackson, L. Reina and D. Wackeroth, Phys. Rev. D **69** (2004) 074027 [hep-ph/0311067].

[43] D. Dicus, T. Stelzer, Z. Sullivan and S. Willenbrock, Phys. Rev. D **59** (1999) 094016 [hep-ph/9811492]; F. Maltoni, Z. Sullivan and S. Willenbrock, Phys. Rev. D **67** (2003) 093005 [hep-ph/0301033].

[44] R. V. Harlander and W. B. Kilgore, Phys. Rev. D **68** (2003) 013001 [hep-ph/0304035].

[45] S. Dittmaier, M. Krämer, A. Mück and T. Schlüter, JHEP **0703** (2007) 114 [hep-ph/0611353]; S. Dawson, C. B. Jackson and P. Jaiswal, Phys. Rev. D **83** (2011) 115007 [arXiv:1104.1631 [hep-ph]].

[46] M. Spira, hep-ph/9510347.

[47] R. Harlander, `www.robert-harlander.de/software/ggh@nnlo`

[48] S. Catani and M. Grazzini, Phys. Rev. Lett. **98** (2007) 222002 [hep-ph/0703012]; M. Grazzini, JHEP **0802** (2008) 043 [arXiv:0801.3232 [hep-ph]]; M. Grazzini and H. Sargsyan, arXiv:1306.4581 [hep-ph].

[49] C. Anastasiou, S. Buehler, F. Herzog and A. Lazopoulos, JHEP **1112** (2011) 058 [arXiv:1107.0683 [hep-ph]].

[50] R. Harlander, `www.robert-harlander.de/software/bbh@nnlo`

[51] E. Bagnaschi, G. Degrassi, P. Slavich and A. Vicini, JHEP **1202** (2012) 088 [arXiv:1111.2854 [hep-ph]].

[52] S. Frixione, P. Nason and C. Oleari, JHEP **0711** (2007) 070 [arXiv:0709.2092 [hep-ph]]; S. Alioli, P. Nason, C. Oleari and E. Re, JHEP **1006** (2010) 043 [arXiv:1002.2581 [hep-ph]].

[53] R. V. Harlander, S. Liebler and H. Mantler, Computer Physics Communications **184** (2013) pp. 1605 [arXiv:1212.3249 [hep-ph]]; `http://sushi.hepforge.org/`

[54] S. Heinemeyer, O. Stål and G. Weiglein, Phys. Lett. B **710** (2012) 201 [arXiv:1112.3026 [hep-ph]].

[55] A. Arbey, M. Battaglia, A. Djouadi, F. Mahmoudi and J. Quevillon, Phys. Lett. B **708** (2012) 162 [arXiv:1112.3028 [hep-ph]].

[56] M. Carena, S. Heinemeyer, O. Stål, C. E. M. Wagner and G. Weiglein, arXiv:1302.7033 [hep-ph].

[57] The LHC Higgs Cross Section Working Group, `https://twiki.cern.ch/twiki/bin/view/LHCPhysics/SMInputParameter`

[58] CDF [Tevatron Electroweak Working Group and D0 Collaborations], arXiv:1305.3929 [hep-ex].

[59] J. H. Kühn, M. Steinhauser and C. Sturm, Nucl. Phys. B **778** (2007) 192 [arXiv:hep-ph/0702103]; K. G. Chetyrkin *et al.*, Phys. Rev. D **80** (2009) 074010 [arXiv:0907.2110 [hep-ph]].

[60] S. Heinemeyer, W. Hollik and G. Weiglein, Comput. Phys. Commun. **124** (2000) 76 [hep-ph/9812320].

[61] M. Frank, T. Hahn, S. Heinemeyer, W. Hollik, H. Rzehak and G. Weiglein, JHEP **0702** (2007) 047 [hep-ph/0611326].

[62] S. Heinemeyer, W. Hollik and G. Weiglein, Eur. Phys. J. C **9** (1999) 343 [hep-ph/9812472].

[63] G. Degrassi, P. Slavich and F. Zwirner, Nucl. Phys. B **611** (2001) 403 [hep-ph/0105096]; A. Brignole, G. Degrassi, P. Slavich and F. Zwirner, Nucl. Phys. B **631** (2002) 195 [hep-ph/0112177].

[64] A. Brignole, G. Degrassi, P. Slavich and F. Zwirner, Nucl. Phys. B **643** (2002) 79 [hep-ph/0206101]; A. Dedes, G. Degrassi and P. Slavich, Nucl. Phys. B **672** (2003) 144 [hep-ph/0305127].

[65] S. Heinemeyer, W. Hollik, H. Rzehak and G. Weiglein, Eur. Phys. J. C **39** (2005) 465 [hep-ph/0411114].

[66] S. Heinemeyer, W. Hollik, H. Rzehak and G. Weiglein, Phys. Lett. B **652** (2007) 300 [arXiv:0705.0746 [hep-ph]].

[67] G. Degrassi, S. Heinemeyer, W. Hollik, P. Slavich and G. Weiglein, Eur. Phys. J. C **28** (2003) 133 [hep-ph/0212020]; B. C. Allanach, A. Djouadi, J. L. Kneur, W. Porod and P. Slavich, JHEP **0409** (2004) 044 [hep-ph/0406166].

[68] S. P. Martin, Phys. Rev. D **66** (2002) 096001 [hep-ph/0206136], Phys. Rev. D **67** (2003) 095012 [hep-ph/0211366], Phys. Rev. D **71** (2005) 016012 [hep-ph/0405022].

[69] S. P. Martin, Phys. Rev. D **75** (2007) 055005 [hep-ph/0701051].

[70] R. V. Harlander, P. Kant, L. Mihaila and M. Steinhauser, Phys. Rev. Lett. **100** (2008) 191602 [Phys. Rev. Lett. **101** (2008) 039901] [arXiv:0803.0672 [hep-ph]], JHEP **1008** (2010) 104 [arXiv:1005.5709 [hep-ph]].

[71] [ATLAS Collaboration], ATLAS-CONF-2013-007.

[72] G. Aad *et al.* [ATLAS Collaboration], JHEP **1310** (2013) 130 [arXiv:1308.1841 [hep-ex]], ATLAS-CONF-2013-047, ATLAS-CONF-2013-061, ATLAS-CONF-2013-062, ATLAS-CONF-2013-089.

[73] S. Chatrchyan *et al.* [CMS Collaboration], Eur. Phys. J. C **73** (2013) 2568 [arXiv:1303.2985 [hep-ex]].

[74] S. Chatrchyan *et al.* [CMS Collaboration], JHEP **1401** (2014) 163 [arXiv:1311.6736 [hep-ex]], CMS-PAS-SUS-13-002, CMS-PAS-SUS-13-008.

[75] S. Chatrchyan *et al.* [CMS Collaboration], arXiv:1311.4937 [hep-ex], arXiv:1402.4770 [hep-ex], CMS-PAS-SUS-13-004.

[76] G. Aad *et al.* [ATLAS Collaboration], arXiv:1403.4853 [hep-ex].

[77] S. Chatrchyan *et al.* [CMS Collaboration], Eur. Phys. J. C **73** (2013) 2677 [arXiv:1308.1586 [hep-ex]], CMS-PAS-SUS-13-015.

[78] [ATLAS Collaboration], ATLAS-CONF-2013-068.

[79] [CMS Collaboration], CMS-PAS-SUS-13-009.

[80] G. Aad *et al.* [ATLAS Collaboration], JHEP **1310** (2013) 189 [arXiv:1308.2631 [hep-ex]].

[81] M. Spira, Fortsch. Phys. **46** (1998) 203 [hep-ph/9705337].

[82] R. Harlander, Eur. Phys. J. C **33** (2004) S454 [hep-ph/0311005].

[83] A. D. Martin, W. J. Stirling, R. S. Thorne and G. Watt, Eur. Phys. J. C **63** (2009) 189 [arXiv:0901.0002 [hep-ph]].

[84] C. Anastasiou, K. Melnikov and F. Petriello, Nucl. Phys. B **724** (2005) 197 [hep-ph/0501130].

[85] E. Boos and T. Plehn, Phys. Rev. D **69** (2004) 094005 [hep-ph/0304034].

[86] K. G. Chetyrkin and M. Steinhauser, Nucl. Phys. B **573** (2000) 617 [hep-ph/9911434]; K. Melnikov and T. v. Ritbergen, Phys. Lett. B **482** (2000) 99 [hep-ph/9912391].

[87] K. G. Chetyrkin, Phys. Lett. B **404** (1997) 161 [hep-ph/9703278]; J. A. M. Vermaseren, S. A. Larin and T. van Ritbergen, Phys. Lett. B **405** (1997) 327 [hep-ph/9703284].

[88] J. Baglio and A. Djouadi, JHEP **1103** (2011) 055 [arXiv:1012.0530 [hep-ph]].

[89] M. I. Kotsky and O. I. Yakovlev, Phys. Lett. B **418** (1998) 335 [hep-ph/9708485]; R. Akhoury, H. Wang and O. I. Yakovlev, Phys. Rev. D **64** (2001) 113008 [hep-ph/0102105].

[90] L. J. Hall, R. Rattazzi and U. Sarid, Phys. Rev. D **50** (1994) 7048 [arXiv:hep-ph/9306309]; R. Hempfling, Phys. Rev. D **49** (1994) 6168.

[91] H. -L. Lai, M. Guzzi, J. Huston, Z. Li, P. M. Nadolsky, J. Pumplin and C. -P. Yuan, Phys. Rev. D **82** (2010) 074024 [arXiv:1007.2241 [hep-ph]].

[92] R. D. Ball, V. Bertone, S. Carrazza, C. S. Deans, L. Del Debbio, S. Forte, A. Guffanti and N. P. Hartland *et al.*, Nucl. Phys. B **867** (2013) 244 [arXiv:1207.1303 [hep-ph]].

[93] F. Demartin, S. Forte, E. Mariani, J. Rojo and A. Vicini, Phys. Rev. D **82** (2010) 014002 [arXiv:1004.0962 [hep-ph]].

[94] S. Alekhin, S. Alioli, R. D. Ball, V. Bertone, J. Blumlein, M. Botje, J. Butterworth and F. Cerutti *et al.*, arXiv:1101.0536 [hep-ph]; M. Botje, J. Butterworth, A. Cooper-Sarkar, A. de Roeck, J. Feltesse, S. Forte, A. Glazov and J. Huston *et al.*, arXiv:1101.0538 [hep-ph].

[95] J. Beringer *et al.* [Particle Data Group Collaboration], Phys. Rev. D **86** (2012) 010001.

[96] A. D. Martin, W. J. Stirling, R. S. Thorne and G. Watt, Eur. Phys. J. C **70** (2010) 51 [arXiv:1007.2624 [hep-ph]].

[97] R. D. Ball, V. Bertone, F. Cerutti, L. Del Debbio, S. Forte, A. Guffanti, J. I. Latorre and J. Rojo *et al.*, Nucl. Phys. B **849** (2011) 296 [arXiv:1101.1300 [hep-ph]].